RAP1-TRIGGERED PATHWAYS FOR TALIN-MEDIATED INTEGRIN ACTIVATION

by

LIANG ZHU

Submitted in partial fulfillment of the requirements for the degree of

Doctor of Philosophy

Dissertation Advisor: Dr. Jun Qin

Department of Biochemistry

CASE WESTERN RESERVE UNIVERSITY

January, 2018

CASE WESTERN RESERVE UNIVERSITY

SCHOOL OF GRADUATE STUDIES

We hereby approve the thesis/dissertation of

Liang Zhu

candidate for the degree of **Doctor of Philosophy** *.

Committee Chair

Vivien Yee, Ph.D.

Committee Member

Jun Qin, Ph.D.

Committee Member

Edward F. Plow, Ph.D.

Committee Member

Focco van den Akker, Ph.D.

Committee Member

Sadashiva S. Karnik, Ph.D.

Date of Defense

November 28, 2017

*We also certify that written approval has been obtained

for any proprietary material contained therein

Table of Contents

List of Tables

List of Figures

Acknowledgement

First of all, I am grateful for everything before 2012 that made happen my journey to U.S. to pursue my doctorate degree. Being the youngest kid from a family with an "unusual size" in my generation in China, I couldn't feel more happy and supportive as I always get unconditional care, love and funds from them, i.e. my parents, my brother and my sister.

Regarding this dissertation and two related first-author publications, I have to express my tremendous gratitude to Dr. Jun Qin. I believe this guy plays an essential role in "Liang's research career". He recruited me even though there was no additional slot in the lab at that time. He "activated" me by patiently explaining the difficult theory of NMR techniques, pushing and trusting me to try those challenging although energy-consuming experiments, and more importantly making me realize that one can be ambitious, humble as well as aggressive. During these five years, we have had "high affinity" interactions and great insightful discussions toward how to make things and projects done. I wish and believe that we will keep doing so in the future.

Thanks to all lab members in Qin lab who create and maintain a harmonic atmosphere for doing research. Thanks to Dr. Jun Yang and Dr. Jianming Liu from whom I have learned a lot important knowledge of NMR techniques. Thanks to Dr. Sujay Ithychanda with whom I always have relaxing chats and discussions. Thanks to Dr. Koichi Fukuda whose dedication to science has touched me somehow deeply. Thanks to Mr. Xiaolun Zhang who has great sense of humor with his own unique style and always brings those hilarious moments to lab. Thanks to Ms. Fan Lu and Dr. Ashley Holly who have

helped me a lot in my project experiments. Thanks to Dr. Julia Vaynberg who has provided useful discussions in my group meeting presentations.

I wish to sincerely acknowledge my committee members, Drs. Edward F. Plow, Sadashiva S. Karnik, Vivien Yee and Focco Van den Akker. They have provided very useful suggestions for my Ph.D. studies as well as my research career. I appreciate them greatly for attending my yearly seminar presentation and commenting insightfully afterwards.

Five years is long if I am reminded of the rough Cleveland winters, but it is pretty short when I recall those great moments of hanging out with my friends. I am grateful for being surrounded by a bunch of nice guys and girls with “strong interaction” as well as “weak interaction”. The time I have spent with them did not delay my project progress at all, but relaxed me down to help me think about my life from where I benefit a lot.

At last, please allow me to be a little be “narcissistic”. Thanks to myself who has shown persistence and successfully handled those “ups and downs” during these five years. Thanks to myself who is always trying to be positive and enthusiastic, and importantly always holds the belief that I can make something different. I am happy, satisfied and grateful.

List of Abbreviations

β-ME, β-mercaptoethanol

C-terminal, carboxyl-terminal

cAMP, cyclic adenosine monophosphate

CC domain, coiled-coil domain

CHO, Chinese hamster ovary

CT, cytoplasmic tail

DAG, diacylglycerol

DM, double mutant or mutations

DTT, dithiothreitol

ECM, extracellular matrix

Ena, *Drosophila* Enabled

FA, focal adhesion

FERM, 4.1/ezrin/radixin/moesin

FL, full length

GAP, GTPase activating protein

GDP, guanosine diphosphate

GEF, guanine nucleotide exchange factor

GMP-PNP, guanosine 5′-[β, γ-imido] triphosphate trisodium salt

GPCR, G protein-coupled receptor

GST, glutathione S-transferase

GTP, guanosine-5'-triphosphate

HNCA, amide proton-to-nitrogen-to-α carbon correlation

HSQC, heteronuclear single quantum coherence

IPTG: isopropyl β-D-1-thiogalactopyranoside

ITC, isothermal titration calorimetry

K_d, dissociation constant

LB: lysogeny broth

Lpd, lamellipodin

LUVs, large unilamellar vesicles

MFI, median fluorescent intensity

MLVs, multilamellar vesicles

MRL, Mig-10/RIAM/Lamellipodin

MST, microscale thermophoresis

N-terminal, Amino-terminal

NMR, nuclear magnetic resonance

NOE, nuclear Overhauser effect

NOESY, nuclear Overhauser effect spectroscopy

PH domain, pleckstrin homology domain

PIP, phosphatidylinositol 4-phosphate

PIP2, phosphatidylinositol 4, 5-bisphosphate

PIPKI, type I phosphatidylinositol phosphate kinase

PIPKIγ, type I phosphatidylinositol phosphate kinase isoform-γ

PKA, protein kinase A

PP, proline-rich regions

PPI, protein-protein interaction

PTB domain, phosphotyrosine-binding domain

PVDF, polyvinylidene fluoride

RA domain, Ras-association domain

RGD, arginine-glycine-aspartate

RIAM, Rap1-GTP-interacting adaptor molecule

RIAM-N, the N-terminus of RIAM

RT, room temperature

TB, talin binding

VASP, vasodilator-stimulated phosphoprotein

WB, western blot

WT, wild type

Rap1-triggered Pathways for Talin-mediated Integrin Activation

Abstract

by

LIANG ZHU

The membrane localization and activation of cytoskeletal protein talin are key steps to trigger the activation of transmembrane receptor integrin to induce cell adhesion – a fundamental process that is involved in almost all life processes. However, the pathways that recruit talin to membrane and activate talin, which critically control talin's action, remained elusive despite decades of studies. Previous studies have identified a canonical "Rap1-RIAM-talin" pathway where membrane-anchored mammalian small GTPase Rap1 recruits one of its downstream effectors called RIAM to membrane which in turn recruits talin by binding to its Rod domain (talin-R). Following talin recruitment, talin gets activated by PIP2-enriched membrane through a previously defined electrostatic "pull-push" mechanism. In the first part of my dissertation, we discover an unexpected role of RIAM, which binds to the N-terminal head of talin (talin-H) and sterically occludes talin-R domain that otherwise masks the integrin-binding site on talin-H to trigger talin activation. Our finding thus calls a revision of the "Rap1-RIAM-talin" pathway, which was recently found to be crucial in regulating leukocyte adhesion. In the second part of

my dissertation, we find a direct “Rap1-talin” interaction crucial for mediating membrane-targeting and activation of talin to activate integrin. This direct Rap1/talin pathway appears to be critical in many non-leukocytes where RIAM has extremely low expression level. We provide structural evidence demonstrating that talin itself is a typical Rap1 effector. We also functionally show that disruption of their binding strongly impairs integrin activation, cell adhesion, and cell spreading. Overall, our findings identify two distinct mechanisms of Rap1-mediated talin localization and activation in regulating cell-specific integrin activation and a wide range of physiological processes.

Chapter 1 Background and Significance

Background

Integrin

Integrins are transmembrane receptors expressed on cell surface and critically regulate cell-extracellular matrix (ECM) adhesion and cell-cell adhesion[1,2]. Integrin is a heterodimer consisting of an α subunit and a β subunit (**Figure 1.1**). Each subunit is composed of a large extracellular domain, a single α-helical transmembrane segment as well as a short cytoplasmic tail. So far, 24 distinct types of integrins assembled by 18 different α subunits and 8 different β subunits have been identified. They can be classified into four major sub-groups based on ligand binding properties or specific cellular function (**Figure 1.2**)[1,3]. Of those, while β1 integrins are wildly expressed in most cells of our body, some individual integrins are cell type specific (e.g. $\alpha_{IIb}\beta_3$ integrin in platelets, β_2 integrins in leukocytes).

Integrin undergoes conformational change from a "bent" inactive state to an "extended" active state to bind ECM ligand to induce cell adhesion (**Figure 1.1**)[4,5]. Such process, also called "integrin activation", has been a central topic of cell adhesion for decades. Integrin activation could be triggered bi-directionally, so called "outside-in" signaling and "inside-out" signaling. Cell-exterior ECM ligands or divalent cations (e.g. Mn^{2+}) are capable of activating some integrins from outside ("outside-in"), but more commonly, majority of integrins are activated by intracellular cytoskeletal proteins, namely talin and kindlin, from cell interior ("inside-out")[6-8].

Integrins are essential for many life processes. For example, $\alpha_{IIb}\beta_3$ integrin is required for platelet aggregation and plays an important role in hemostasis and thrombosis[9]. β_2 integrins are essential for regulating leukocyte adhesion which critically controls the migration of leukocytes to inflammation site[10]. Besides, $\alpha_v\beta_3$ integrin is primarily involved in mediating osteoclast function to regulate the resorption of bone[11]. Dysfunctional integrins can lead to multiple human diseases, e.g. thrombosis, inflammation, osteoporosis and cancer[1-3]. Thus, to thoroughly study the mechanism of integrin signaling improves our knowledge of the underlying causes of integrin-related diseases and provides a solid basis for drug development.

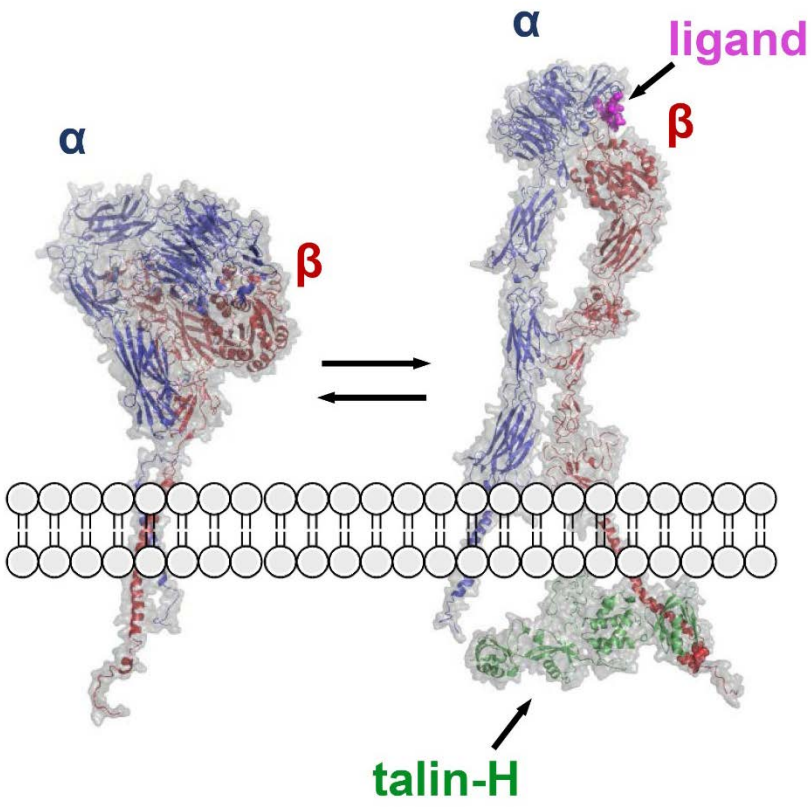

Figure 1.1 The structural model of integrin activation

Integrin undergoes conformational change from a “bent” inactive state to an “extended” active state to bind extracellular matrix (ECM) ligands. Integrin and talin head domain (talin-H) are shown in both cartoon and surface representations. Integrin α subunit, β subunit and talin-H are colored in blue, red, and green respectively. The polypeptide (“HHLGGAKQRGDV”) of fibrinogen (an ECM ligand) is colored in magenta and shown in sphere representation. This model is generated with known X-ray crystal structures (PDB codes: 3FCS, 2VDQ, 3IVF, and 3G9W) and an NMR solution structure (PDB code: 2KNC).

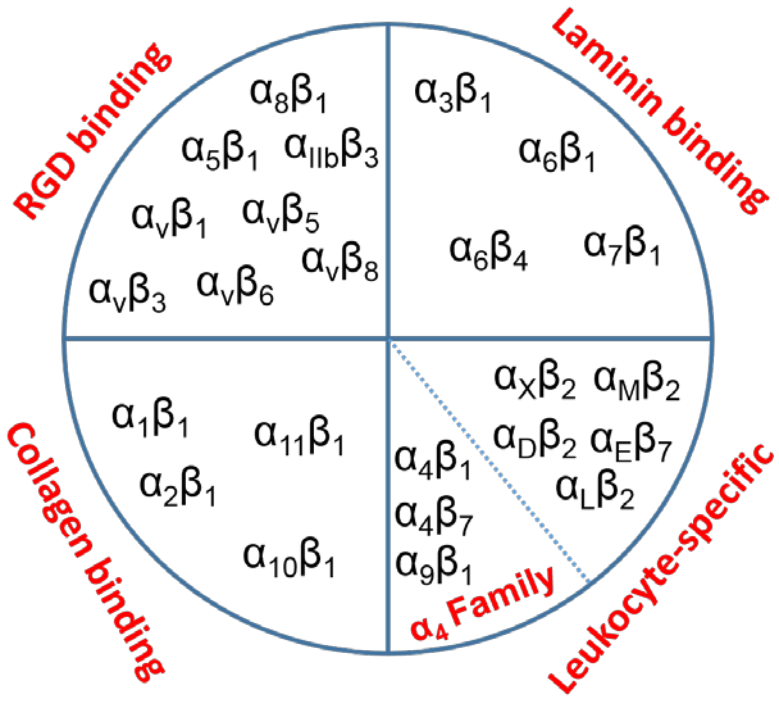

Figure 1.2 The classification of integrins

24 types of integrins are classified into 4 sub-groups, “arginine-glycine-aspartate (RGD)”-binding integrins, collagen-binding integrins, laminin-binding integrins and leukocyte-specific integrins.

Talin

Talin is a large scaffold protein (MW: ~270 kD) that links "ECM-integrin" complex and actin cytoskeleton[7]. It has two isoforms, namely talin-1 and talin-2. Talin-1 is ubiquitously expressed, whereas talin-2 is more enriched in heart and brain. Talin is essential and plays a critical role in integrin activation. Mice with talin-1 knock-out are embryonically lethal by embryonic day E8.5 due to gastrulation defects. Talin-2 knockout mice are viable and fertile, but show early and severe dystrophic phenotype in skeletal muscle. Besides, tissue-specific depletions of talin-1 in mice can lead to integrin-dependent phenotypes, such as impaired platelet aggregation, and defects in B lymphocytes homing to lymph nodes[7,12,13].

Talin consists of an N-terminal head domain (talin-H), and a C-terminal rod domain (talin-R) followed by a small dimerization domain (talin-DD) (**Figure 1.3**). Talin-H is further divided into a preceding F0 subdomain and a FERM (4.1/ezrin/radixin/moesin)-like domain (including F1, F2 and F3 subdomains). Talin-R is made up of 13 consecutive helical bundles. As a critical integrin activator, talin has been found to trigger the activation of β_1, β_2 and β_3 integrins[7,13]. To do so, talin-F3, a PTB (phosphotyrosine-binding domain)-like domain directly binds to the membrane proximal "NPxY" motif of integrin β cytoplasmic tail, which result in the separation of integrin α and β subunit at the cytoplasmic face. Such change is further relayed to integrin extracellular domain and leads to the overall conformational change or activation of integrin.

Interestingly, talin randomly distributes in cytosol in resting cells and remains inactive by adopting an auto-inhibitory conformation in which the integrin binding site of

talin-F3 is masked by talin-R[14,15]. Upon cellular stimulation, talin rapidly localizes to the plasma membrane[16,17] and gets activated to induce integrin activation. Extensive studies have shown that Rap1, RIAM and PIPKIγ/PIP2 are capable of regulating membrane recruitment and activation of talin[18], however, the exact mechanisms have not been fully understood.

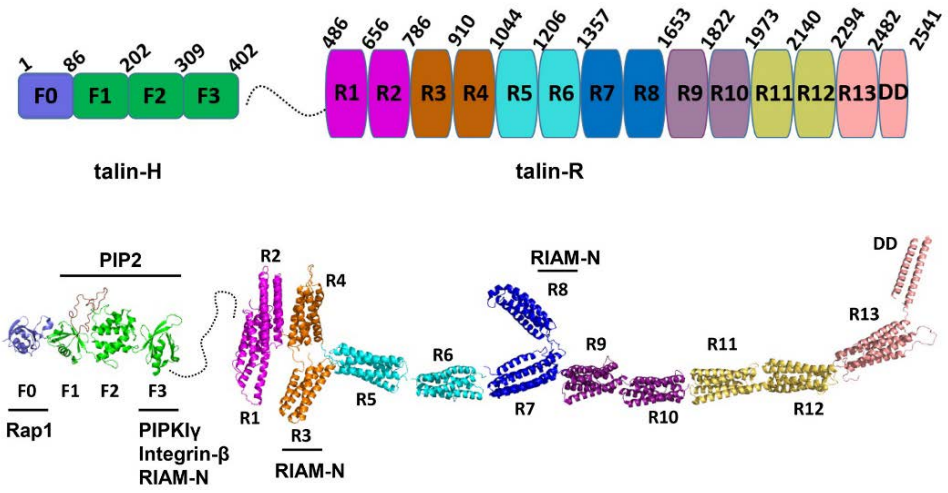

Figure 1.3 Domain organization and a linear structural model of talin

The model was generated from known crystal and NMR structures of talin fragments and shown in cartoon representation. Critical talin binding partners involved in talin membrane recruitment and activation are indicated in the figure. PIP2, phosphatidylinositol 4,5-bisphosphate. RIAM-N, the N-terminus of RIAM. PIPKIγ, type I phosphatidylinositol phosphate kinase isoform-γ. Note that talin-F3/RIAM-N interaction and talin-F0/Rap1 interaction are studied in Chapter 2 and Chapter 3 of this dissertation respectively.

Rap1

Rap1 is a small GTPase from Ras superfamily. It has two isoforms with ~95% identity encoded by separate genes, namely Rap1a and Rap1b. Both isoforms are ubiquitously expressed in tissues. Particularly, Rap1a is the major isoform in neutrophils, whereas Rap1b is more predominant in platelets[19]. Rap1 triggers integrin activation through "inside-out" signaling and critically regulates integrin-dependent cell adhesion[20,21]. Mice with Rap1a/b double knock-out are not viable due to embryonic lethality suggesting a developmental role of Rap1[22]. Although mice lacking either isoform are viable indicating the functional redundancy of these two isoforms, severe tissue-specific phenotypes have been observed. For example, loss of Rap1a impaired the cell adhesion, migration and phagocytosis of leukocytes, whereas Rap1b deficiency led to severe defect in integrin-dependent platelet function[23,24].

Like other Ras-family GTPases, Rap1 localizes at the plasma membrane *via* a geranylgeranyl group that is post-translationally added to its C-terminal "CAAX" motif by prenylation[25]. The membrane dissociation of Rap1 could be otherwise regulated by protein kinase A (PKA)-dependent phosphorylation[26]. Rap1 cycles between an inactive form (GDP-bound) and an active form (GTP-bound). The activation and inactivation of Rap1 are regulated by Rap-specific guanine nucleotide exchange factors (GEFs) and GTPase activating proteins (GAPs) respectively. Rap1 activation is initiated by extracellular stimulation of various agonists including growth factors, hormones, neurotransmitters and cytokines, which results in the increased cellular level of second messengers (e.g. calcium, cAMP, diacylglycerol) and subsequently activates GEFs[21] (**Figure 1.4**). Activated Rap1 has been found to recruit multiple downstream effectors (e.g.

RAPL, RIAM, KRIT1) to regulate different signaling pathways including cell proliferation, secretion, adhesion and migration [20,27,28].

RIAM

Rap1-GTP-interacting adaptor molecule (RIAM), belongs to the MRL (Mig-10/RIAM/Lamellipodin) family, was first identified as a Rap1 effector to regulate β1 and β2 integrin-mediated adhesion in T lymphocytes[29]. RIAM is an adaptor protein with a molecular weight of ~73 kDa (**Figure 1.5**). The N-terminus of RIAM contains a talin-binding (TB) region that binds to talin-R, a short proline-rich region and two coiled-coil domains. The central part of RIAM comprises a Ras-association (RA) domain and a pleckstrin homology (PH) domain which interact with Rap1 and PIP2-membrane respectively. The C-terminus of RIAM is another proline-rich region that may bind to Profilin and Ena/VASP family proteins to regulate actin dynamic[29].

For a long while, RIAM was considered as a bridge that links Rap1 and talin to trigger the membrane-targeting of talin for integrin activation[30,31]. Other MRL family protein like lamellipodin (Lpd) also has similar function[30,32]. RIAM or Lpd forms a so called "MIT" complex with integrin and talin at the leading edge of cells to trigger the assembly of "sticky fingers" that guide cell migration[33]. However, RIAM or Lpd has low expression level in non-leukocytes[34,35] indicating an alternative pathway for talin membrane-targeting.

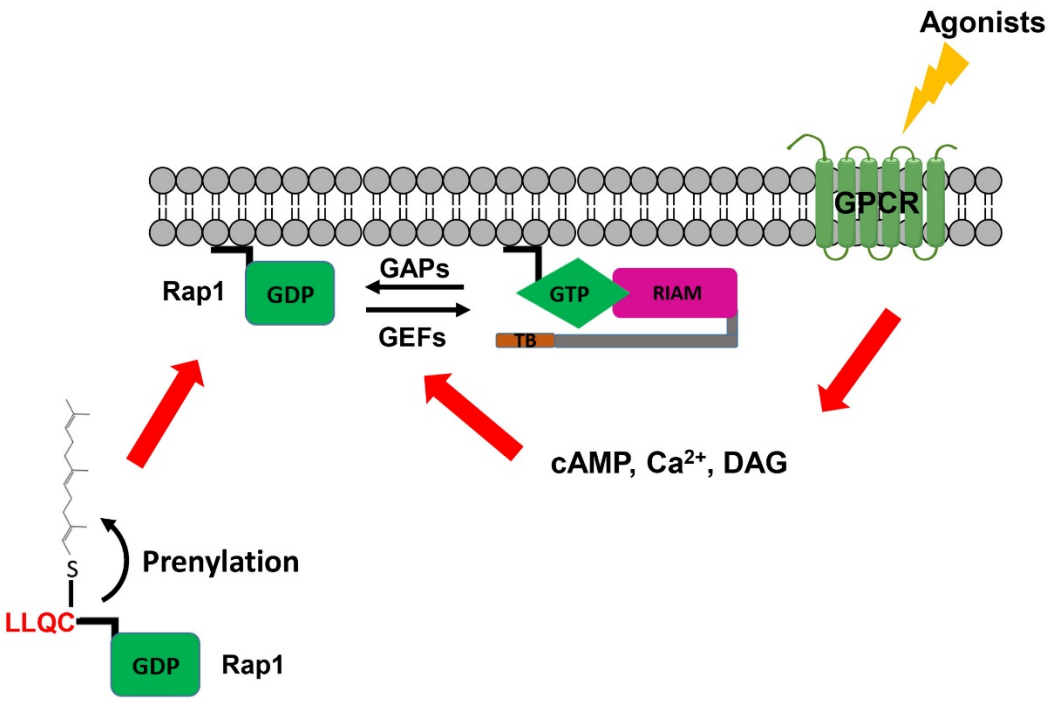

Figure 1.4 The mechanism of Rap1 activation

Agonist stimulation through G-protein-coupled receptors (GPCRs) results in the increased cellular level of second messengers including calcium, cyclic adenosine monophosphate (cAMP), and diacylglycerol (DAG). Subsequently, guanine nucleotide exchange factors (GEFs) get activated and in turn promote the GTP loading of Rap1.

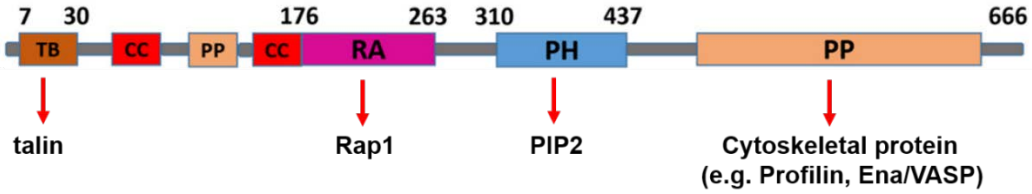

Figure 1.5 Domain organization of RIAM

RIAM comprises a talin binding site (TB), a Ras association domain (RA), a pleckstrin homology domain (PH), two coiled-coil domains (CC) and two proline-rich regions (PP). Its binding partners include talin, Rap1, PIP2, and other cytoskeletal proteins (e.g. Profilin and Ena/VASP family proteins).

PIPKI

Type I phosphatidylinositol phosphate kinases (PIPKIs) are kinases that phosphorylate phosphatidylinositol 4-phosphates (PIPs) to phosphatidylinositol 4,5-bisphosphates (PIP2s) which are critical lipid molecules that regulate many cellular processes[36]. Three isoforms (α, β and γ) of PIPKI have been identified[37]. All of them contain a similar kinase domain at the central part and have similar kinase activity, however, these isoforms vary a lot at the amino- and carboxyl-terminal regions. Distinct from the other two isoforms, PIPKIγ contains a talin-binding (TB) region at its C-terminus and directly interacts with talin-F3 domain[38,39]. Such interaction allows PIPKIγ to be co-localized with talin in focal adhesions (FAs) and also enhances the kinase activity of PIPKIγ [38,39] . On the other hand, the recruitment and activation of PIPKIγ by talin provide a positive feedback for membrane-targeting and FAs assembly of talin. PIPKIγ-derived PIP2 lipid molecules at the membrane site could associate with talin to promote its membrane localization, and activate talin through a previously defined electrostatic "pull-push" mechanism to facilitate its binding to integrin[14,16].

The C-terminus of PIPKIγ contains a motif of "WVYSPLHY" (called PIPKIγ peptide here) that interacts with talin-F3 in a similar mode to that of integrin-β "NPxY" motif (**Figure 1.6**)[40-43]. In Particular, W642 of PIPKIγ and W775 of integrin β-tail occupy the same pocket of talin-F3 (**Figure 1.6**). Apparently, PIPKIγ and Integrin are mutually exclusive for talin-F3 binding, however, these two binding events could be spatiotemporally regulated by Src-mediated tyrosine-phosphorylation. Phosphorylation of PIPKIγ peptide at Y644 enhances its binding ability to talin-F3, whereas phosphorylation of Integrin β-tail at Y783 displays the opposite effect[44].

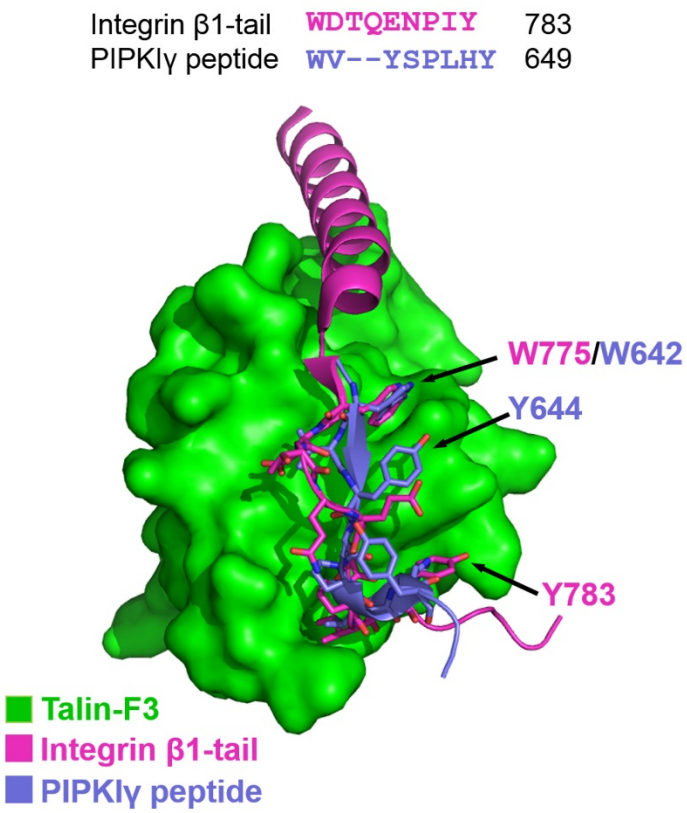

Figure 1.6 PIPKIγ peptide and integrin β-tail bind to talin-F3 in a similar mode

Talin-F3 (green) is shown in surface representation. PIPKIγ peptide (blue) and integrin β-tail (magenta) are shown in cartoon representation. W642 of PIPKIγ peptide and W775 of integrin β-tail bind to the same pocket of talin-F3. Phosphorylation of Y644 by Src increases the binding of PIPKIγ peptide to talin-F3, whereas phosphorylation of Y783 by Src decreases the binding of integrin β-tail to talin-F3. This figure is generated with known X-ray crystal structures (PDB codes: 1Y19 and 3G9W).

Significance

Extensive studies in the past decades have demonstrated that talin-mediated integrin activation is Rap1-dependent, but the underlying mechanism has remained controversial and elusive. Although "PIPKIγ-PIP2-talin" loop plays an important role in talin membrane-targeting and activation, the direct link between such loop and Rap1 is lacking. The specific ablation of PIPKIγ only partially and temporally impaired talin-mediated cell adhesion[45] and platelets lacking PIPKIγ showed normal integrin activation[46]. These evidence suggest that there are additional factors to regulate talin activity. "Rap1-RIAM-talin" axis has been considered as the major pathway for membrane-targeting of talin to regulate integrin "inside-out" signaling[8,13]. However, a study published in 2014 showed that RIAM knock-out mice are apparently healthy and fertile with normal platelet integrin activation and function[34] indicating the existence of an alternative mechanism for talin membrane-targeting.

In this dissertation, we try to improve the understanding of this complicated and mysterious mechanism. By exploiting a combination of biochemical, biophysical and cell-biological studies, we identified another two major pathways that are triggered by Rap1 for talin-mediated integrin activation. First, we discovered an unexpected role of RIAM, which binds to the N-terminal head of talin (talin-H) and sterically occludes talin-R domain that otherwise masks the integrin-binding site on talin-H to trigger talin activation. Second, we found a direct "Rap1-talin" interaction crucial for mediating membrane-targeting and activation of talin to activate integrin.

Overall, our studies in this dissertation combined with previously defined pathways by our group and others, provide an elaborate and convincing model for Rap1-

mediated talin localization and activation in regulating cell-specific integrin activation and a wide range of physiological processes.

Chapter 2 Conformational Activation of Talin by RIAM Triggers Integrin-mediated Cell Adhesion

The study of this chapter was published in

Jun Yang[#], Liang Zhu[#], Hao Zhang[#], Jamila Hirbawi, Koichi Fukuda, Pallavi Dwivedi, Jianmin Liu, Tatiana Byzova, Edward F. Plow, Jinhua Wu, and Jun Qin. Conformational activation of talin by RIAM triggers integrin-mediated cell adhesion. *Nat Commun*. 2014, 5: 5880. (# denotes co-first authorship)

Abstract

The membrane localization and activation of cytoskeletal protein talin are key steps to initiate the integrin transmembrane receptors' activation, which mediates many cellular adhesive responses such as cell migration, spreading and proliferation. RIAM, a membrane anchor and small GTPase Rap1 effector, is known to bind to the C-terminal rod domain of talin (talin-R) and promote localizations of talin to the membrane. Through systematic mapping analysis, we find that RIAM also binds to the N-terminal head of talin (talin-H), a crucial domain involved in binding and activating integrins. We show that the RIAM binding to talin-H sterically occludes the binding of a talin-R domain that otherwise masks the integrin-binding site on talin-H. We further provide functional evidence that such RIAM-mediated steric unmasking of talin triggers integrin activation. Our findings thus uncover a novel role for RIAM in conformational regulation of talin during integrin activation and cell adhesion.

Introduction

Almost every life process involves the adhesion of cells to their surroundings, the extracellular matrix (ECM). A major mediator of such an adhesion is integrin, a heterodimeric (α/β) transmembrane receptor that binds to the ECM proteins via its large ectodomains and connect to intracellular cytoskeleton via its small cytoplasmic tails (CTs) [2,5,47]. The ability of the integrin binding to the ECM proteins is controlled by a distinct 'inside-out' signaling mechanism (integrin activation), that is, an agonist-induced intracellular signal induces a conformational change of integrin cytoplasmic face, which is relayed via the transmembrane region to the ectodomain, converting it from low to high-affinity ligand-binding state[2,5,47]. As a vital step for controlling all cell adhesive processes, this integrin activation process has been the subject of intensive studies for decades. A major breakthrough from these studies was the discovery of talin as an intracellular activator of integrins[7,12].

Talin is a large protein that can be divided into an amino-terminal (N-terminal) head (1–433, talin-H, 50 kDa) that contains a FERM domain (including F1, F2 and F3 subdomains) and a preceding F0 domain, and a carboxyl-terminal (C-terminal) rod (482–2541, talin-R, 220 kDa) that is made up of 13 consecutive helical bundles followed by a C-terminal dimerization domain (DD)[7,12] (see also **Figure 1.3**). Extensive structural/biochemical studies have indicated that talin-H is responsible for activating integrin by disrupting the integrin α/β cytoplasmic clasp and initiating the inside-out conformational change of the receptor[43,48,49]. The key integrin-binding site is located on talin-F3. Interestingly, talin is randomly distributed[17] and autoinhibited in unstimulated cells with this integrin-binding site being masked by talin-R via an intramolecular

interaction[14,15,50]. On cellular simulation, talin rapidly localizes to the plasma membrane[17] and becomes activated to bind and activate integrin[14,15,50]. Thus, talin autoinhibition and activation allow the dynamic regulation of cell adhesion processes such as cell shape change and migration. Phosphatidylinositol-4,5-bisphosphate (PIP2) has been shown to act as a talin activator[16,50,51] through an electrostatic 'pull–push' mechanism[14]. However, the specific ablation of PIP2-producing enzyme PIPKIγ in the integrin adhesion sites only partially and temporally impaired the talin-mediated cell adhesion[45], suggesting that there are additional pathways/factors to regulate the talin activity. One emerging pathway involves small GTPase Rap1 and its effector RIAM, which was shown to engage talin in the plasma membrane and promote the integrin activation and signaling[29,30,32,52-54].

RIAM contains a Ras association (RA) domain, a pleckstrin homology (PH) domain and a proline-rich region[29](see also **Figure 1.5**). RIAM RA binds to Rap1 that attaches to the membrane and RIAM PH domain also preferentially binds to PIP2 in vivo[31]. With this combined membrane-anchoring capacity, the Rap1/RIAM complex was shown to localize talin to the plasma membrane[30,32]. A specific N-terminal fragment (residue 7–30, referred to as RIAM-N hereafter) of RIAM was recently found to bind to talin[30], which plays a key role in the talin/RIAM interaction. Deletion and NMR studies have identified some RIAM-N-binding sites in talin-R in a manner analogous to vinculin binding to multiple sites of talin-R[55]. More recent crystallographic and biochemical analyses revealed two major RIAM-binding sites in talin-R, which clearly promote the talin recruitment[56]. However, the molecular basis as to how the RIAM/talin interaction ultimately triggers the integrin activation remains obscure.

In this study, we undertake a detailed mechanistic investigation of the talin–RIAM interaction. Through a systematic mapping analysis, we find surprisingly that RIAM not only binds to talin-R but also to a distinct site in talin-F3. We further discover that RIAM binding to this talin-F3 site sterically occludes inhibitory talin-R, thereby freeing up talin-F3 for binding to integrin. Combined with the functional data, our findings unravel a dual role of RIAM in recruiting as well as unmasking talin for spatiotemporal regulation of integrin activation and cell adhesion.

Results

A novel RIAM-binding site on talin-F3

The talin-binding site on RIAM was previously mapped to the 1–306 containing RA domain (RIAM-1–306) and further narrowed down to the N-terminal Leu-rich region 7–30 (RIAM-N)[30]. As mentioned above, RIAM-N was recently shown to recognize multiple sites in talin-R, suggesting that multiple RIAM molecules bind to a single talin[55,56] with primary sites located in talin-R3 and talin-R8, respectively[56]. Consistently, we also observed that RIAM-1–306 binds to multiple fragments of talin-R (data not shown). Surprisingly, when we expanded our analysis to include talin-H, we found that, while RIAM-1–306 had no interaction with talin-F0F1 (**Figure 2.1A**), it specifically bound to talin-F2F3 (**Figure 2.1B**). Glutathione S-transferase (GST) pull-down experiments confirmed the RIAM/talin-H interaction (**Figure 2.2 A**). NMR-based chemical shift mapping analysis further narrowed down the RIAM-1–306 binding to talin-F3 (**Figure 2.2B**). Isothermal titration calorimetry (ITC) experiment revealed a 1:1 binding at a moderate affinity with K_d ~ 32 μM between talin-F2F3 and RIAM-1–306 (**Figure 2.2C**). Since both talin-H and full-length RIAM are membrane associated[14,16,43] once being activated, we anticipate the K_d between talin-H and intact RIAM to be much stronger in the presence of cell membrane. A similar case was recently shown for the interaction between talin-H and integrin β3 CT with K_d being ~ 438 μM in the absence of membrane[57] but becoming ~0.86 μM in the presence of membrane that binds to both talin-H and β3 CT[58].

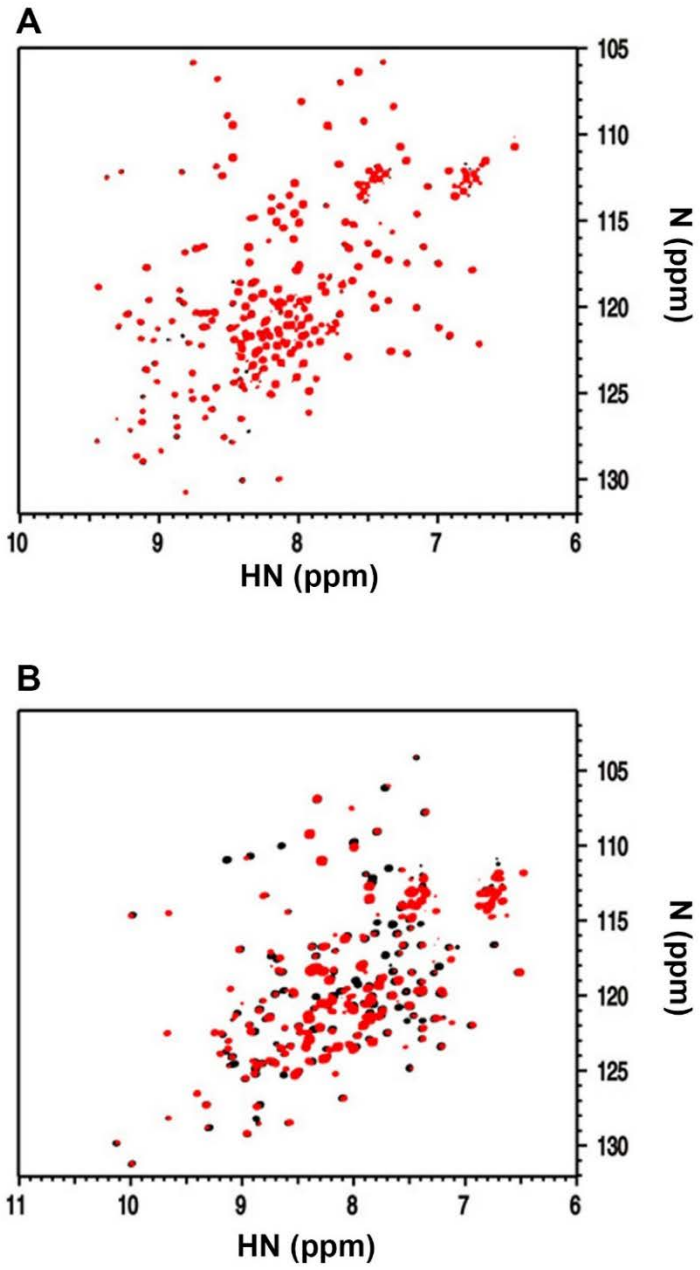

Figure 2.1 RIAM interacts with talin-F2F3 but not talin-F0F1

(A) The HSQC spectra of 40 μM ^{15}N-labeled talin-F0F1 in the absence (black) and presence of 80 μM RIAM 1-306 (red). (B) The HSQC spectra of 40 μM ^{2}H, ^{15}N-labeled talin-F2F3 in the absence (black) and presence of 80 μM RIAM 1-306 (red).

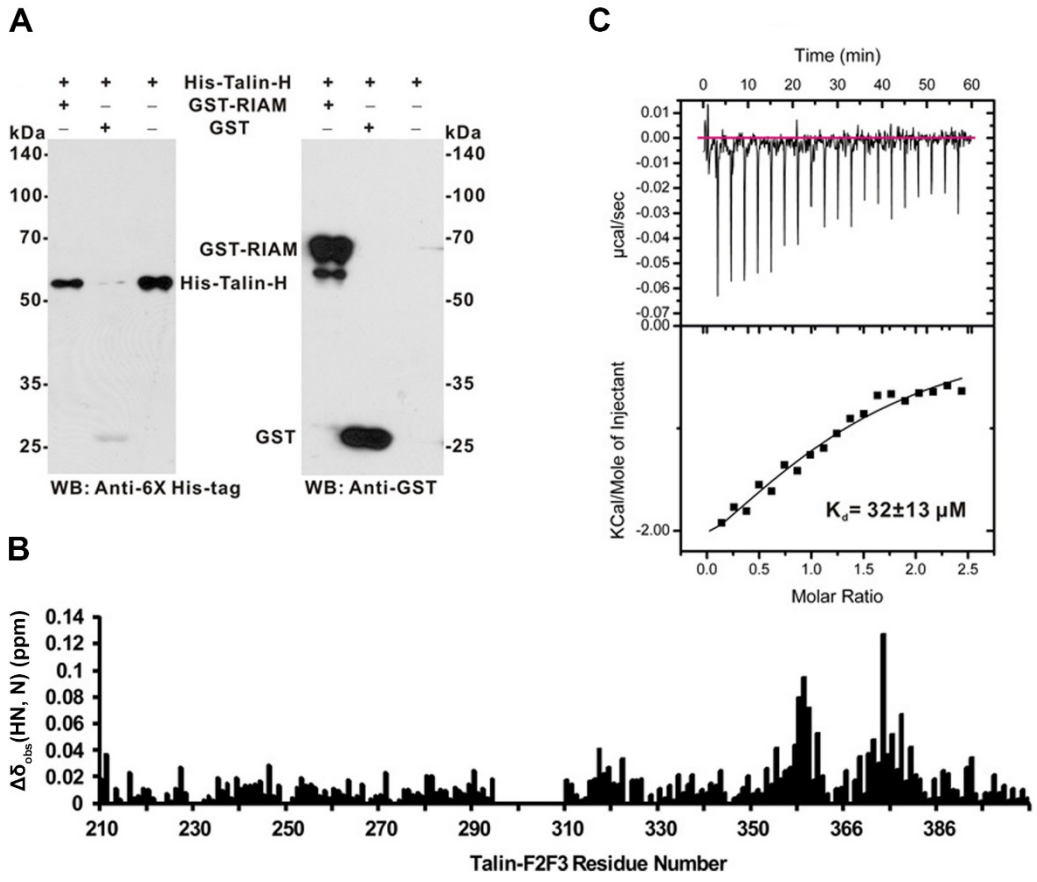

Figure 2.2 RIAM specifically interacts with talin-H F3 domain

(A) GST pull down assay to show that GST-RIAM 1-306 but not GST control interacts with talin-H. (B) The profile of chemical shift changes of 40 µM ^{2}H, ^{15}N-labeled talin-F2F3 induced by 80 µM RIAM 1-306. (C) The affinity between talin-F2F3 and RIAM 1-306 measured by ITC.

RIAM-N binds next to integrin site in talin-F3 to occlude talin-R9

Since previous studies have indicated that RIAM-N is the primary binding segment of talin[30], we further examined the RIAM-N binding to talin-F2F3 as compared with RIAM-1–306. Talin-F2F3 underwent smaller chemical shift changes but with the same spectral perturbation pattern by RIAM-N as that by RIAM-1–306 (**Figure 2.3A**), suggesting that RIAM-N plays a predominant role in the RIAM/talin-F3 interaction.

Dr. Jun Yang in our lab solved the solution structure of RIAM-N binding to talin-F3 (**Figure 2.3B**). In the complex, M11, L15, L16, M19 and L22 of the RIAM-N helix forms a hydrophobic interface with talin-F3 L325, A360, T367 methyl, methylenes of R358, S362, and S379, and side-chain of Y377 (**Figure 2.3B**). Superposition of the complex structure with the crystal structure of the autoinhibited talin-F3/talin-R9 complex[14] shows clearly that RIAM-N would sterically interfere with the autoinhibitory interface of talin (**Figure 2.4A**). This was also supported by a pull-down experiment in which RIAM competes with talin-R9 for binding to talin-F3[59]. Interestingly, by superimposing the talin-F3/RIAM-N structure with the crystal structure of talin-F3/integrin-β1 CT complex, we found that RIAM binds to a region that is next to the binding site of integrin-β1D CT on talin-F3 (**Figure 2.4B),** suggesting that RIAM sterically occludes talin-R9 and further may promote the β CT binding to talin-F3. Indeed, Dr. Jun Yang and Dr. Koichi Fukuda in our lab experimentally demonstrated that talin-F3, RIAM-N and integrin β3 CT could form ternary complex by both NMR HSQC analyses and GST-pull down assays[59]. These data thus indicate that RIAM competes with the autoinhibitory talin-R9 for binding to talin-F3 and thereby promotes the unmasking of talin to allow its binding to integrin.

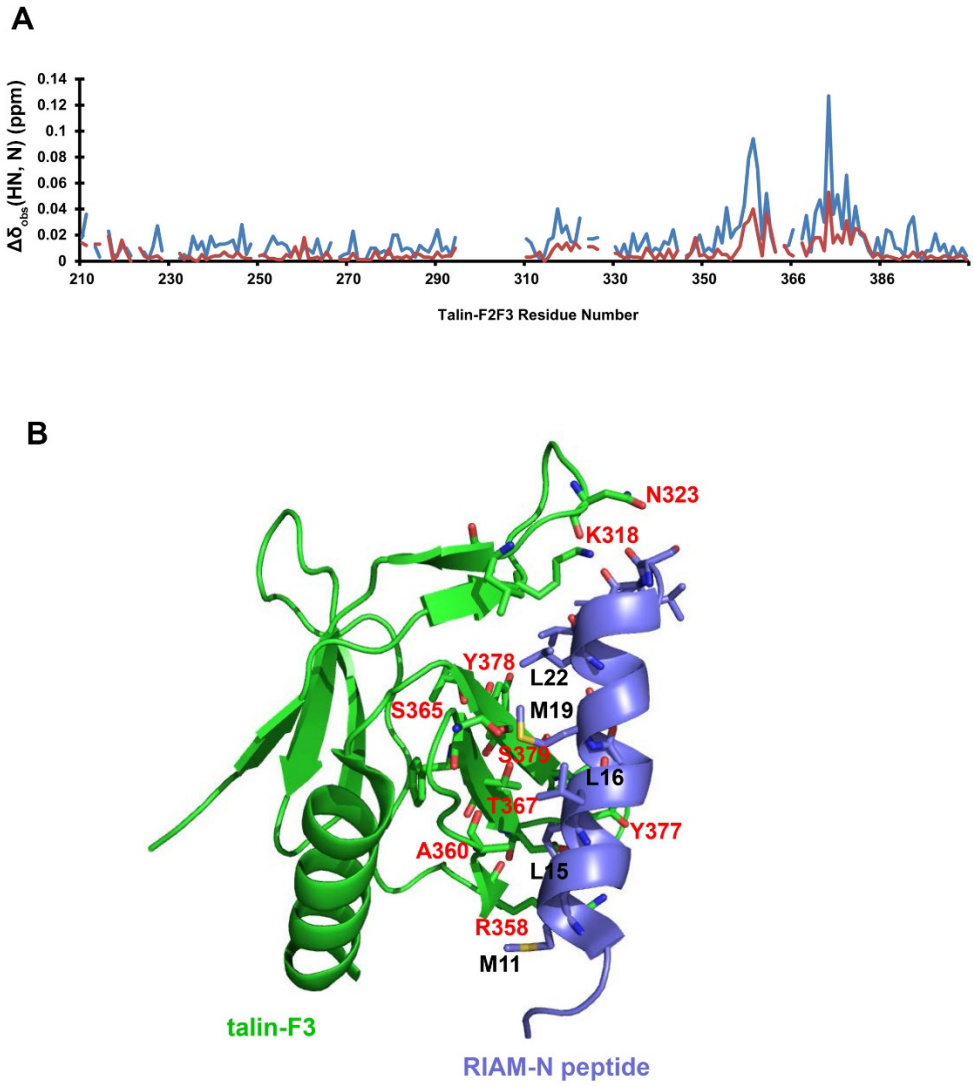

Figure 2.3 The interface between talin-F3 and RIAM-N

(A) Comparison of the chemical shift perturbation of ^{15}N-labeled talin-F2F3 by RIAM-1-306 (light blue) and RIAM-N (salmon), showing similar perturbation patterns. (B) The complex structure (shown in cartoon representation) of talin-F3 (green) and RIAM-N (blue) with the lowest energy (PDB code: 2MWN). Critical interface residues of talin-F3 and RIAM-N within the cut-off of 4 Å are labeled in red and black respectively.

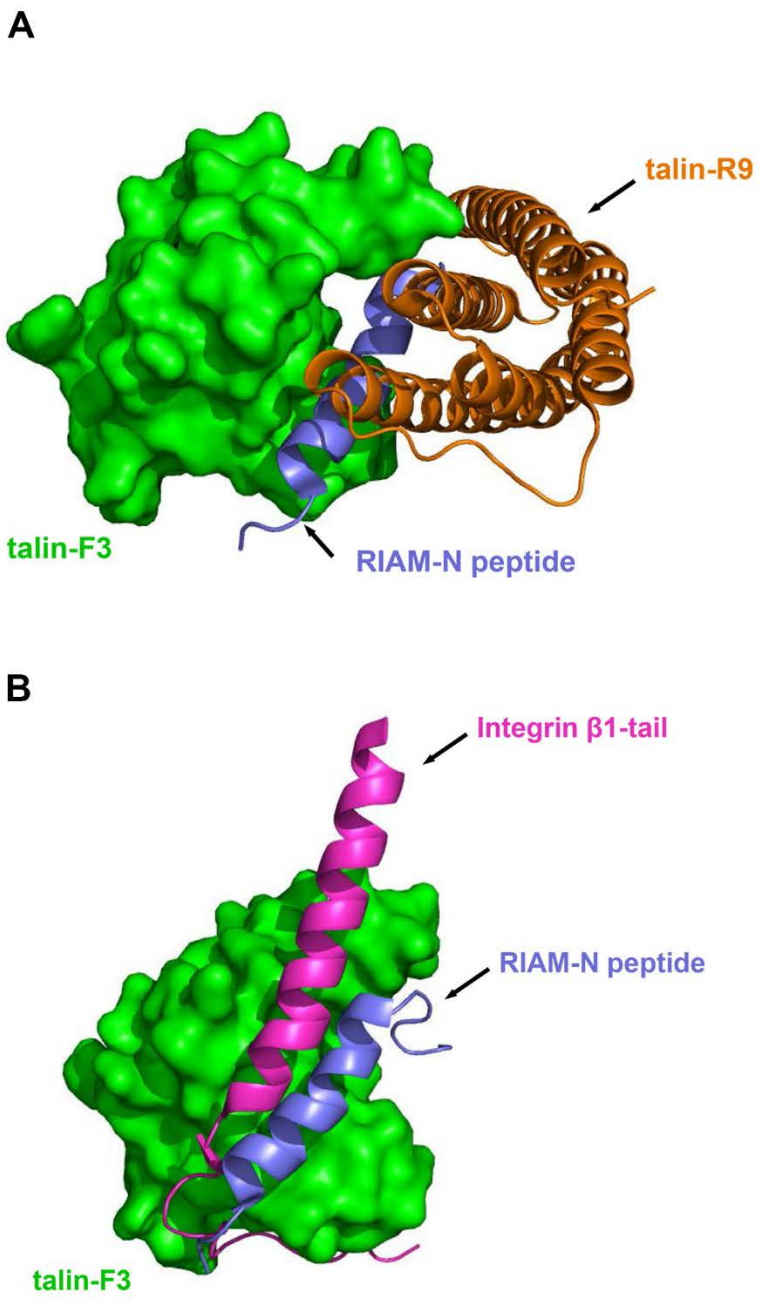

Figure 2.4 RIAM-N occludes talin-R from binding to talin-F3 and may otherwise promote integrin binding to talin-F3

(A) A structural model showing that RIAM-N (blue, cartoon representation) competes with talin-R (cyan, cartoon representation) for talin-F3 (green, surface representation)

binding. The model was derived by superimposition of talin-F3/RIAM-N (NMR solution structure with a PDB code of 2MWN) and talin-F2F3/talin-R9 (X-ray crystal structure with a PDB code of 4F7G) complex structures. (B) A structural model showing that talin-F3 (green, surface representation), RIAM-N (blue, cartoon representation) and integrin β-tail (magenta, cartoon representation) may form ternary complex. This model was derived by superimposition of talin-F3/RIAM-N (NMR solution structure with a PDB code of 2MWN) and talin-F2F3/integrin-β1D CT (X-ray crystal structure with a PDB code of 3G9W) complex structures.

RIAM promotes talin unmasking to activate integrin

Next we decided to functionally evaluate the importance of the RIAM binding to talin-F3. First, we co-expressed talin-H or full-length talin (talinFL) with RIAM, which revealed that while RIAM has no effect on the talin-H-mediated integrin activation, it substantially enhanced talinFL-mediated integrin activation, demonstrating that the talinFL activity depends on RIAM (**Figure 2.5A**). Second, we made talin binding-defective RIAM mutant (M11E/F12E/L15E/L16E, RIAM-4E), which failed to induce talinFL-mediated integrin activation, further demonstrating that the RIAM binding to talinFL controls the talin activity (**Figure 2.5A**). However, since the 4E mutations abolish the RIAM binding to both talin-H and talin-R, this experiment cannot distinguish the importance of RIAM binding to talin-H versus its binding to talin-R. Two possible mutagenesis approaches can be performed to address this issue: (a) point mutation in talin-H to abolish its binding to RIAM but retain the talin-R binding to RIAM; (b) point mutation in talin-R to abolish its binding to RIAM while retaining the talin-H binding to RIAM. Because the RIAM-binding site on F3 of talin-H resides in the talin autoinhibitory interface and is also very close to the integrin-binding site (**Figure 2.3 B and 2.4B**), approach (a) would cause complicated effects including unmasking of talin versus reduced talin-H binding to RIAM and/or integrin. We therefore chose (b) by generating a structure-based talinFL mutant where V871 and V1540 in talin-R were both substituted into Y (talinFL-DM) to diminish the talin-R binding to RIAM[56]. **Figure 2.5B** confirms that while purified talin-R1–9, which contains the major RIAM-binding sites[56], binds to RIAM-1–306, the V871Y/V1540Y double mutations abolished the binding. As a result, purified talinFL-DM binds to RIAM-1–306 much more weakly than to wild-type (WT) talinFL

(**Figure 2.5B**). Remarkably, while talinFL-DM is equally inactive as WT talinFL, which is consistent with the inactive talin structure where both V871 and V1540 are outside the talin autoinhibitory domain talin-R9[14], the co-expression of talinFL-DM with RIAM still potently induced the integrin activation as the co-expression of WT talinFL with RIAM (**Figure 2.5C**). These data strongly indicate that while the RIAM/talin-R interaction promotes the talin recruitment to membrane, it is the RIAM/talin-H interaction that ultimately leads to integrin activation by unmasking talin.

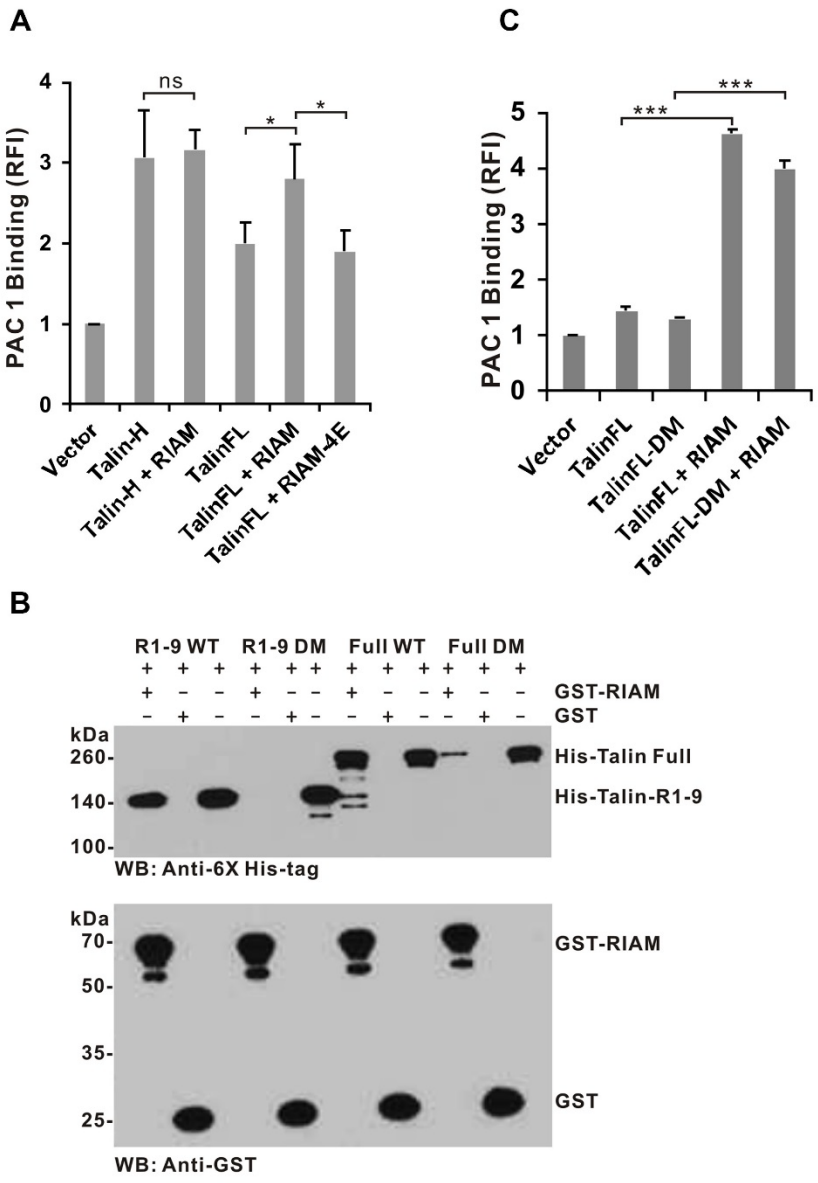

Figure 2.5 RIAM promotes talin unmasking to activate integrin

(A) Effects of integrin activation by talin in the presence of RIAM and talin-binding defective RIAM M11E/F12E/L15E/L16E mutant (RIAM-4E). ns, not significant, *, significant with $p<0.05$. The comparison clearly suggests that RIAM significantly enhanced the activation of full length talin (talinFL + RIAM vs. talinFL) but not talin-H ($p>0.79$, Talin-H + RIAM vs Talin-H), suggesting the role of RIAM in unmasking

autoinhibited talin. The 4E mutation impairs the RIAM binding to talin and substantially reduces its activation capacity (talinFL + RIAM-4E vs. talinFL + RIAM). (B) GST-based pull down assay showing that GST-RIAM 1-306 binds to talin-R1-9 but not talin-R1-9 DM (V871Y/V1540Y) mutant. As a result, GST-RIAM 1-306 binds to talinFL but only weakly to talinFL DM. The residual binding of talinFL-DM to RIAM may be due to talin-H/RIAM interaction as shown in **Figure 2.2A**. (C) Despite the loss of RIAM binding to talin-R, inactive talinFL-DM is still potently activated by RIAM that binds and unmasks talin-H, leading to enhanced integrin αIIbβ3 activation. ***, significant with $p<0.001$. The data in (A) and (C) are presented as mean ± S.E.M. from three independent experiments, and the statistical significance was assessed using t-test. (The data of panel A and C were provided by Dr. Jamila Hirbawi.)

Discussion

In this study, we have uncovered a novel regulatory mechanism of talin by RIAM. Specifically, we have shown that RIAM binds to a previously unrecognized site in talin-F3 near that for integrin binding. Using a combination of structural, biochemical and functional approaches, we further showed that the RIAM/talin-F3 interaction promotes the conformational opening of latent talin, leading to the binding and activation of integrin. By binding to the membrane-associated Rap1 via the RA domain and PIP2 via the PH domain, RIAM was previously suggested to promote the membrane co-localization of talin[30-32,56]. However, our results now suggest that RIAM has an additional key role in conformationally activating talin. The multiple binding sites of RIAM on talin-R may allow a strengthened RIAM binding to talin, thus leading to effective RIAM/talin co-localization to the membrane (**see also Figure 4.1A**). However, it is the RIAM-N interaction with talin-H that sterically repels talin-R and leads to the talin activation (**see also Figure 4.1A**). Such steric occlusion mechanism is distinctly different from the previously described 'pull–push' activation mechanism of talin by PIP2[14]. The presence of this RIAM pathway also explains why the ablation of the PIP2 pathway by deleting PIPKIγ at the integrin adhesion sites only partially impaired the talin-mediated cell adhesion. On the other hand, since RIAM binds to PIP2 in vivo[31], it is possible that the RIAM and PIP2 pathways may converge at the membrane surface in certain cellular conditions to orchestrate the potent talin activation (**see also Figure 4.1**).

How is the RIAM/talin interaction regulated after the integrin activation? As mentioned above, RIAM was found to bind to the overlapping sites in talin-R as vinculin—a major focal adhesion adaptor. Structural and functional analyses revealed that

vinculin can displace RIAM as a switch for promoting the maturation of focal adhesions and its turnover[55,60]. Thus, after integrin activation, RIAM may be dissociated from talin by vinculin, triggering the focal adhesion reassembly. RIAM was also shown to regulate the subcellular localization of PLC-gamma1 that dephosphorylates PIP2 to PIP[17], which would in turn weaken/dissociate the membrane association with talin and RIAM, respectively. Since RIAM also binds to VASP[53]—a major regulator for actin assembly, RIAM may be involved in a more complex network of cytoskeleton remodeling including talin, vinculin and VASP, which all bind to F-actin. More detailed investigation is necessary to elucidate how RIAM is spatiotemporally regulated to mediate dynamic integrin signaling and its linkage to cytoskeleton.

In conclusion, we have obtained important insights into the RIAM function in regulating the integrin-mediated cell adhesion. We showed that RIAM can induce conformational opening/activation of talin, which may be also coupled with the well-known PIP2-mediated pathway for the talin activation. The finding not only defines a novel mechanism of talin activation by RIAM but also highlights how talin is under the dynamic control of a multi-faceted regulatory system to allow complex integrin signaling events, actin cytoskeleton reorganization, cell spreading and migration.

Materials and Methods

Protein preparation and purification

Mouse full-length talin, talin-R1-R9 (486-1848), or mouse talin-H (1-429) was subcloned into a pET28t vector with an N-terminal His tag. RIAM (residues 1–306) was subcloned into a pGEX4T-1 vector (GE Healthcare) with an N-terminal GST tag. Talin-F0F1 (1–205), or talin-F2F3 (206–405) was subcloned into a pET30a vector (EMD Millipore) with an N-terminal His tag. Double mutations (V871Y, V1540Y) of full-length talin and talin-R1-R9 were obtained by using QuickChange multi-site directed mutagenesis Kit (Agilent Technologies). Note that pET28t is a modified pET28a vector where the thrombin cleavage site is substituted with a TEV protease cleavage site.

Above constructs were transformed into E.*coli* BL21 (DE3) strain (New England Biolabs) for Protein expression. Proteins with fusion tag were purified by using either GST or nickel gravity column. Proteins were always purified by size-exclusion chromatography using either Superdex-75 (16/60), Superdex-200 (16/60) or Superose-6 (10/300) (GE Healthcare) in the final step. ^{15}N and/or ^{13}C isotope labelling was achieved by employing $^{15}NH_4Cl$ (1.1 g l^{-1}) and/or ^{13}C glucose (3 g l^{-1}) as the sole nitrogen and carbon sources in the minimal medium. ^{2}H isotope labelling was achieved by using ^{2}H-glucose (3 g l^{-1}) as the sole carbon source and preparing the minimal medium in 99.8% D_2O.

NMR spectroscopy

All NMR experiments were performed at 25 °C on Bruker Avance 600 or 900 MHz spectrometers equipped with cryogenic triple resonance probes and shielded z-gradient units. NMR samples were prepared in buffer containing 50 mM NaH_2PO_4/Na_2HPO_4 (pH 6.8), 50 mM NaCl, 2 mM NaN_3, 1 mM DSS, and 5% D_2O (v/v). The weighted chemical shift changes of amide proton and nitrogen were calculated using the equation: $\Delta\delta_{obs[HN,N]}=([\Delta\delta_{HN}W_{HN}]^2+[\Delta\delta_N W_N]^2)^{1/2}$, where W_{HN} (1.0) and W_N (0.154) are weighting factors based on the gyromagnetic ratios of ^1H and ^{15}N.

Isothermal titration calorimetry (ITC) experiment

ITC experiments were performed using a Microcal iTC 200 system at 25 °C. The buffer contained 50 mM NaH_2PO_4/Na_2HPO_4 (pH 6.8), and 50 mM NaCl. 380 μM His-talin-F2F3 in the syringe (~40 μl) was injected 20 times in 2.0 μl aliquots into the sample-cell (~200 μl) containing 30 μM GST-RIAM-1–306 or GST or buffer only. Data were analyzed by fitting to a single-site binding model with Origin Software.

GST pull-down assay

Purified GST-fused RIAM (1-306) or GST (~ 20 μg each) was first immobilized on 15 μl of glutathione-Sepharose 4B resin (beads) and equilibrated in the binding buffer containing 25 mM Tris-HCl (pH 7.5), 150 mM NaCl, 1 mM DTT, 0.1% Nondiet, P-40 and supplemented with complete EDTA-free Protease Inhibitor (Roche, Indianapolis, IN). The desired His-tagged proteins were then added in and incubated with beads for 2 h at 4 °C. The beads were washed by 500 μl binding buffer for three times, and then subjected

to be denatured by adding 35 μl 2xSDS loading buffer and boiling for 5 min. After centrifuge down, supernatants were analyzed by western blotting.

For western blotting, samples were resolved by SDS-PAGE and then transferred onto a 0.45 μm PVDF membrane (Millipore). The membrane was blocked with 5% non-fat milk in TBST buffer overnight at 4 ℃. After that, the membrane was incubated with primary antibody (6xHis epitope tag antibody, Catalog# MA1-21315, Thermo Fisher Scientific) at room temperature (RT) for 3 hours and then incubated with HRP-conjugated secondary antibody (Anti-mouse IgG, HRP linked Antibody, Catalog# 7076, Cell Signaling Technology) at RT for 1 hour. The blots were detected by Pierce ECL Western Blotting Substrate (Thermo Fisher Scientific). All pull down experiments were performed in triplicate independently.

Integrin activation assay

Mouse full-length talin-1, talin-1 DM (V871Y/V1540Y) or talin-H was subcloned into a pEGFP-N1 vector (Clontech Lab, Mountain View, CA) encoding a C-terminal EGFP tag. Full-length RIAM fused to EGFP was a kind gift from Dr. Frank Gertler at MIT and was used to subclone RIAM-1–306 and the RIAM mutant into EGFP or dsRED vector, (pDsRed-Express-N1, Clontech Lab, Mountain View, CA). RIAM was also subcloned into a pCGN vector with an N-terminal HA tag.

The effects of full-length talin, talin-H and RIAM on integrin activation were analyzed using CHO cells stably expressing integrin $\alpha_{IIb}\beta_3$ and an activation-specific anti-αIIbβ3 mAb (PAC1). For Figure 2.5A, mouse GFP talin1 alone or together with dsRED

RIAM was transiently transfected into CHO cells with stably expressed integrin αIIbβ3 using Lipofectamine 2000 (Invitrogen). PAC1 binding to the different transfectants (EGFP and dsRed double-positive cells) was analyzed by flow cytometry after incubating the transfected cells with anti-PAC1 mAb. Integrin activation was expressed in terms of relative median fluorescence intensities (MFI) by defining the basal PAC1 binding to WT $\alpha_{IIb}\beta_3$ cells positive for EGFP and DsRed as 1.0. For Figure 2.5C, CHO cells were co-transfected with GFP-TalinFL or GFP-TalinFL–DM with HA-RIAM and harvested 24 hours after transfection. GFP positive cells were gated on to detect PAC-1 binding. The relative MFI of each transfectant was obtained by normalizing to that of the GFP empty vector transfectant, where MFI was defined as 1.0. The data were represented by the means±S.E.M. and the unpaired t-test was performed to calculate the *p* value using GraphPad software.

Chapter 3 Structure of Rap1b Bound to Talin Reveals a Pathway for Triggering Integrin Activation

The study of this chapter was published in

Liang Zhu[#], Jun Yang[#], Thomas Bromberger[#], Ashley Holly, Fan Lu, Huan Liu, Kevin Sun, Sarah Klapproth, Jamila Hirbawi, Tatiana V. Byzova, Edward F. Plow, Markus Moser, and Jun Qin. Structure of Rap1b bound to talin reveals a pathway for triggering integrin activation. *Nat Commun*. 2017, 8(1):1744.

Abstract

Activation of transmembrane receptor integrin by talin is essential for inducing cell adhesion. However, the pathway that recruits talin to membrane, which critically controls talin's action, remains elusive. Membrane-anchored mammalian small GTPase Rap1 is known to bind talin F0 domain but the binding was shown to be weak and thus hardly studied. Here we show structurally that talin F0 binds to human Rap1b like canonical Rap1 effectors despite little sequence homology, and disruption of the binding strongly impairs integrin activation, cell adhesion, and cell spreading. Furthermore, while being weak in conventional binary binding conditions, the Rap1b/talin interaction becomes strong upon attachment of activated Rap1b to vesicular membranes that mimic the agonist-induced microenvironment. These data identify a crucial Rap1-mediated membrane-targeting mechanism for talin to activate integrin. They further broadly caution the analyses of weak protein-protein interactions that may be pivotal for function but neglected in the absence of specific cellular microenvironments.

Introduction

The adhesion of cells to extracellular matrix (ECM) is essential for regulating a variety of physiological or pathological responses such as platelet aggregation, blood clotting, stroke, wound healing and cancer metastasis. Such adhesion critically depends upon integrins, a class of cell surface receptors that are (α/β) heterodimers with each subunit containing a small cytoplasmic tail (CT), a transmembrane segment, and a large extracellular domain. In unstimulated cells, integrin adopts an inactive conformation with low affinity for ECM ligands (e.g. collagen, fibronectin and laminin) but upon agonist stimulation, integrin CT is bound by intracellular proteins, in particular talin and/or kindlin, which trigger global conformational change of the extracellular domain to acquire high affinity for ECM ligand and initiate firm adhesion. This process, widely regarded as inside-out signaling or integrin activation, has been the central topic of cell adhesion research for nearly three decades[2,5-7,61,62]. Extensive efforts have been focused on investigating the mechanism of integrin activation by talin — a major cytoskeletal protein comprising an N-terminal head domain (talin-H) and a C-terminal rod domain (talin-R). Talin-H contains four subdomains F0, F1, F2, and F3 in which F1-F3 constitutes a so-called FERM (4.1/ezrin/radixin/moesin)-like domain. Talin-R is made up of 13 consecutive helical bundles followed by a C-terminal dimerization domain (also see **Figure 1.3**). Intact talin adopts an inactive conformation where the major integrin binding site located in talin-H F3 domain is masked by talin-R (autoinhibition)[14,15,50,63]. Talin may be unmasked *via* multiple mechanisms to bind integrin β CT[14,16,50,59,64]and trigger the receptor activation[42,48,49,65].

While a great deal has been learned about talin, a fundamental issue still remains unresolved: how is cytoplasmic talin recruited to plasma membrane – a crucial step for talin to bind and activate integrin? A previous dogma, largely derived from studying prototypic integrin $\alpha_{IIb}\beta_3$ from platelets, is that agonist stimulation activates small GTPase Rap1 on membrane to recruit an effector called RIAM that in turn recruits talin[7,47]. However, while both Rap1 and talin are highly abundant[35], RIAM is present at very low levels in platelets with no other homologs detected[34]. More importantly, mice lacking RIAM are viable and the platelet functions including the $\alpha_{IIb}\beta_3$ activation are totally normal[34,66,67]. By contrast, Rap1 and talin are both essential for integrin activation[4-5,18]. For example, ablation of the Rap1 isoform Rap1b severely impairs $\alpha_{IIb}\beta_3$ activation and platelet aggregation[23] – defects that were also observed in talin knock-out mice [68,69]. These observations strongly suggest a RIAM-independent engagement between Rap1 and talin to regulate integrin activation. Interestingly, previous studies reported a direct interaction between Rap1 and talin in mammals[70] and in Dictyostelium[71] but the affinity of the interaction was found to be low especially for that in mammals ($K_d \sim 0.14$ mM)[70]. Since weak protein-protein interactions are typically assumed to be non-specific and RIAM was widely regarded as a key bridge between Rap1 and talin, the Rap1/talin interaction was hardly studied at mechanistic level. Through comprehensive structural, biochemical, and cell biological analyses, we discovered that talin is actually a distinct effector of Rap1 that recruits talin to membrane and triggers integrin activation. We further found that while being weak in conventional binary binding assays, Rap1/talin interaction became strong when activated Rap1 was anchored to membrane that mimics the cellular condition. Our results thus uncover a mechanism of membrane-targeting of talin by Rap1 and also

highlight the importance of weak protein-protein interactions that may be neglected in the absence of specific cellular microenvironments.

Results

Rap1 recognizes talin F0 domain in a GTP-dependent manner

Rap1 is known to contain two highly homologous isoforms called Rap1a and Rap1b[72-75]. In this study, we choose to focus on examining the interaction between the platelet-rich Rap1b and talin-F0. Like other small GTPases, Rap1b exists in inactive (GDP bound) and active (GTP bound) states. We first used a highly sensitive NMR technique called heteronuclear single quantum coherence (HSQC)[76] to examine the Rap1b/talin-F0 interaction. **Figure 3.1A, B** show that Rap1b loaded with GTP analog GMP-PNP induced residue-specific chemical shift changes of ^{15}N-talin-F0. Inactive Rap1b loaded with GDP also binds to talin-F0 but at weaker affinity as evidenced by smaller chemical shift changes than those with GMP-PNP (**Figure 3.2A**). Thus, talin-F0 binds favorably to the active form of Rap1b but, as shown in **Figure 3.2B**, the binding affinity is quite low (K_d ~162 μM) as previously concluded[70]. On the other hand, talin-F0 does not bind H-Ras (**Figure 3.3A**) that is near 90% homologous in terms of binding interface (overall similarity is ~76%) to Rap1b (**Figure 3.3B**), suggesting that despite being weak, the talin-F0/Rap1b interaction is specific. To further investigate the specificity of Rap1b/talin-F0 interaction, we examined the Rap1b binding to F0 domain of another integrin activator kindlin-2 that is homologous to talin-H (**Figure 3.4A**)[77], but no interaction was detected (**Figure 3.4B**). Since talin-H contains FERM domain (F1-F3) prior to F0 and F1-F2 of KRIT1 FERM domain was shown to bind Rap1b[78], we also wondered if F1-F2 of talin FERM would be

involved in binding to Rap1b. However, **Figure 3.5** shows that Rap1b does not interact with talin FERM F1-F2. Overall, these data suggest that Rap1b engages with talin-F0 in a highly specific manner. Interestingly, NMR (**Figure 3.6A, B**) and GST pull-down (**Figure 3.7**) experiments revealed that active Rap1b also binds talin-H and full-length talin in the same manner as to talin-F0. Given that full-length talin is autoinhibited with F0 being unmasked[50], these data suggest that active Rap1b specifically recognizes the F0 domain of resting talin.

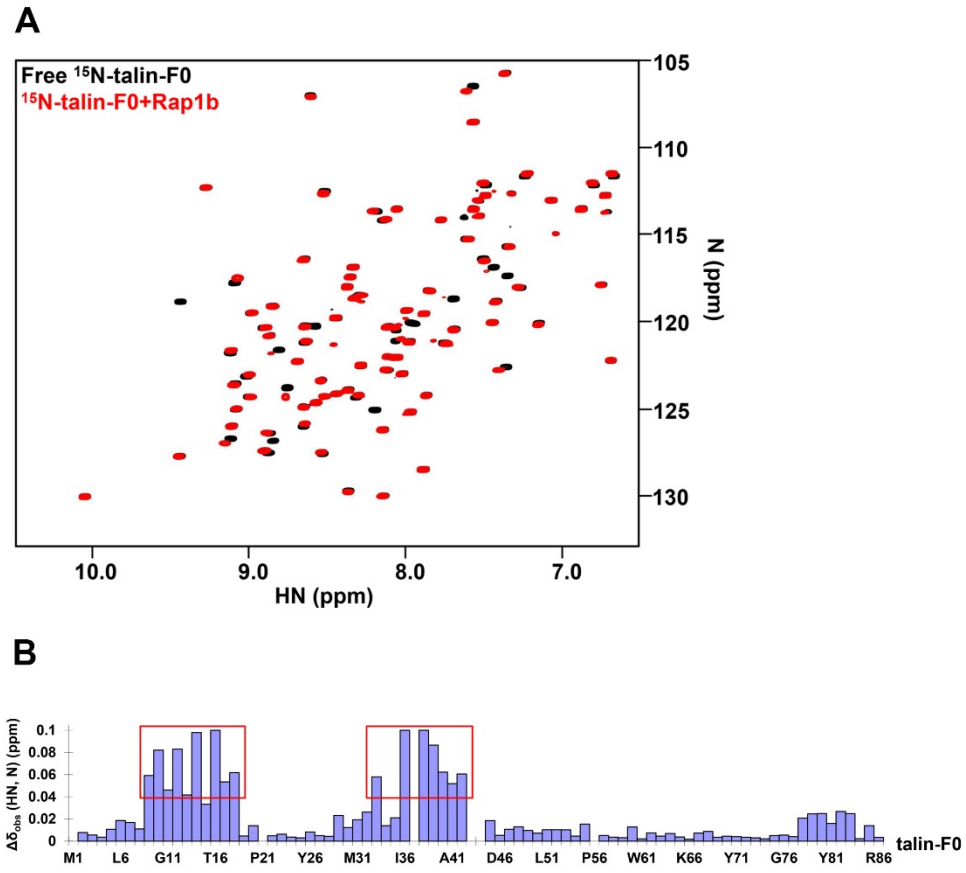

Figure 3.1 Rap1b induces residue-specific chemical shift changes of ^{15}N-labeled talin-F0

(A) The HSQC spectra of 50 μM ^{15}N-labeled talin-F0 in the absence (black) and presence of 125 μM GMP-PNP loaded Rap1b (red). (B) The profile of chemical shift changes of 50 μM ^{15}N-talin-F0 induced by 125 μM GMP-PNP loaded Rap1b. The chemical shift changes of completely broadened residues (T16, I36 and E38) were set to 0.1 ppm. The most perturbed regions are boxed in red.

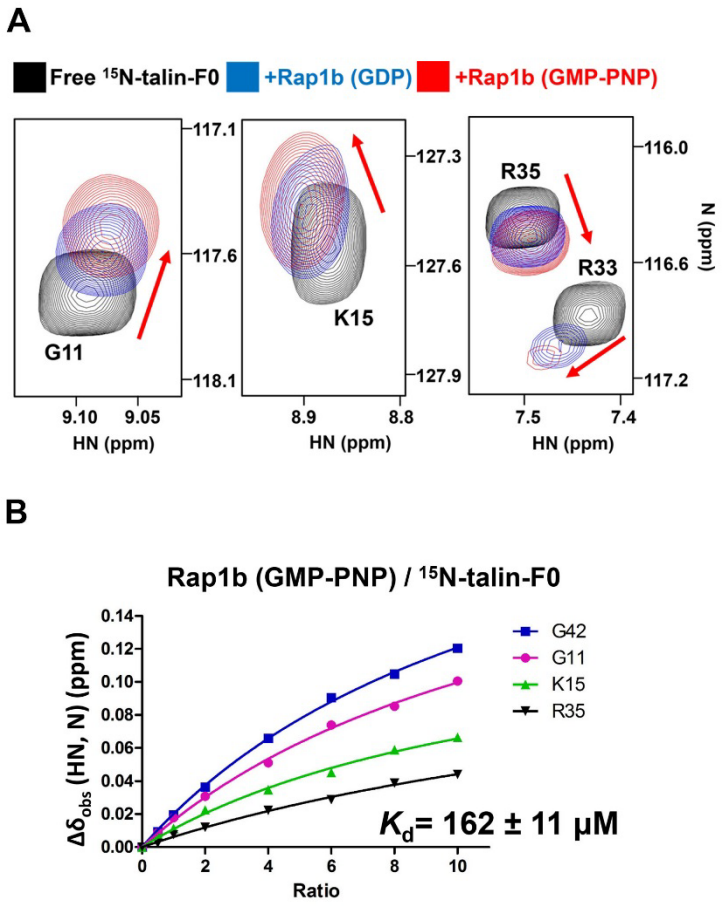

Figure 3.2 Rap1b/talin-F0 interaction is GTP dependent but of weak affinity

(A) The HSQC spectra (four representative residues were shown) of 50 μM ^{15}N-labeled talin-F0 in the absence (black) and presence of 125 μM GDP loaded Rap1b (blue) or GMP-PNP loaded Rap1b (red). Note that Rap1b-GDP induced the same overall pattern of chemical shift changes of ^{15}N-labeled talin-F0 as Rap1b-GMP-PNP does but with less peak shifts and broadenings, indicating a weaker affinity. (B) The Affinity of Rap1b (GMP-PNP)/talin-F0 interaction measured by HSQC titration.

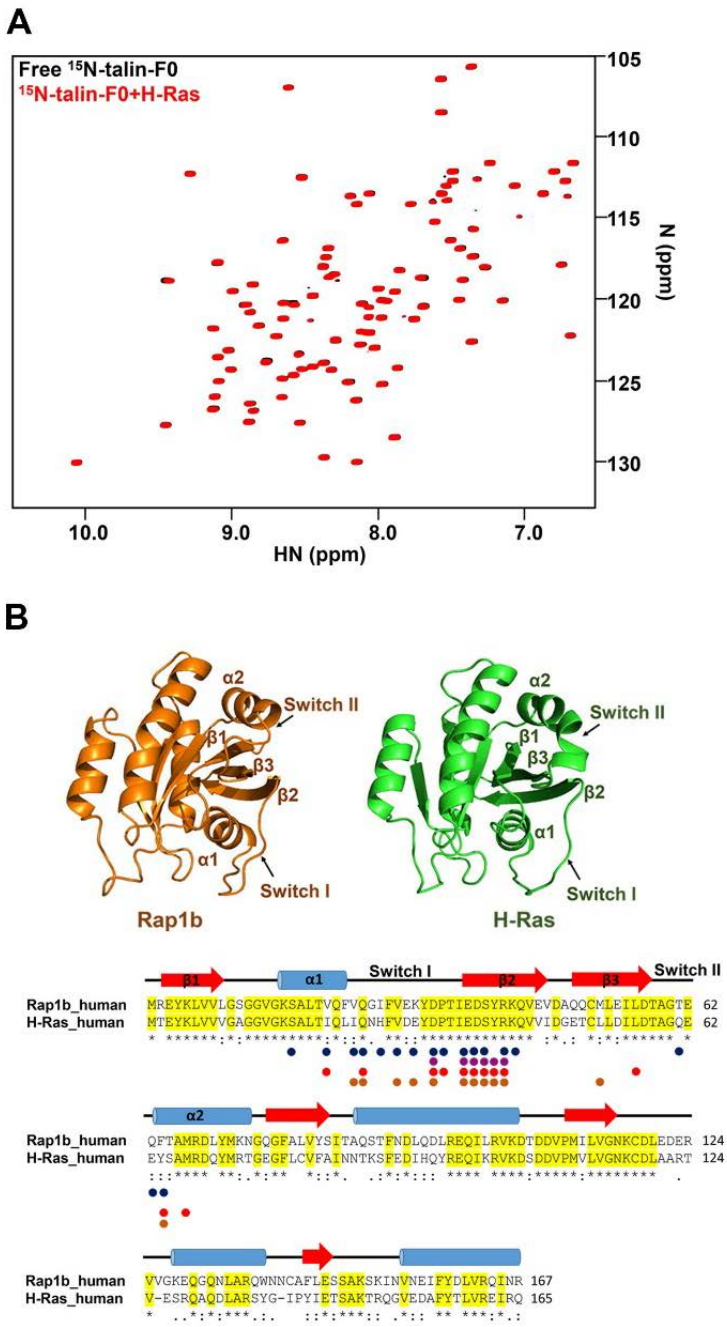

Figure 3.3 H-Ras does not interact with talin-F0

(A) The HSQC spectra of 50 μM ^{15}N-labeled talin-F0 in the absence (black) and presence of 125 μM GMP-PNP loaded H-Ras (red). (B) Sequence alignment of Rap1b and H-Ras. Identical residues are highlighted in yellow. (‘*’ indicates fully conserved residue, ‘:’

indicates residues with strongly similar properties, and '.' indicates residues with weakly similar properties. Residues of Rap1b involved in the binding interface (cut-off of 4 Å) with talin-F0, RIAM-RA, KRIT1-F1, and c-Raf1-RA are indicated in the figure with blue, purple, red and brown solid circles respectively.

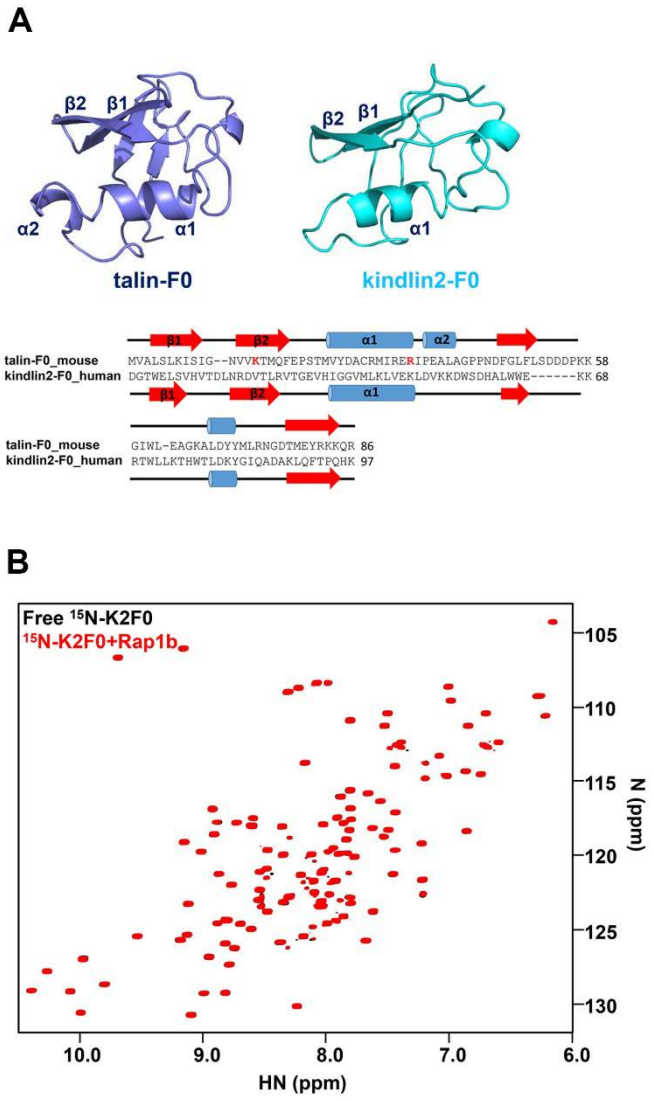

Figure 3.4 Kindlin2-F0 does not interact with Rap1b

(A) Structure-based sequence alignment of talin-F0 and kindlin2-F0. (B) The HSQC spectra of 50 μM ^{15}N-labeled kindlin2-F0 in the absence (black) and presence of 125 μM GMP-PNP loaded Rap1b (red).

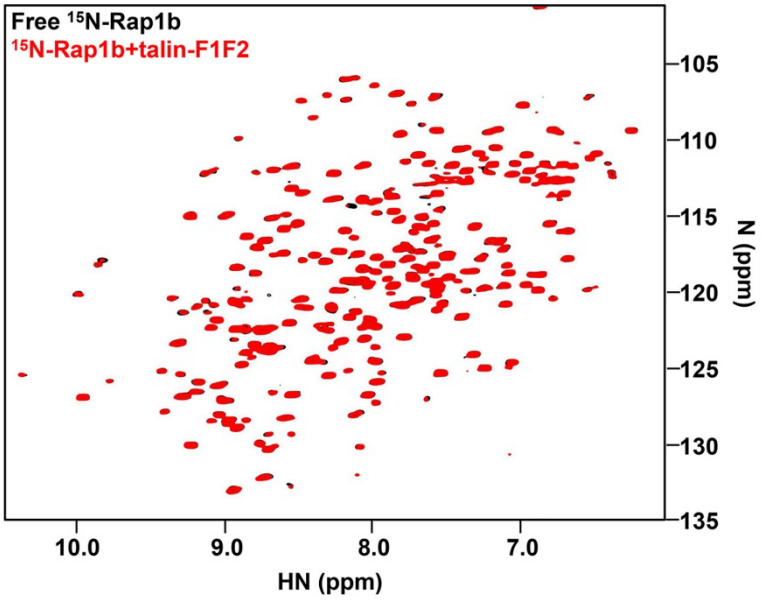

Figure 3.5 Talin-F1F2 does not interact with Rap1b

The HSQC spectra of 45 μM GMP-PNP loaded ^{15}N-labeled Rap1b (1-167) in the absence (black) and presence of 90 μM talin-F1F2 (red).

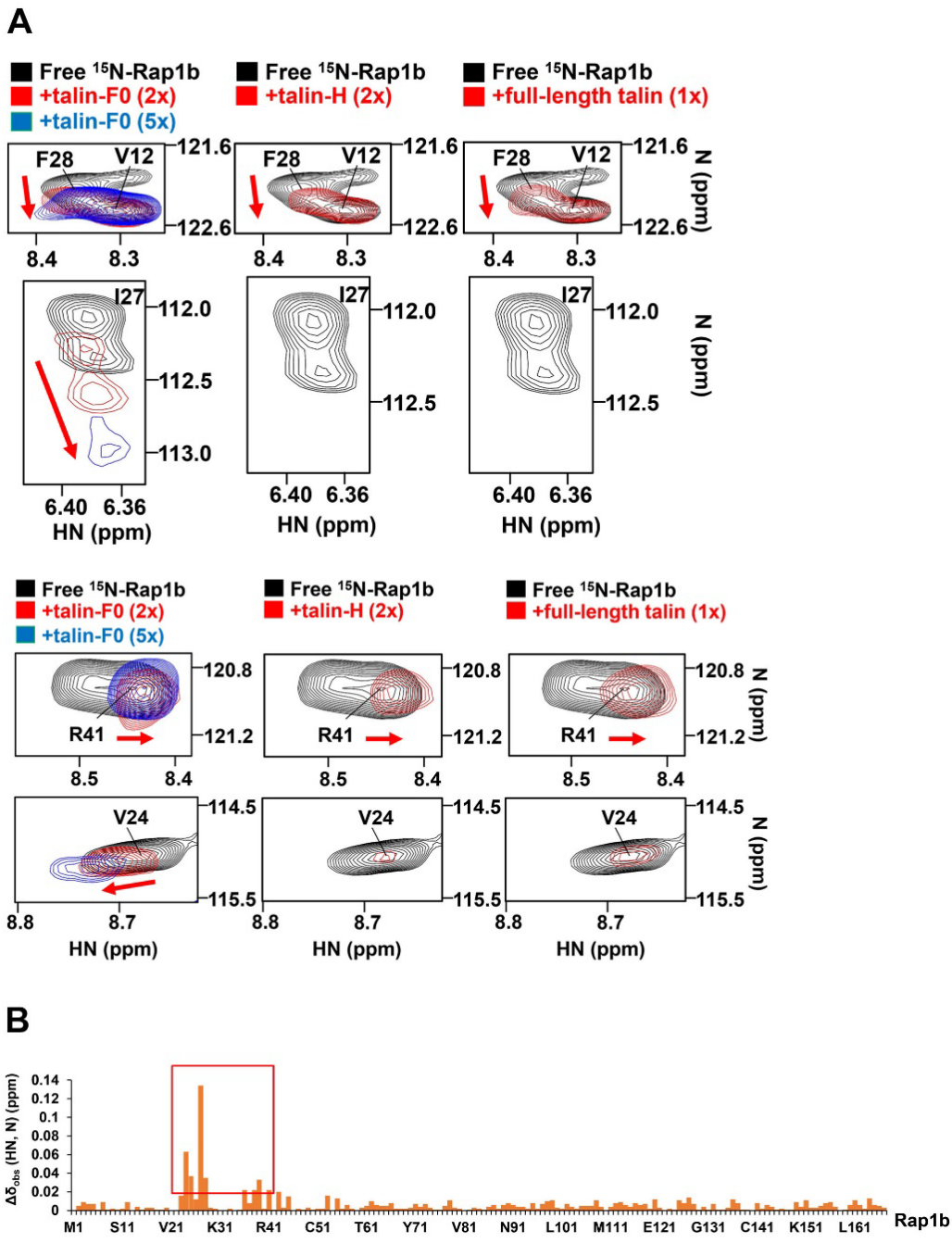

Figure 3.6 Talin-F0 induced residue-specific chemical shift changes of ^{15}N-labeled Rap1b

(A) The HSQC spectra (representative regions were shown) of 45 μM GMP-PNP loaded

^{15}N-labeled Rap1b (1-167) in the absence (black) and presence of 90 μM talin-F0 (red), 225 μM talin-F0 (blue), 90 μM talin-H (red) or 45 μM full-length talin (red). Note that the peaks of I27 and V24 were broadened in the presence of talin-H or full-length talin. (B) The profile of chemical shift changes of 45 μM GMP-PNP loaded ^{15}N-labeled Rap1b (1-167) induced by 225 μM talin-F0. The most perturbed region is boxed in red.

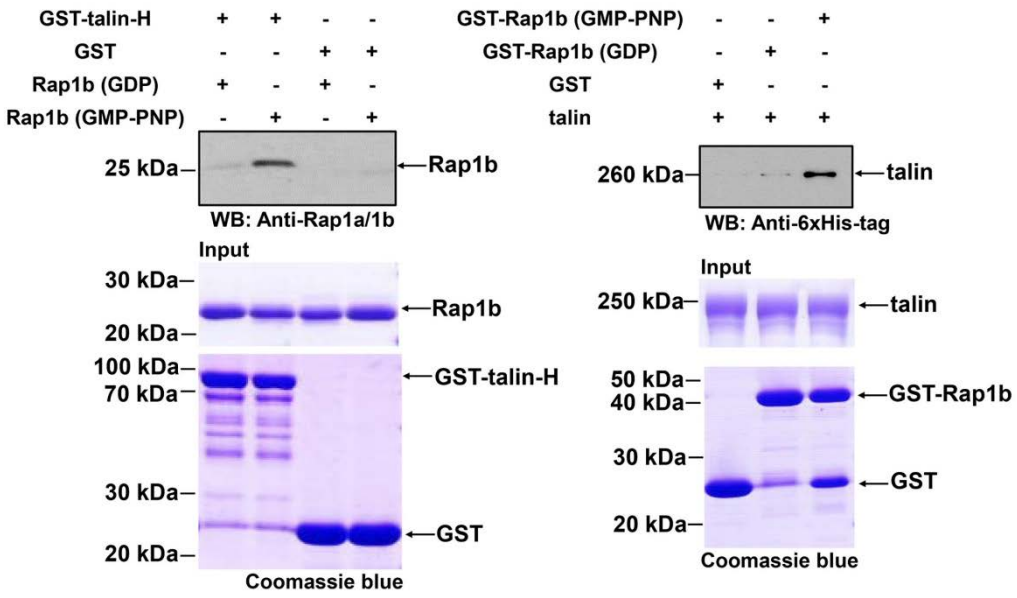

Figure 3.7 Rap1b recognizes F0 domain of talin in a GTP-dependent manner

GST pull down assays to show that Rap1b interacts with both talin-H and full-length talin in a GTP dependent manner.

Rap1b/talin interface exhibits distinct features

To understand how Rap1b recognizes talin, we decided to pursue the total structure of active human Rap1b (~20 kDa) in complex with talin-F0 (~10 kDa). Solution NMR is particularly suitable for structure determination of weak protein complexes[76]. By performing a series of 3D heteronuclear experiments using a combination of $^{1}H/^{15}N/^{13}C$-labeled and $^{2}H/^{15}N$-labeled samples, we were able to obtain nearly complete resonance assignment, 3422 intramolecular NOEs, and 78 intermolecular NOEs (**Figure 3.8**), which allowed determination of the complex structure (**Figure 3.9A** and **Table 3.1**). **Figure 3.9B** displays the cartoon diagram of the overall complex in which individual subunits, Rap1b and talin-F0, adopt a Ras family GTPase fold and an ubiquitin-like fold respectively, as expected. The ubiquitin-like fold of talin-F0 has similarity to Ras association (RA) domain present in known Rap1 effectors such as KRIT1, RIAM, and c-Raf1 (**Figure 3.9C**). However, despite this similar fold, talin-F0 has little sequence homology with these Rap1b RAs (**Figure 3.9D**) with only three positively charged residues being relatively conserved. The detailed Rap1b/talin-F0 interface is summarized in **Figure 3.10A-C** and compared with other Rap1b effectors (**Table 3.2**). Majority of the contacts in the Rap1b/talin-F0 complex are different from other Rap1b/effector complexes (**Table 3.2**) apparently due to the scant sequence homology of talin-F0 with other Rap1b effectors (**Figure 3.9D**). A particularly distinct feature in the Rap1b/talin-F0 complex is the existence of a hydrophobic core between I36/P37 of talin-F0 and V21/I27/V29 of Rap1b (**Figure 3.10D**). Such core was not observed in other Rap1b/effector complexes. To understand how Rap1b but not the highly homologous H-Ras binds talin-F0 (**Figure 3.3A**), we mutated I27 and K31 of Rap1b, which closely contact with talin-F0, into corresponding H-Ras residues,

Histidine and Glutamate respectively. Both mutations showed reduced binding to talin-F0 (**Figure 3.11A**). By contrast, both Rap1b and H-Ras bind equally well to RIAM as shown before[31] as also confirmed in **Figure 3.11B**. These data provide insight into the high specificity of the talin binding to Rap1b despite the weaker affinity than that between talin and RIAM (**Figure 3.11C**).

Further analysis revealed that while the Rap1b/talin-F0 interface exhibits distinct features (**Figure 3.10A, D**, and **Table 3.2**), the overall topology of the complex shares similarity with other Rap1b/effector complexes (**Figure 3.9 B, C**). A key determinant for this similarity appears to be the antiparallel β-sheet between Rap1b β2 strand and talin-F0 β2 strand (**Figure 3.9B and 3.10B**), as also present in other Rap1b/effector complexes (**Figure 3.9C**). In addition, charge-charge interactions in talin-F0/Rap1b complex, which involve talin-F0 K7 with Rap1b E37 and talin-F0 K15/R35 with Rap1b D33, are relatively conserved in other Rap1b/effector complexes (**Figure 3.9D** and **Table 3.2**). By contrast, kindlin2-F0, which is not a Rap1b effector (**Figure 3.4B**) but is highly homologous to talin-F0 (**Figure 3.4A**), lacks two positively charged residues in the corresponding positions (**Figure 3.9D**).

In summary, the Rap1b/talin-F0 interface is quite unique yet resembles other Rap1b/effector complexes in overall topology. These structural and binding data suggest that talin is a direct effector of Rap1. Interestingly, the interface residues are highly conserved in both talin/Rap1 isoforms and in different species (**Figure 3.12A, B**), suggesting that Rap1/talin recognition is evolutionally conserved.

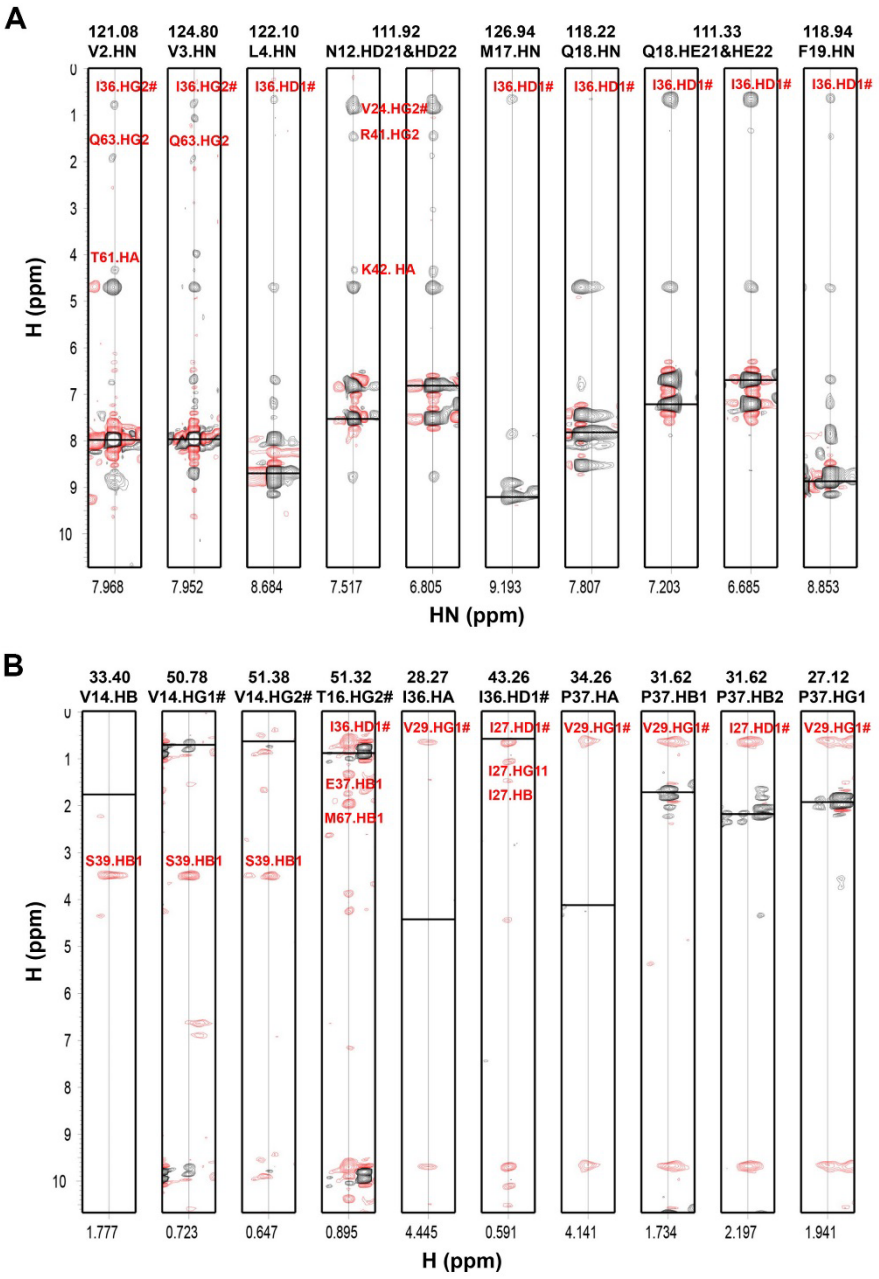

Figure 3.8 Representative intermolecular NOEs for the structure calculation of Rap1b/talin-F0 complex

(A) Representative intermolecular NOEs obtained from 3D ^{15}N-edited NOESY experiment (300 ms mixing time) with sample 3: 0.5 mM ^{15}N/100% ^{2}H-labeled talin-F0

in the presence of 0.7 mM unlabeled Rap1b. Selected residues of talin-F0 were indicated on top of each strip. (B) Representative intermolecular NOEs obtained from 3D $^{15}N/^{13}C$-filtered NOESY experiment (120 ms mixing time) with sample 4: 0.5 mM $^{15}N/^{13}C$-labeled talin-F0 in the presence of 0.7 mM unlabeled Rap1b prepared in 99.8% D_2O. Selected residues of talin-F0 were indicated on top of each strip. Cross-peaks shown in both (A) and (B) which were unambiguously assigned to the specific proton of unlabeled Rap1b residues are labeled in red. The horizontal black line of each strip is diagonal line whose position indicates the chemical shift of the specific proton labeled on top of each strip.

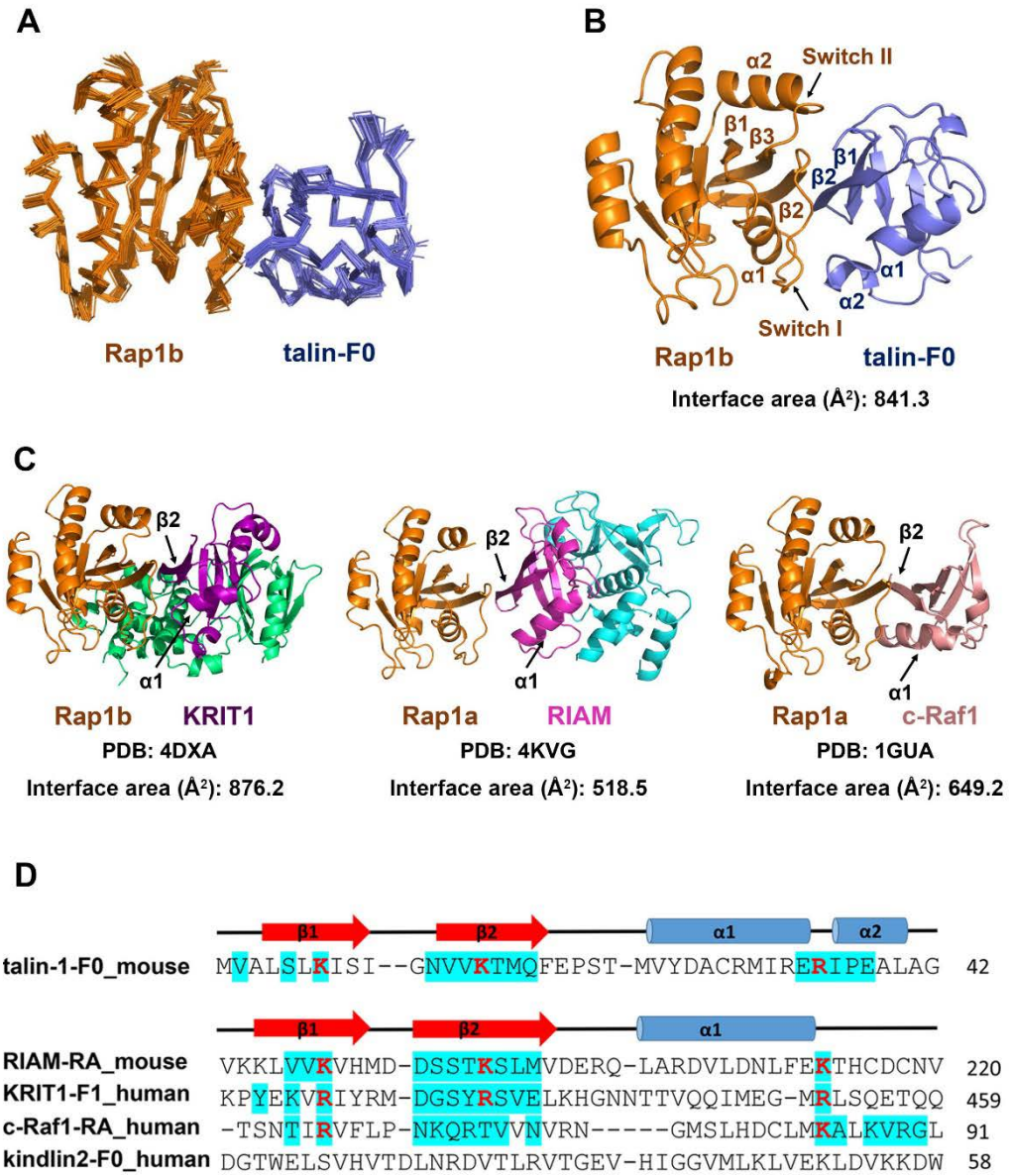

Figure 3.9 Solution structure of Rap1b/talin-F0 complex by NMR

(A) Superposition of 20 calculated Rap1b/talin-F0 complex structures with lowest energies (shown in ribbon representation). (B) Cartoon representation of the Rap1b/talin-F0 complex structure with the lowest energy. (C) Current solved complex structures of Rap1 and its effector proteins (shown in cartoon representation). Interface area ($Å^2$) of

each complex was calculated by an online tool called PDBePISA. The value is calculated as the difference in total accessible surface areas of isolated domains and complex divided by two. (D) Structure-based sequence alignment of talin-F0 and RA domain containing Rap1b effector proteins or kindlin2-F0 (only binding interfaces were shown). Residues involved in the binding interface with a cut-off of 4 Å are highlighted in cyan. Conserved residues are colored in red.

Table 3.1 Structural Statistics of the Rap1b/talin-F0 complex

	Complex
NMR distance & dihedral constraints	3802
Distance constraints	3500
Total NOE	3500
Intra-residue	894
Inter-residue	
Sequential (|i-j| = 1)	1158
Medium-range (|i-j| < 5)	620
Long-range (|i-j| ≥ 5)	750
Intermolecular	78
Hydrogen bonds[a]	
Total dihedral angel restraints	302
phi	151
psi	151
Structure Statistics	
Violations (mean±s.d.)[a]	
Distance constraints (Å)	0.12780 ± 0.00229
Dihedral angel constraints (°)	2.47094 ± 0.31544
Max. dihedral angle violation (°)	5
Max. distance constraint violation (Å)	0.5
Deviations from idealized geometry	
Bond lengths (Å)	0.00796 ± 0.00014
Bond angles (°)	0.94224 ± 0.01034
Impropers (°)	0.73831 ± 0.01966
Average pairwise r.m.s.d. (Å)	
Backbone atoms	0.584 ± 0.106
All heavy atoms	1.177 ± 0.097
Ramachandran Plot	
Residues in allowed region (%)	98.8
Residues in disallowed regions (%)	1.2

[a] Statistics were calculated over 20 structures with lowest energies.

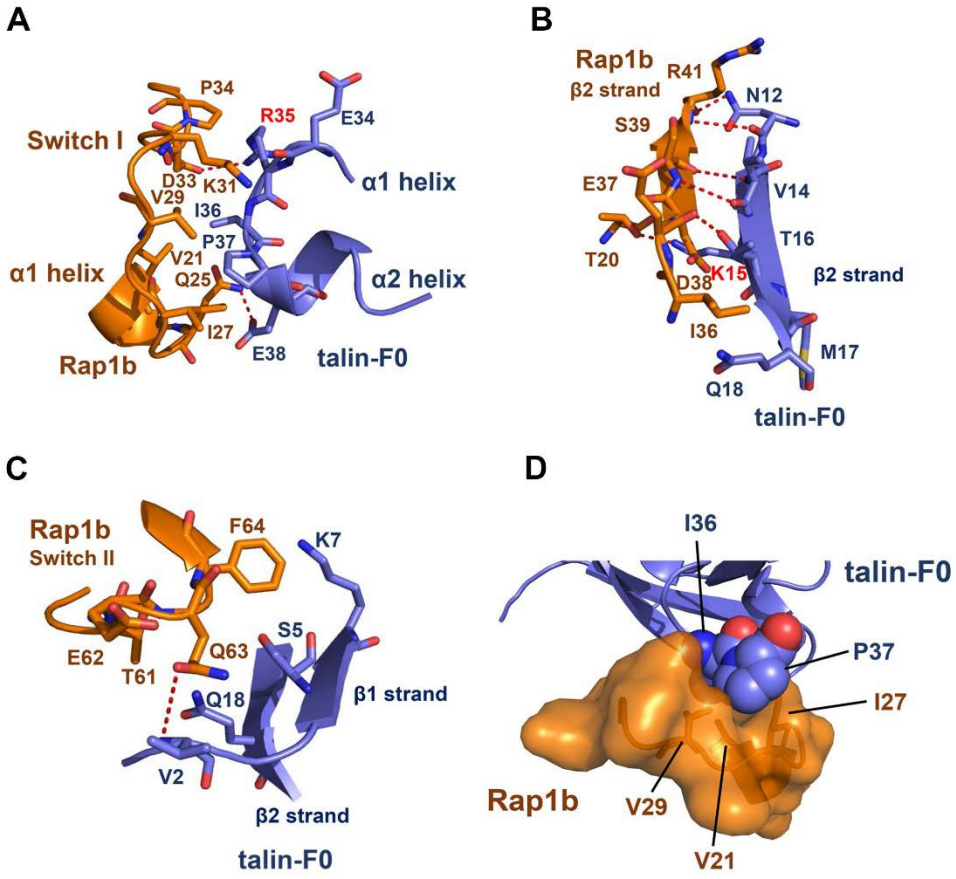

Figure 3.10 Detailed binding interface between Rap1b and talin-F0

(A) Detailed binding interface between the α1 helix and switch I of Rap1b and the α2 helix of talin-F0. (B) Detailed binding interface between β2 strand of Rap1b and talin-F0. (C) Detailed binding interface between switch II region of Rap1b and talin-F0. Hydrogen bonds are represented in red dashed lines. (D) A distinct hydrophobic core formed between I36/P37 (shown in spheres representation) of talin-F0 and V21/I27/V29 of Rap1b (shown in surface representation).

Table 3.2 Comparison of binding interface between Rap1 and its effector proteins[a,b,c]

	Rap1	F0	RIAM-RA PDB: 4DXA	KRIT1-F1 PDB: 4KVG	cRaf-1 PDB: 1GUA
	S17	**K15**			
α1 helix	V21	**K15**, I36		**R452**	
	V24	N12, V13			V88
	Q25	V13, I36, E38		**R452**	K87, V88, R89, G90
	I27	P37, E38			
	V29	P37			**K84**
Switch I	K31	E34, **R35**			**K84**
	D33	**K15**, **R35**	**K213**	**R432**, **R452**	**K84**
	P34	T16, **R35**		**R432**	
	I36	S5, T16, M17, Q18	V182, S194, L195, M196	S433, V434, E435	I57, V69, N71
	E37	**K7**, T16	**K193**, S194	**R423**, Y431, S433	**R59**, R67, T68, V69
	D38	V14	T192, **K193**, S194	Y431, **R432**, S433	R67, T68, R89
β2 strand	S39	V14	S191, T192	S430, Y431	Q66, R67, R89
	Y40		**K193**	**R452**	Q66, R89
	R41	N12, V13, V14	S190	D428, G429	N64, K65, Q66
	K42	N12			
β3 strand	M52				N64
	L56			Y431	
	T61	Q18			
Switch II	Q63	V2, Q18			
	F64	S5, **K7**, G76		F419	
	M67			K421	

[a] A cut-off of 4 Å was used to define the interface. The residues were identified in PyMOL 1.3 (Schrödinger, LLC.) and then manually organized into the table.

[b] Conserved residues are highlighted in red.

[c] The Rap1b/talin-F0 complex with the lowest energy was analyzed in this table.

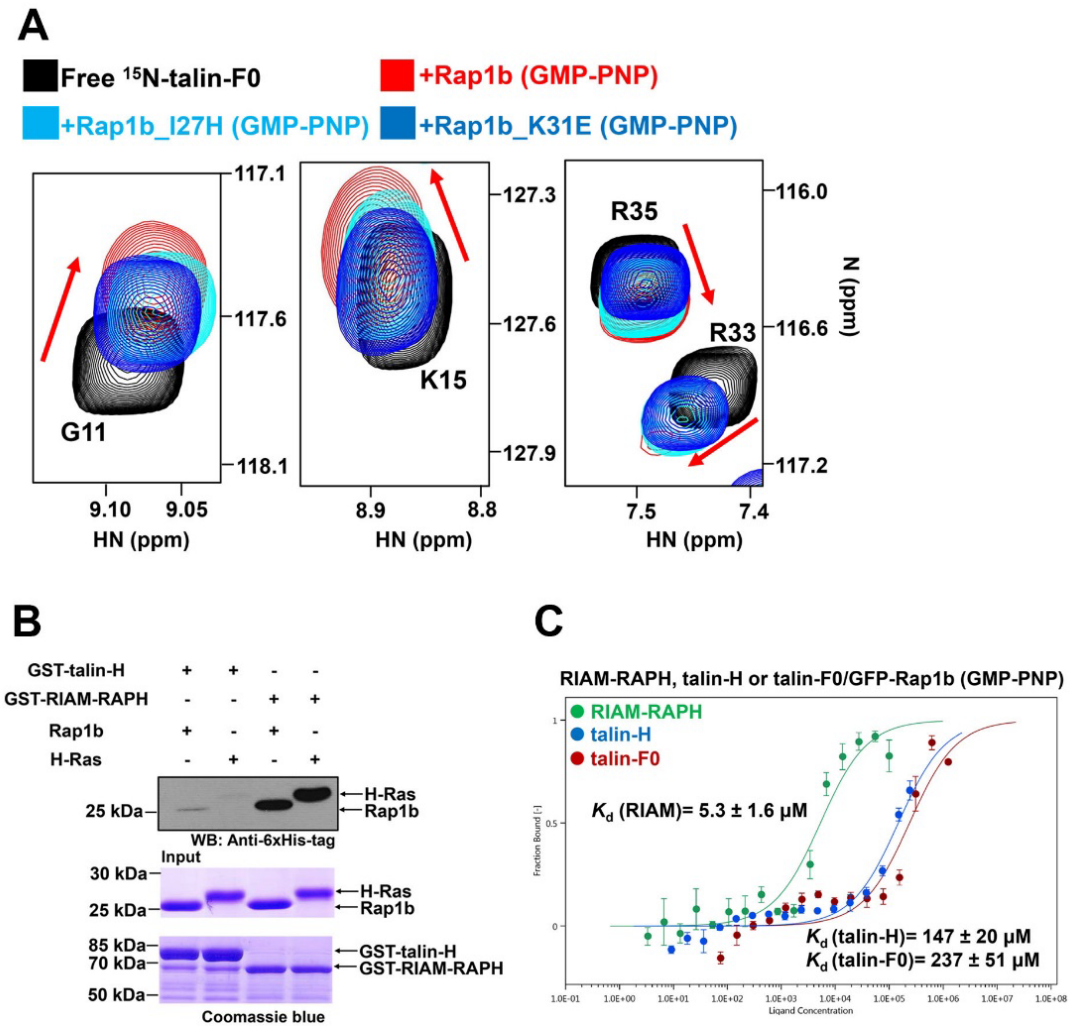

Figure 3.11 Rap1b/talin-F0 interaction is modest but highly specific

(A) The HSQC spectra (four representative residues were shown) of 50 μM ^{15}N-labeled talin-F0 in the absence (black) and presence of 125 μM GMP-PNP loaded Rap1b (red), K31E mutant (blue) or I27H mutant (cyan). Note that all Rap1b variants also bear a G12V mutation. K31E and I27H mutations resulted in overall less chemical shift changes and less extent of line broadening. (B) GST pull down assay to show that talin-H interacts specifically with Rap1b, while RIAM interacts with both Rap1b and H-Ras equally. (C)

The affinity between GMP-PNP loaded GFP-Rap1b and RIAM-RAPH, talin-F0 or talin-H measured by Nanotemper. Experiments were done in triplicates. The affinity of GFP-Rap1b/talin-H shown here is an estimated value because the saturation step was not reached due to the aggregation issue of talin-H at high concentration.

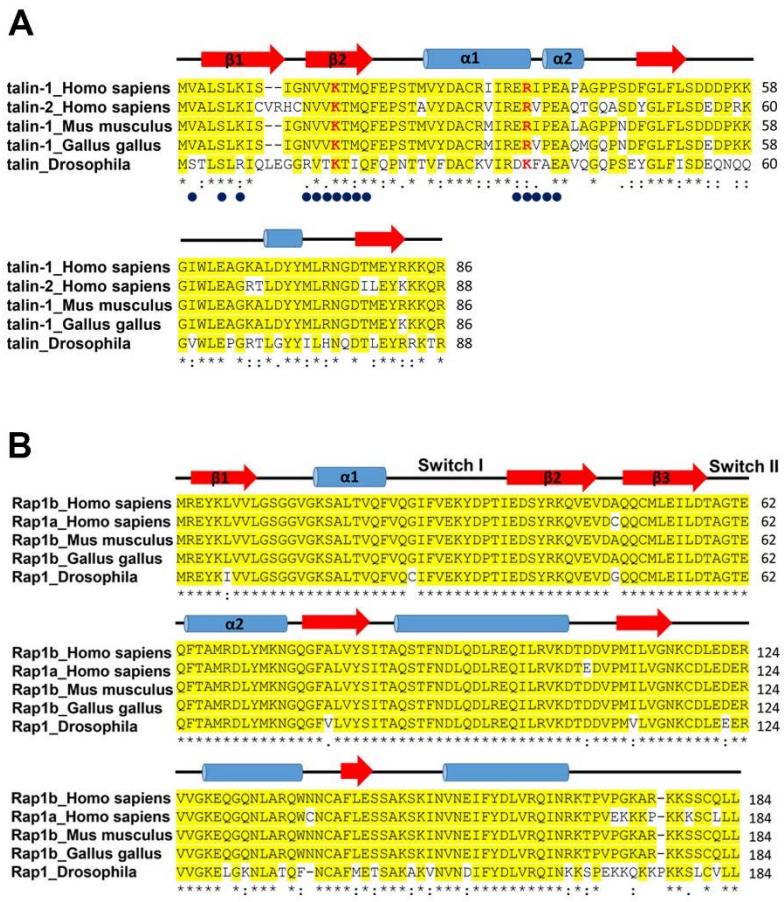

Figure 3.12 Rap1/talin interaction is evolutionally conserved

(A) Sequence alignment of talin-F0 from different species. Residues of talin-F0 involved in the binding interface (cut-off of 4 Å) with Rap1b are indicated in the figure with blue solid circles. (B) Sequence alignment of Rap1 from different species. (Residues identical to human talin-1 or Rap1b are highlighted in yellow. '*' indicates fully conserved residue, ':' indicates residues with strongly similar properties, and '.' indicates residues with weakly similar properties).

Rap1b binding to talin is crucial for integrin activation

To further evaluate the importance of the Rap1b/talin interaction, we performed the structure-based analysis and mutated two critical interface residues K15 and R35 of talin-F0 (**Figure 3.10A, B**) into alanines. **Figure 3.13A, B** show that K15A/R35A double mutations (DM) drastically reduced the Rap1b interaction to talin-F0 as well as talin-H. Since talin-H is the unit responsible for binding and activating integrin[7,12], we next tested the impact of the Rap1b binding defective mutations on its ability to activate $\alpha_{IIb}\beta_3$ – the prototypic integrin widely used to study integrin activation. To this end, we transfected wild-type (WT) talin-H or talin-H DM into CHO A5 cells stably expressing $\alpha_{IIb}\beta_3$. **Figure 3.14A** shows that as compared to the WT talin-H, the talin-H mutant-induced $\alpha_{IIb}\beta_3$ activation was substantially reduced. These results provide strong evidence that the interaction of talin-H with Rap1b is crucial for the talin-H-mediated integrin activation. They also explain a previously reported phenomenon where deletion of F0 domain in talin-H significantly impaired the integrin activation[79]. To further demonstrate that the impaired interaction between talin DM with Rap1 impacts on integrin-mediated functions, we retrovirally transduced talin-null fibroblasts (talin$^{1/2dko}$), which show a strong defect in cell adhesion and spreading[80], with C-terminally ypet-tagged talin WT as well as talin DM. The transduced cells were FACS-sorted for equal talin and talin DM expression as confirmed by flow cytometry and western blotting (**Figure 3.14B**). Re-expression of both WT talin and talin DM induced cell spreading of talin$^{1/2dko}$ cells with WT and mutant talin localizing to paxillin positive focal adhesions (FAs) (**Figure 3.14C, D**). We then performed adhesion assays on various integrin ligands and observed that talin DM only partially rescued cell adhesion of talin$^{1/2dko}$ cells to fibronectin (FN), laminin-111 (LN),

and vitronectin (VN) compared to WT talin, whereas integrin-independent adhesion to poly-L-lysine was unchanged (**Figure 3.15A**). As expected, talin$^{1/2dko}$ cells expressing ypet as a control hardly adhered to any integrin ligand (**Figure 3.15A**). Importantly, expression of mutant talin did not alter the expression levels of surface integrins nor those of RIAM and Rap1 (**Figure 3.14B, E**). Next we plated the cells on FN and measured cell spreading for 4 hours. While ypet transduced talin$^{1/2dko}$ cells remained roundish and did not spread, talin DM cells displayed a significant spreading defect compared to talin WT transduced cells (**Figure 3.15B**).

We hypothesize that the reduced PAC-1 binding, cell adhesion and spreading of talin DM expressing cells are due to impaired integrin activation caused by deficient talin recruitment to the integrin site at the plasma membrane. To test this hypothesis experimentally, we seeded WT talin and talin DM expressing cells on FN-coated micropatterns for 4 hours and measured the number and size of paxillin-positive focal adhesions. This analysis reveals that indeed the focal adhesion (FA) area and number per cell are significantly reduced in cells expressing talin DM compared to those expressing WT talin (**Figure 3.15C-E**). The mean FA size (**Figure 3.15F**) was also reduced by talin DM although with a *p* value of 0.09. To further test whether impaired talin/Rap1 interaction affects the recruitment of talin DM to FAs, we measured the intensity of ypet fluorescence within FAs and correlated it to the total cellular ypet fluorescence intensity. We observed a significantly reduced relative intensity of ypet signal within FAs in talin DM transduced cells, which suggests that the talin/Rap1b interaction is important for talin recruitment to FAs (**Figure 3.15G**). Collectively, our data provide strong evidence for the physiological importance of direct Rap1/talin interaction in integrin regulation.

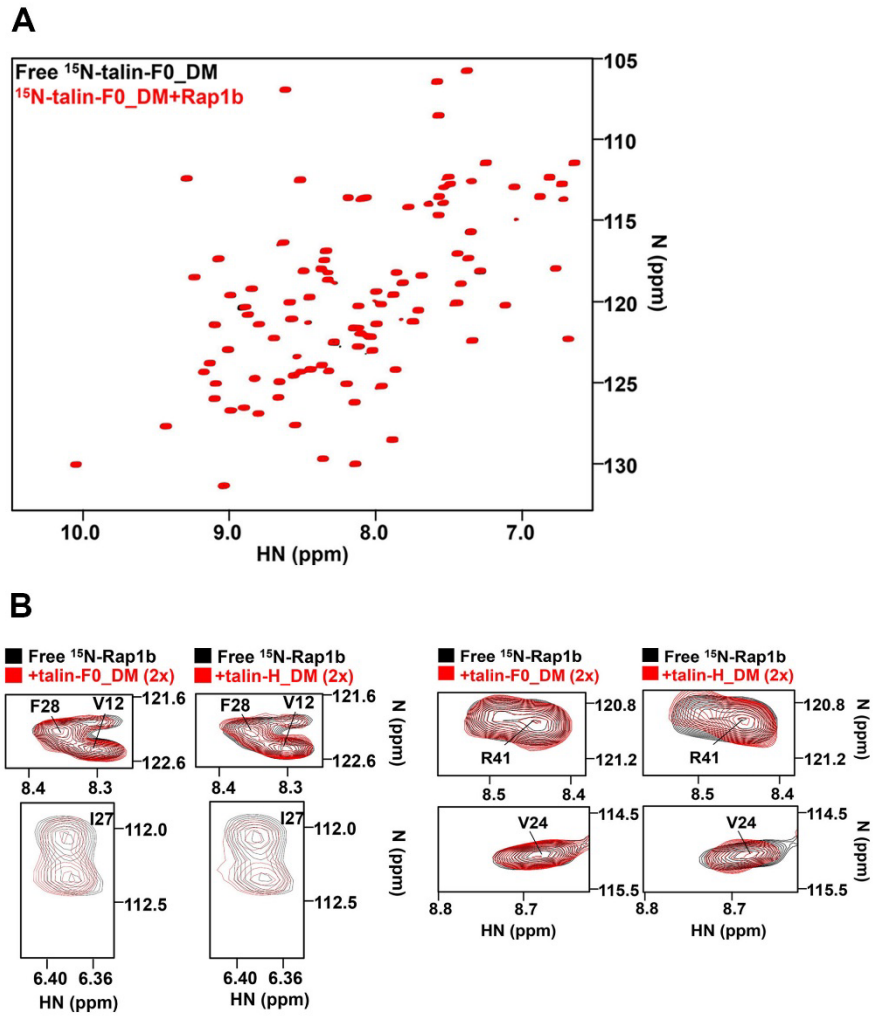

Figure 3.13 Rap1b/talin interaction is drastically reduced by double mutations (K15A, R35A) in talin-F0 domain

(A) The HSQC spectra of 50 μM ^{15}N-labeled talin-F0_DM (K15A, R35A) in the absence (black) and presence of 125 μM GMP-PNP loaded Rap1b (red). (B) The HSQC spectra (representative regions were shown) of 45 μM GMP-PNP loaded ^{15}N-labeled Rap1b (1-167) in the absence (black) and presence of 90 μM talin-F0_DM or talin-H_DM (red).

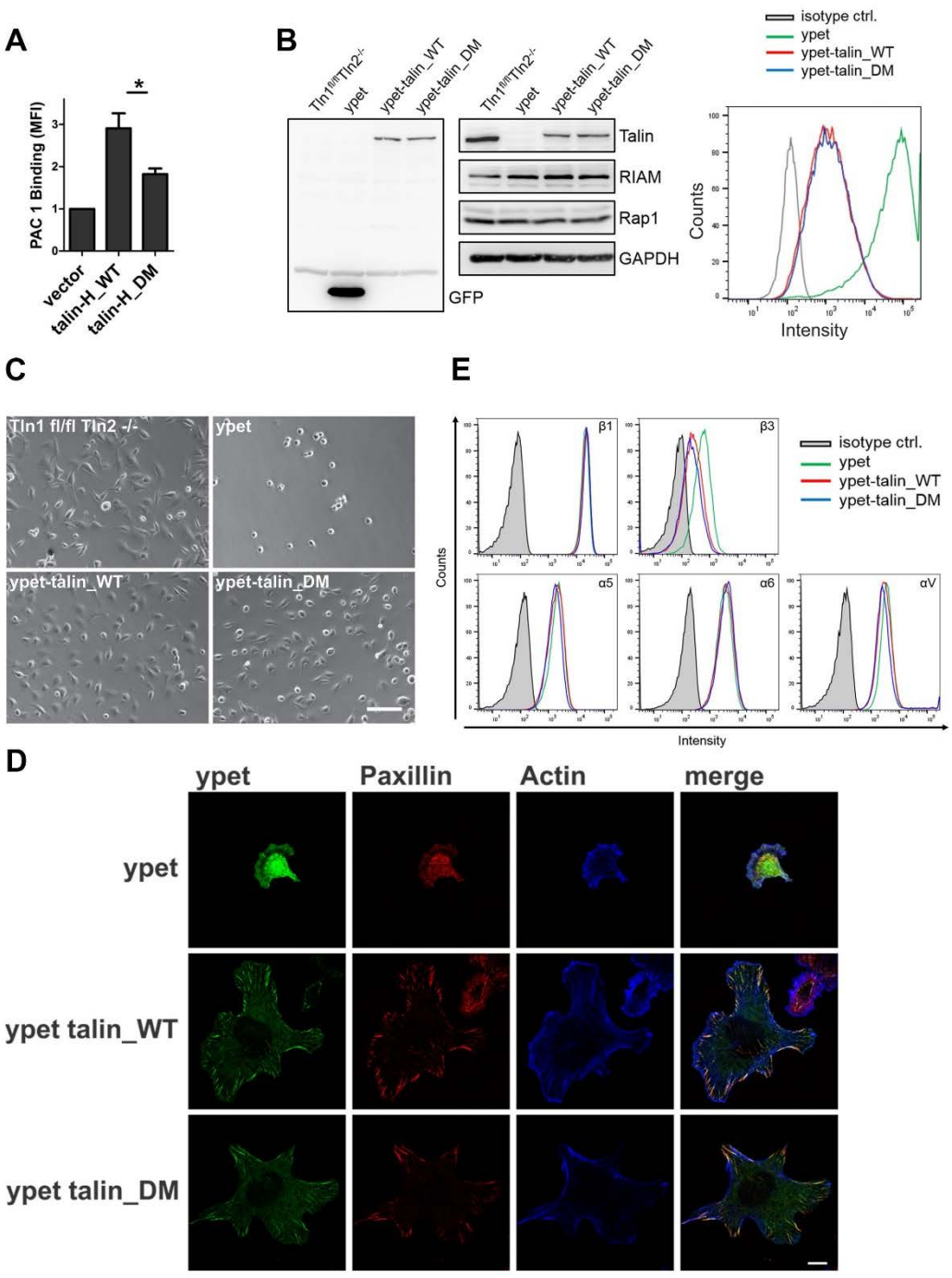

Figure 3.14 Impaired Rap1/talin interaction results in defective integrin activation

(A) Integrin activation assay in CHO A5 cells which stably express integrin $\alpha_{IIb}\beta_3$. Double mutations (K15A, R35A) in talin-H substantially decreases integrin activation. The data

are shown as means ± S.E.M. from four independent experiments. * denotes $p < 0.05$. (B) Left, western blot analyses of talin control (talin-$1^{fl/fl}$/talin-$2^{-/-}$) and talin$^{1/2dko}$ fibroblasts which were retrovirally transduced with either ypet alone, ypet-tagged talin WT or ypet-tagged talin DM (K15A, R35A) to show expression levels of ypet and ypet-tagged talin (recognized by GFP antibody), talin, RIAM and Rap1. GAPDH served as loading control. Right, flow cytometric analysis of talin control (talin-$1^{fl/fl}$/talin-$2^{-/-}$) (grey) and talin$^{1/2dko}$ fibroblasts retrovirally transduced with ypet alone (green), ypet-tagged talin WT (red) or ypet-tagged talin DM (blue) to quantify expression levels of the transduced proteins. (C) Phase contrast images of talin-$1^{fl/fl}$/talin-$2^{-/-}$ control cells and talin$^{1/2dko}$ cells expressing ypet, ypet-talin WT or ypet-talin DM plated on fibronectin. Scale bar 100 μm. (D) Confocal images of the ventral side of talin$^{1/2dko}$, ypet-talin WT or ypet-talin DM cells stained for paxillin (red) and F-actin (blue). Ypet-signal is shown in green. Scale bar 10 μm. (E) Surface expression levels of integrin β1, β3, α5, α6 and αV on talin control (grey) and talin$^{1/2dko}$ fibroblasts expressing ypet (green), ypet-tagged talin WT (red) or ypet-tagged talin double mutant (DM) (blue) analyzed by flow cytometry. (The data of panel A were provided by Dr. Ashley Holly in our lab, the data of panel B-E were provided by Dr. Markus Moser's lab.)

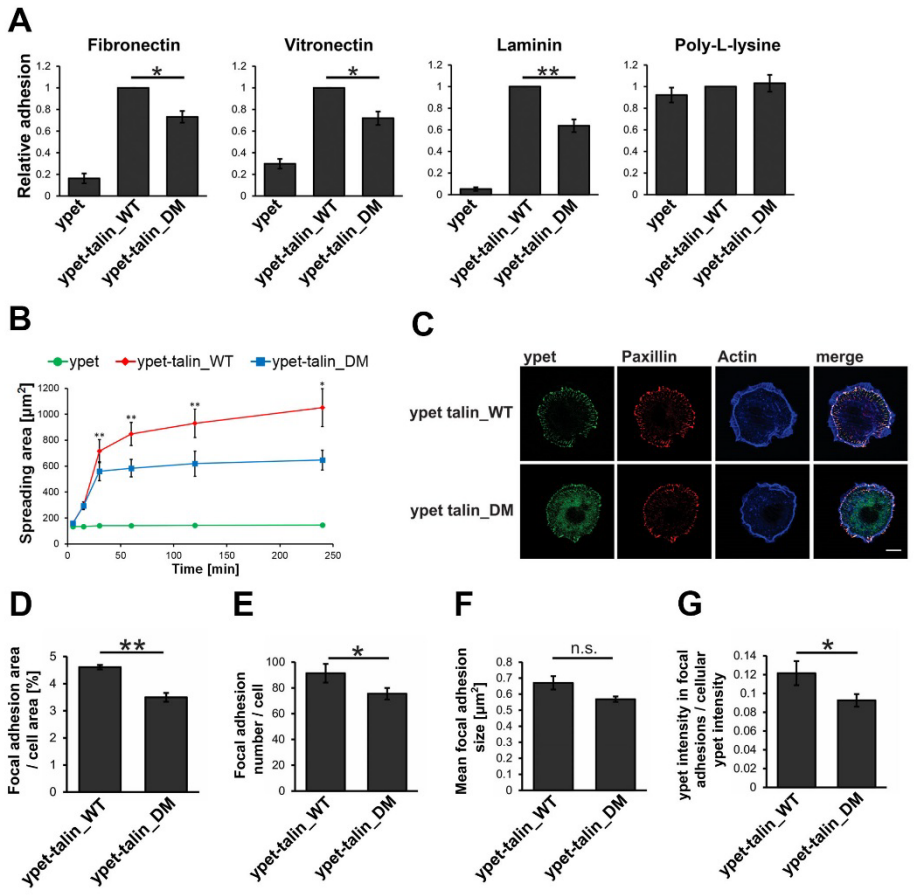

Figure 3.15 The Rap1b binding to talin is crucial for cell adhesion and spreading

(A) Static adhesion of talin$^{1/2dko}$ fibroblasts, expressing either ypet alone, ypet-tagged talin WT or ypet-tagged talin DM (K15A, R35A). Number of adherent cells was quantified by measuring absorbance of crystal violet staining. Values measured for talin WT transduced cells were set to 1 in each of 6 independent experiments. Values are given as mean ± S.E.M.. * denotes $p < 0.05$, and ** denotes $p < 0.01$. (B) Spreading of talin$^{1/2dko}$ fibroblasts expressing ypet (green), ypet-tagged talin WT (red) or ypet-tagged talin DM (blue) on a fibronectin coated surface, measured 5 min, 15 min, 30 min, 1 h, 2 h and 4 h after plating. N=5. (C) Confocal images of ypet-tagged talin WT or ypet-tagged talin DM cells on FN-

coated round micropatterns stained for paxillin (red) and F-actin (blue). Ypet signal is shown in green. Scale bar 10 μm. Focal adhesion area per cell area (D), focal adhesion number per cell (E) and focal adhesion size (F) of ypet-tagged talin WT and ypet-tagged talin DM cells on FN-coated micropatterns. (G) Ypet fluorescence intensity within paxillin-positive focal adhesion area in relation to the cellular ypet fluorescence. N=5; 10 to 15 talin WT and talin DM expressing cells in each measurement were analyzed. All values are given as mean ± S.E.M. * denotes $p < 0.05$, and ** denotes $p < 0.01$. (All the data in this figure were provided by Dr. Markus Moser's lab.)

Membrane anchored Rap1b shows enhanced binding to talin

While the forgoing data demonstrated the unique specificity of Rap1b/talin interaction and its importance in regulating integrin mediated functions, a key issue still remains: how can such interaction with ~ 0.16 mM affinity be effective since protein concentration in cells is typically much lower than 0.16 mM? We attempted to address this issue from two angles. First, both Rap1 and talin are highly abundant in cells. For example, recent proteomic studies showed that Rap1b and talin belong to the top most abundant proteins in platelets with copy numbers of ~ 200,000 which are nearly1/4 of the most abundant platelet protein actin[35]. The high levels of Rap1 and talin in platelets are consistent with our protein expression analysis (**Figure 3.16A**). Given that the average concentration of actin is above 200 μM in platelets[81], the estimated concentration of Rap1b or talin in platelets should be at least 50 μM. By contrast, the RIAM level is very low in both human and murine platelets (**Figure 3.16A**) which was also confirmed by quantitative mass spectrometry with a copy number of only 162[35]. Thus, the high concentrations of Rap1 and talin increase the chance for their direct interaction to occur. Second, given that Ras family GTPases including Rap1 are all known to be attached to membrane *via* Cys prenylation of their C-terminal CAAX motif[73] and talin-H also binds to membrane *via* a large positively charged surface on F1, F2, and F3 domains[14,82], we reasoned that Rap1 and talin-H might be more tightly associated if Rap1 were prenylated with membrane to mimic the true cellular microenvironment (**Figure 3.16B**). Our Rap1b/talin-F0 structure superimposed with the structure of talin-H supports this possibility in that the CAAX containing C-terminus of Rap1b and the positively charged surface of talin-H align well to all face towards the membrane surface (**Figure 3.16B**). To

address this possibility experimentally, we prepared membrane vesicles with anchored Rap1b using the well-established thiol-maleimide crosslinking method[83] (**Figure 3.17A**). As shown in **Figure 3.17B**, membrane-anchored Rap1b indeed bound much more robustly to talin-H than Rap1b unanchored to membrane. Isothermal titration calorimetry (ITC) experiments revealed a K_d of ~2.6 μM for membrane-anchored active Rap1b to bind to talin-H (**Figure 3.18**), which indicates a more than two orders of magnitude stronger binding than that measured without membrane (**Figure 3.2B and 3.11C**). Consistently, the membrane binding capacity of talin-H was also substantially enhanced by Rap1 anchored to membrane, but such enhancement was diminished for talin-H DM that is defective for binding to Rap1 (**Figure 3.19A**). Importantly, the binding of membrane-anchored Rap1b to talin-H is GTP dependent as shown by two independent methods: GST pull-down assay (**Figure 3.17C**) and co-sedimentation assay (**Figure 3.19B**). Such GTP-dependence indicates that the effective membrane targeting of talin requires active Rap1b. These findings provide key evidences for talin being a bona fide Rap1 effector and suggest how agonist-activated and membrane-anchored Rap1 can effectively recruit talin to the membrane surface. Although full-length talin binds to membrane more weakly than talin-H possibly due to some degree of autoinhibition for the former, membrane with anchored Rap1b clearly binds more potently to full-length talin contrasting to the scenario where Rap1b was not attached to membrane (**Figure 3.19C**). Similar to membrane-mediated Rap1b/talin-H binding (**Figure 3.19B**), membrane-anchored Rap1b also interacts with full-length talin in a GTP dependent manner (**Figure 3.19D**). Importantly, since full-length talin adopts an autoinhibited conformation[50,63], which may be unmasked through a pull-push mechanism by binding to the membrane[14] , our data further suggest that Rap1

not only promotes the membrane targeting but also leads to activation of talin *via* this mechanism (**Figure 3.16B**). In order to test this hypothesis, we performed NMR-based competition experiments by examining the interaction of $^{15}N/^{2}H$-labeled inhibitory talin rod domain 9 (talin-R9) with talin-H in the absence and presence of membrane-anchored Rap1b. **Figure 3.20** shows that while talin-H induces residue-specific chemical shift changes of talin-R9 as the signature of the autoinhibition[14], such chemical shift changes were suppressed by membrane-anchored Rap1b, thus demonstrating the talin unmasking process.

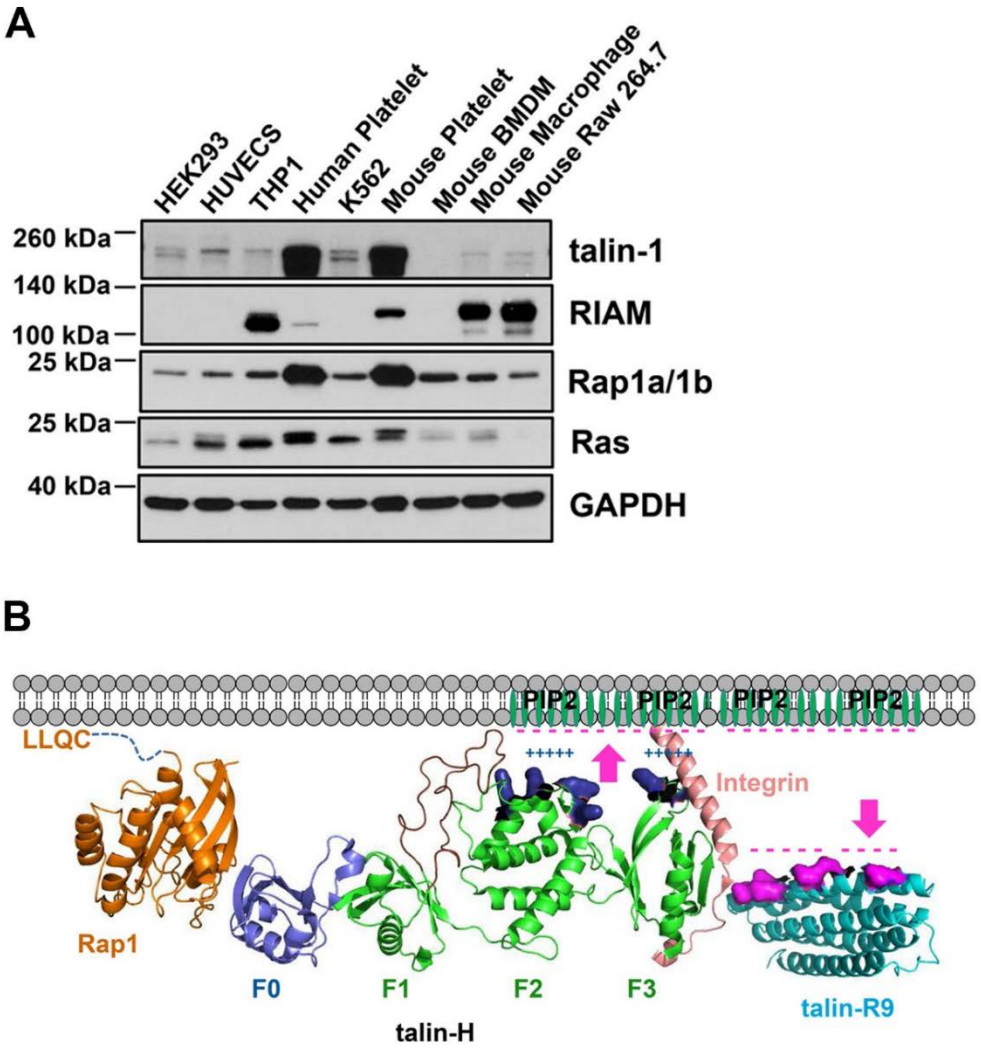

Figure 3.16 The mechanism of talin recruitment by Rap1

(A) Protein expression levels of talin, RIAM, Rap1, Ras GTPases, and GAPDH in various types of cell lines indicated in the figure. (B) A model of membrane-associated Rap1b recruiting talin for integrin activation. Proteins are shown in cartoon representation. Talin F1 loop is colored in maroon, the positive charged residues of talin-F2F3 domains (green) which interact with PIP2 are colored in deep blue and shown in surface representation, and the negative charged residues of talin-R9 (cyan) are colored in magenta and shown in surface representation.

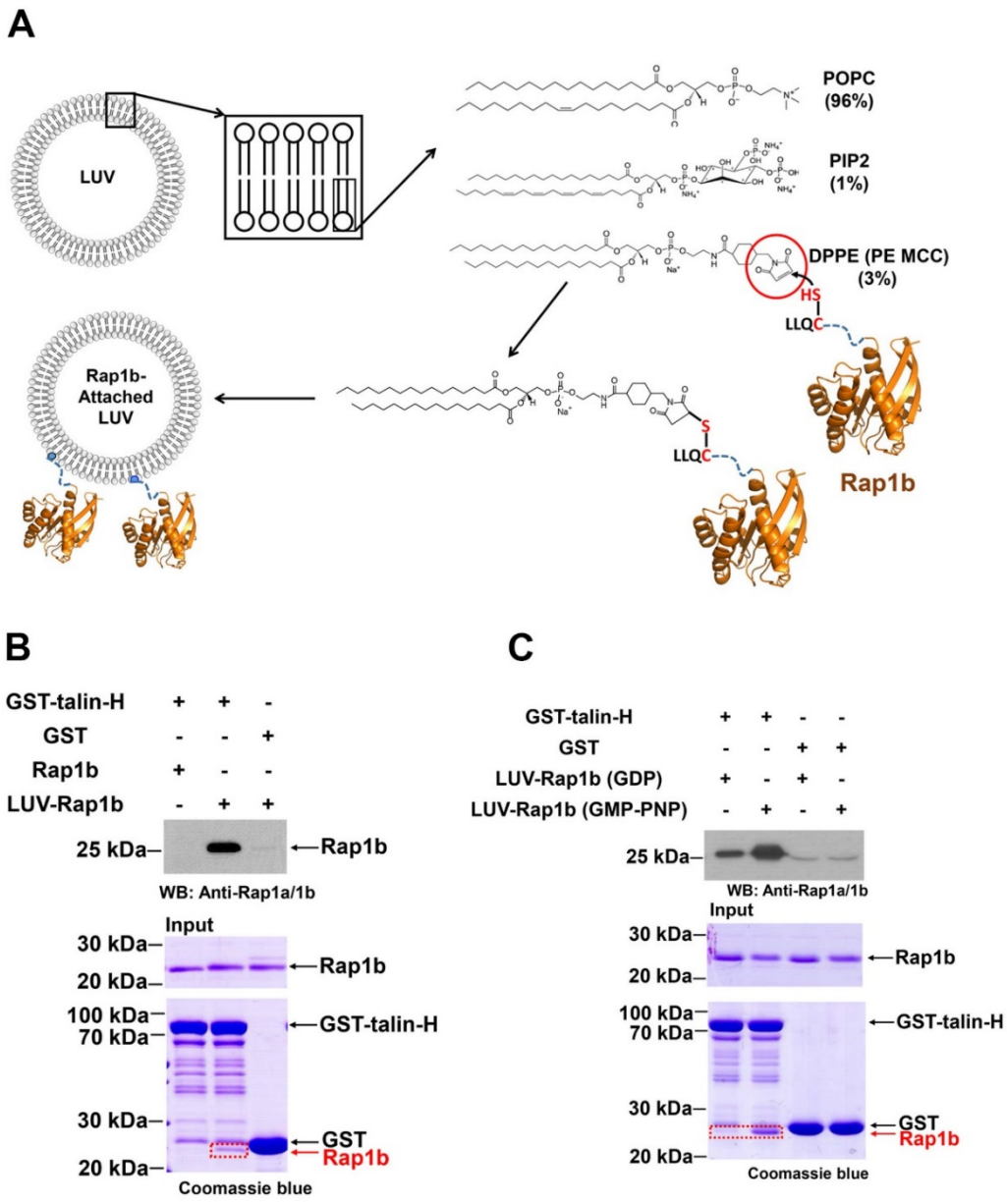

Figure 3.17 Membrane anchored Rap1b robustly enhances its binding to talin-H

(A**)** The diagram procedure of generating Rap1b-anchored LUVs. (B) GST pull down assay to show the robustly enhanced interaction between membrane-anchored Rap1b and talin-H. Rap1b was loaded with GMP-PNP in this assay and "LUV-Rap1b" represents that Rap1b was anchored to large unilamellar vesicles (LUVs). LUV- Rap1b could be easily

pulled down by GST-talin-H and the band was visible in coomassie-blue staining gel (boxed in red) and intense in WB analysis, while free Rap1b pulled down by GST-talin-H was hardly seen in the same condition. (C) GST pull down assay to show that the interaction between membrane-anchored Rap1b and talin-H is also in a GTP dependent manner.

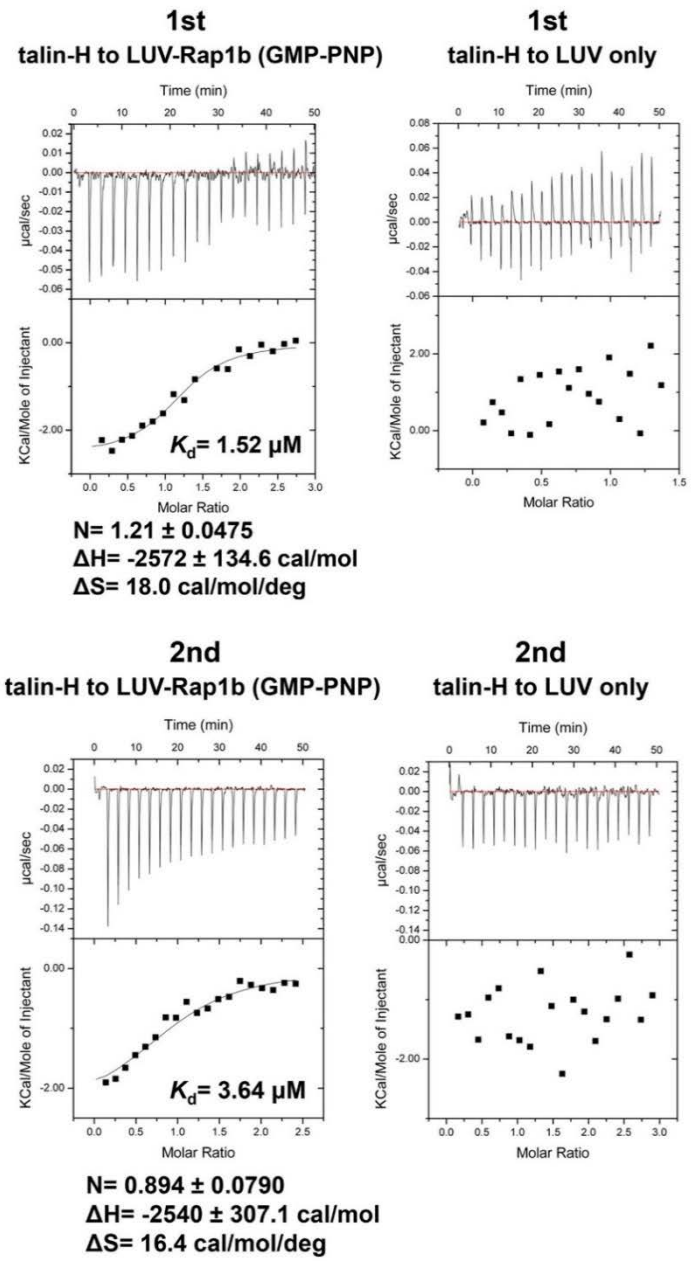

Figure 3.18 Binding affinity between membrane-anchored Rap1b and talin-H measured by isothermal titration calorimetry (ITC)

The titrations of talin-H to LUV-only showed different background heats due to different batches of LUVs, but the enthalpy changes and affinities of talin-H/LUV-Rap1b were

consistent after subtraction. The average affinity of this interaction is ~ 2.6 μM. N, the number of binding sites. ΔH, enthalpy change. ΔS, entropy change.

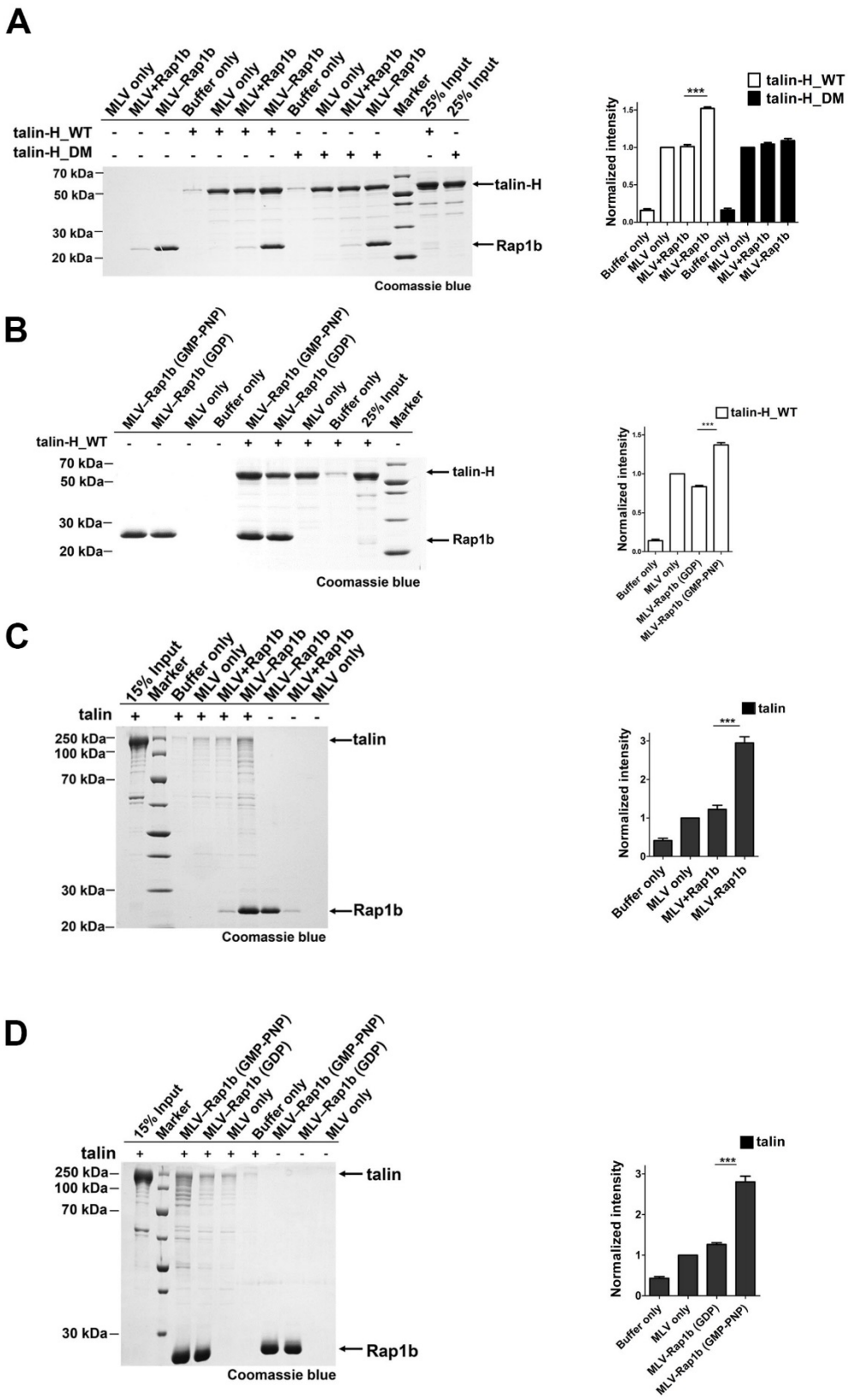
A
MLV only
MLV+Rap1b
MLV–Rap1b
Buffer only
MLV only
MLV+Rap1b
MLV–Rap1b
Buffer only
MLV only
MLV+Rap1b
MLV–Rap1b
Marker
25% Input
25% Input
talin-H_WT - - - + + + + - - - - + -
talin-H_DM - - - - - - - + + + + - +
70 kDa
50 kDa
30 kDa
20 kDa
talin-H
Rap1b
Coomassie blue
talin-H_WT
talin-H_DM
***
Normalized intensity
Buffer only
MLV only
MLV+Rap1b
MLV–Rap1b
Buffer only
MLV only
MLV+Rap1b
MLV–Rap1b
B
MLV–Rap1b (GMP-PNP)
MLV–Rap1b (GDP)
MLV only
Buffer only
MLV–Rap1b (GMP-PNP)
MLV–Rap1b (GDP)
MLV only
Buffer only
25% Input
Marker
talin-H_WT - - - - + + + + + -
70 kDa
50 kDa
30 kDa
20 kDa
talin-H
Rap1b
Coomassie blue
talin-H_WT
***
Normalized intensity
Buffer only
MLV only
MLV–Rap1b (GDP)
MLV–Rap1b (GMP-PNP)
C
15% Input
Marker
Buffer only
MLV only
MLV+Rap1b
MLV–Rap1b
MLV–Rap1b
MLV+Rap1b
MLV only
talin + + + + + - - -
250 kDa
100 kDa
70 kDa
30 kDa
20 kDa
talin
Rap1b
Coomassie blue
talin
***
Normalized intensity
Buffer only
MLV only
MLV+Rap1b
MLV–Rap1b
D
15% Input
Marker
MLV–Rap1b (GMP-PNP)
MLV–Rap1b (GDP)
MLV only
Buffer only
MLV–Rap1b (GMP-PNP)
MLV–Rap1b (GDP)
MLV only
talin + + + + + - - -
250 kDa
100 kDa
70 kDa
30 kDa
talin
Rap1b
Coomassie blue
talin
***
Normalized intensity
Buffer only
MLV only
MLV–Rap1b (GDP)
MLV–Rap1b (GMP-PNP)

Figure 3.19 Membrane anchored Rap1b interacts with talin in a GTP dependent manner

(A) Left, a representative vesicle co-sedimentation assay showing that the interaction between talin-H_WT and membrane is enhanced by around 1.5 folds when Rap1b (GMP-PNP) is attached to membrane but not for talin-H_DM. “MLV+Rap1b” represents that Rap1b remained as free form in solution without being attached to multilamellar vesicles (MLVs) which were pre-incubated with β-mercaptoethanol. “MLV-Rap1b” represents that Rap1b was anchored to MLVs. Right, the quantification of four independent experiments. The intensity of talin-H_WT or talin-H_DM band was normalized to that of corresponding “MLV only” group and the data are shown in means ± S.E.M. *** denotes $p < 0.0001$. (B) Left, a representative vesicle co-sedimentation assay showing that the interaction between talin-H and membrane-anchored Rap1b is GTP dependent. Right, the quantification of four independent experiments. The intensity of talin-H_WT band was normalized to that of “MLV only” group and the data are shown in means ± S.E.M.*** denotes $p < 0.0001$. (C) Left, a representative vesicle co-sedimentation assay showing that the interaction between full-length talin and membrane is significantly enhanced by around 3 folds when Rap1b (GMP-PNP) is attached to membrane. Right, the quantification of four independent experiments. The intensity of talin band was normalized to that of the “MLV only” group and the data are shown as means ± S.E.M. *** denotes $p<0.0001$. (D) Left, a representative vesicle co-sedimentation assay showing that the interaction between full-length talin and membrane-anchored Rap1b is GTP dependent. Right, the quantification of four independent experiments. The intensity of

talin band was normalized to that of “MLV only” group and the data are shown as means ± S.E.M. *** denotes $p<0.0001$.

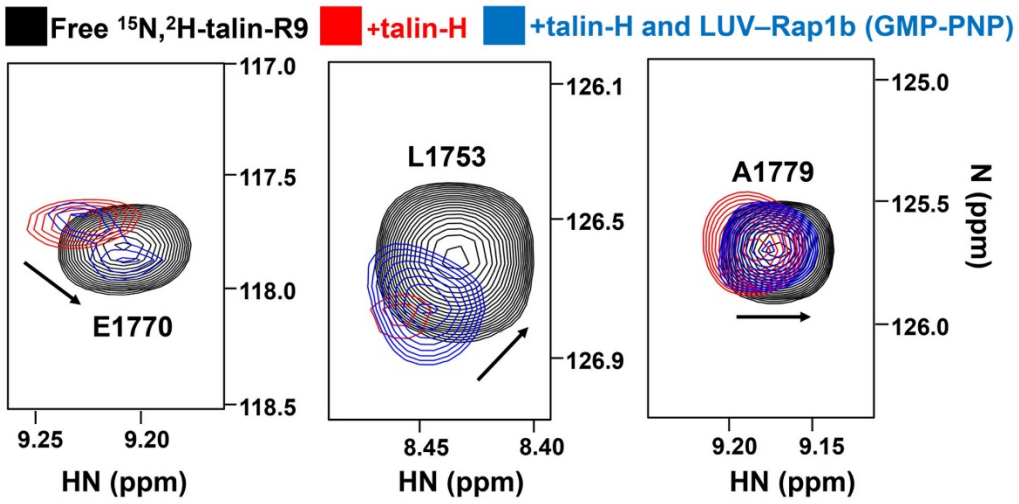

Figure 3.20 Membrane anchored Rap1b promotes talin unmasking

HSQC-based spectral changes (three representative residues were shown) of 30 μM ^{15}N/80% ^{2}H-labeled talin-R9 in the absence (black) and presence of 22 μM talin-H (red) showing the talin-H masking by the autoinhibitory talin-R9 as reported before[14]. Addition of 11 μM membrane-anchored Rap1b shifts the peaks towards the free form of talin-R9 (blue) indicating the talin unmasking. Note that the concentrations of the proteins were kept low, which cause less pronounced chemical shift changes but to avoid precipitation. The peak intensity for each dataset was set to the same scale. These experiments were performed at 28.5 ℃ on Bruker 900 MHz NMR spectrometer. The buffer contained 25 mM NaH_2PO4/Na_2HPO4 (pH 6.8), 100 mM NaCl, 5 mM $MgCl_2$, 5 mM β-mercaptoethanol and 5% D_2O.

Discussion

Rap1 was discovered nearly three decades ago[84] and its two isoforms Rap1a and Rap1b (with ~ 95% identity, see also **Figure 3.12B**) are regarded as the key membrane-associated small GTPases to target proteins to the plasma membrane to regulate diverse cellular responses[72-75]. A large body of data have indicated that Rap1 is critically involved in activation of integrins[7,47,85], but the immediate downstream effector of Rap1 has been highly elusive. Our studies have now obtained an important clue on this longstanding mystery. We found that the activated Rap1b interacts with the F0 domain of talin – the key mediator of integrin activation, and we determined the NMR structure of the Rap1b/talin-F0 complex. Despite little sequence homology between talin-F0 and other Rap1 effectors, the overall topology of the complex was found to resemble those known Rap1/effector complexes. Moreover, disruption of the Rap1b/talin interface substantially impaired the integrin $\alpha_{IIb}\beta_3$ activation, cell adhesion and cell spreading. Interestingly, we found that while being weak measured in conventional binary conditions[26], the Rap1b/talin interaction became quite strong when Rap1b was anchored to membrane – a condition mimicking the cellular microenvironment of Ras family GTPases[83] and also favoring talin unmasking as indicated previously[8]. Overall, our data suggest a crucial pathway by which agonist-activated Rap1 directly promotes the membrane recruitment of talin, which further leads to the talin unmasking and integrin activation (**Figure 3.16B**). Our data also provide an explanation of why Rap1 and talin are essential for integrin activation whereas RIAM is dispensable for activation of most integrins expressed on many cell types as indicated by the recent series of genetic studies[34,66,67]. On the other hand, RIAM, which is highly abundant in leukocytes, was shown to play an important role

in regulating leukocyte integrin function[66,67] by possibly forming so called "MIT complex" with talin and integrin[33], indicating that the direct Rap1/talin pathway plays a minor role in regulating the leukocyte β_2 integrins. The fact that talin DM still partially supports cell adhesion and spreading of talin$^{1/2dko}$ cells (**Figure 3.15A, B**) further indicates the existence of other compensatory pathways including "Rap1-RIAM-talin" and "PIPKIγ/PIP2-talin" [14,16,50]. More detailed investigations are needed to understand how these different pathways are turned on or cooperate in a spatiotemporal manner. Nevertheless, our data, combined with the genetic evidence of Rap1 and talin in integrin activation, suggest that direct Rap1-talin interaction critically regulates integrin activity.

In addition to uncovering the physiological role of the Rap1b/talin interaction, our findings also bear broad implications in the analyses of protein-protein interactions (PPIs). Tens of thousands of PPIs in cells form a web of intricate communication networks for regulating diverse biological processes[86]. Interestingly, recent proteomic analyses have suggested that weak protein-protein interactions dominate in these cellular PPI networks[87]. However, because cellular protein concentrations, which are typically estimated on whole cell volumes, are low (e.g., nM), weak binary PPIs, as detected by conventional *in vitro* methods, were commonly treated to be non-specific and therefore disregarded for further investigations. Nevertheless, these weak PPIs may be enhanced and exert crucial functions at specific microenvironments, which is strongly demonstrated in our study. Specifically, while isolated Rap1b and talin-F0 binds at sub-mM affinity, the binding became very strong in the presence of membrane that mimics the cellular microenvironment. As illustrated in **Figure 3.16B**, the membrane anchoring ability of both Rap1b and talin may increase the local concentration of both proteins, thereby dramatically strengthening their

association. Other types of cellular strategies may also exist to enhance the association of otherwise weak binary interactions, which remain to be further investigated. With the completion of human genome and rapidly growing data of weak PPIs[87], our study emphasizes cautious treatment of a wide variety of weak PPIs by including specific microenvironments. In this regard, NMR is particularly valuable for deciphering the detailed structural basis of weak PPIs[76] *in vitro*, laying down the foundation for further analysis of the interaction in certain networks both *in vitro* and *in vivo*, as exemplified in our study. Such approach would complement with other techniques such as crystallography and CryoEM that are advantageous for elucidating large high affinity complexes, together, facilitating a thorough and unbiased view of how proteins function in cells.

Materials and Methods

Plasmid constructs and mutagenesis

The following constructs for bacterial expression were used in this study: mouse talin-F0 (1-86) subcloned into a pHis-1 vector, mouse full-length talin subcloned into a pET28t vector, human kindlin2-F0 (1-105) subcloned into a pGST-1 vector, mouse talin-H (1-429) subcloned into a pET28t and a pGST-1 vector, mouse RIAM-RAPH (149-438) subcloned into a pGST-1 vector, human full-length Rap1b subcloned into a pGST-1 vector, and C-terminal truncated Rap1b (1-167) subcloned into a pET28t vector. Human wild-type Rap1b and H-Ras (G12V) subcloned into pET28a vectors (6xHis tag) were kind gifts from Dr. Matthias Buck at Case Western Reserve University. Construct mutagenesis was conducted by using QuickChange lightning site-directed mutagenesis Kit (Agilent Technologies). Mutated constructs generated in this study include talin-F0_DM (K15A, R35A), talin-H_DM (K15A, R35A), Rap1b (G12V), Rap1b (1-167, G12V), Rap1b (G12V, I27H), Rap1b (G12V, K31E), Rap1b_TM1 (C51S, C118S, C141S), and Rap1b_TM2 (G12V, C51S, C118S, C141S). Note that pET28t is a modified pET28a vector where the thrombin cleavage site is substituted with a TEV protease cleavage site.

Protein expression and purification

Recombinant proteins with fusion tag (6xHis-tag or GST-tag) were expressed in E.*coli* BL21 (DE3) strain (New England Biolabs). Typically, bacteria was initially grown in 50 ml LB medium and then amplified in 1~2 l LB at 37 ℃. The culture was induced by 0.4 mM IPTG at 20 ℃ or RT for overnight when it reached an A_{600} of 0.7. The pellet was

then collected and suspended in buffer and frozen at -80 ℃. For protein purification, the pellet was lysed by incubation with lysozyme and sonication. After high speed centrifuge, the supernatant was subjected to affinity column purification by using either nickel or GST gravity column. Ion exchange chromatography was an optional purification step depending on protein purity (in this study, full-length Rap1b was purified by anion exchange method using Hi-trap Q column). Gel filtration was always performed in the final step by using either Superdex-75 (16/60) or Superdex-200 (16/60) (GE Healthcare). Note that Superose-6 (10/300) was used for full-length talin purification. Purified protein was checked by SDS-PAGE. Proteins with 90% purity or above were used in this study. According to experimental requirement, fusion tag (either His-tag or GST tag) was removed by TEV protease during protein purification if necessary. Isotope-labeled (^{15}N and/or ^{13}C) proteins were achieved by employing minimal medium with $^{15}NH_4Cl$ and/or ^{13}C-glucose as the sole nitrogen and carbon sources. ^{2}H labeled protein was achieved by using the minimal medium prepared in 99.8% D_2O with ^{2}H-glucose as the carbon source. Protein concentration was measured by absorbance at 280 nm or Pierce 660 nm protein assay reagent (Thermo Fisher Scientific).

GTPase nucleotide exchange

Non-hydrolyzable analogs of GDP and GTP, named Guanosine 5′-[β-thio] diphosphate trilithium salt (GDP-β-S) and Guanosine 5′-[β, γ-imido] triphosphate trisodium salt (GMP-PNP) respectively were purchased from Sigma-Aldrich. In this study, wild-type Rap1b loaded with GDP-β-S was used as an inactive form, and Rap1b (G12V)

or H-Ras (G12V) loaded with GMP-PNP was used as an active form. 50 μM purified wild-type Rap1b, Rap1b (G12V) or H-Ras (G12V) was first incubated with 2 mM EDTA and 2 mM GDP-β-S or GMP-PNP at RT for 35 min, $MgCl_2$ was then added in to reach a final concentration of 7 mM and incubated for another 30 min. After that, they were kept on ice and concentrated into a high concentration for experiment use.

NMR 2D-HSQC and HSQC titration

2D-HSQC experiments were performed on Bruker 600 MHz NMR spectrometer, and samples containing 50 μM ^{15}N-labeled protein were studied. For ^{15}N-labeled talin-F0 or kindlin2-F0, experiments were performed at 25 ℃ in buffer containing 20 mM NaH_2PO4/Na_2HPO4 (pH 6.6), 50 mM NaCl, 5 mM $MgCl_2$, 2 mM Dithiothreitol (DTT) and 5% D_2O. For ^{15}N-labeled Rap1b (1-167), experiments were performed at 25 ℃ in buffer containing 25 mM NaH_2PO4/Na_2HPO4 (pH 6.8), 150 mM NaCl, 5 mM $MgCl_2$, 2 mM DTT and 5% D_2O. Chemical shift change ($\Delta\delta_{obs\ [HN,N]}$) was calculated with the equation $\Delta\delta_{obs\ [HN,N]} = [(\Delta\delta_{HN}W_{HN})^2 + (\Delta\delta_N W_N)^2)]^{1/2}$, where W_{HN} and W_N are weighting factors based on the gyromagnetic ratios of ^{1}H and ^{15}N ($W_{HN} = 1$ and $W_N = 0.154$), and $\Delta\delta$ (ppm) = $\delta_{bound} - \delta_{free}$. For HSQC titration, samples containing 45 μM ^{15}N-labeled talin-F0 with increasing amount of GMP-PNP loaded Rap1b (G12V) were used to collect 2D-HSQC spectra. Dissociation constant (K_d) was achieved by fitting the chemical shift changes into the equation as shown below[88]. Four independent well resolved residues were selected for fitting and an average K_d was obtained.

$$\Delta\delta_{obs}=\Delta\delta_{max}\{(K_d+[P]_t+[L]_t)-[(K_d+[P]_t+[L]_t)^2-4*[P]_t*[L]_t\ ]^{1/2}\}/2[P]_t$$

($\Delta\delta_{max}$, maximum chemical shift change. $[P]_t$, labeled protein concentration. $[L]_t$, ligand or titrant concentration)

GST pull down

~25 μg purified GST or GST-fused protein was immobilized on 15 μl glutathione-Sepharose 4B resin (beads) via incubation on a rotator for 1.5 hours at 4 ℃ in the binding buffer containing 25 mM Tris-HCl (pH 7.5), 150 mM NaCl, 5 mM $MgCl_2$, 1 mM DTT, 0.01% Nondiet P-40, and supplemented with Complete EDTA-free Protease Inhibitor (Roche, Indianapolis, IN). Desired amount of prey protein was then added in and incubated with beads for another 2 hours at 4 ℃. After that, the beads were washed by 600 μl binding buffer twice and subjected to be denatured by adding 35 μl 2xSDS loading buffer and boiling for 5 min. After centrifuge down, supernatants were resolved by SDS-PAGE or western blotting. All the pull down experiments were performed in triplicate independently.

Western blotting and antibodies

After SDS-PAGE, samples were transferred onto a 0.45 μm PVDF membrane (Millipore, Billerica, MA). The membrane was blocked with 5% non-fat milk in TBST buffer overnight at 4 ℃. After that, the membrane was incubated with primary antibody

at RT for 3 hours and then incubated with HRP-conjugated secondary antibody at RT for 1 hour. The blots were detected by Pierce ECL Western Blotting Substrate (Thermo Fisher Scientific). The following primary antibodies were used in this study: 6xHis epitope tag antibody (Catalog# MA1-21315, Thermo Fisher Scientific), Rap1a/Rap1b (26B4) Rabbit mAb (Catalog# 2399, Cell Signaling Technology), Ras (27H5) Rabbit mAb (Catalog# 3339, Cell Signaling Technology), GAPDH (D16H11) Rabbit mAb (Catalog# 5174, Cell Signaling Technology), Anti-Talin 1 antibody (Catalog# ab57758, Abcam Inc.), and Anti-RIAM antibody [EPR2806] (Catalog# ab92537, Abcam Inc.). The following secondary antibodies were used in this study: Anti-mouse IgG, HRP linked Antibody (Catalog# 7076, Cell Signaling Technology) and Anti-rabbit IgG, HRP linked Antibody (Catalog# 7074, Cell Signaling Technology). Primary antibodies were used at 1:1000 dilution, and secondary antibodies were used at 1:3000 dilution.

Assignment of Rap1b and talin-F0 and their bound forms

C-terminal truncated Rap1b (1-167) with G12V mutation was used in all the following structure determination studies. For assignment of Rap1b, $^{15}N/^{13}C$-labeled Rap1b was purified and the N-terminal 6xHis tag was removed during purification. Standard triple-resonance experiments were conducted with 0.6 mM GMP-PNP loaded Rap1b. Rap1b sequential assignment was performed using PASA software[89]. For assignment of talin-F0, the complete chemical shift–assignment table of talin-F0 from Biological Magnetic Resonance Data Bank (accession code 15458) was downloaded and used in this study [70]. HNCA experiment was performed on 1.0 mM $^{15}N/^{13}C$-labeled talin-

F0 to confirm the assigned resonances. All these experiments were performed on Bruker 600 MHz NMR spectrometer, and at 25 ℃ in the buffer which contained 20 mM NaH_2PO4/Na_2HPO4 (pH 6.6), 50 mM NaCl, 5 mM $MgCl_2$, 2 mM d-DTT, and 5% D_2O. For assignments of the bound Rap1b and talin-F0 forms, the chemical shifts of majority of residues were readily transferred from the free forms with slight adjustments as they are similar to those of the free forms. A few residues (e.g. I27, R41) exhibited duplex peaks in the free form of Rap1 likely due to local conformational flexibility and most of these peaks were merged into single peaks in the complex. All assignments were also verified by through-bond NOESY experiments of the complex.

3D-NOESY experiments

The following samples were prepared: (1) 0.6 mM $^{15}N/^{13}C$-labeled Rap1b in the presence of 0.9 mM unlabeled talin-F0, (2) 0.5 mM $^{15}N/^{13}C$- labeled talin-F0 in the presence of 0.7 mM unlabeled Rap1b, (3) 0.5 mM ^{15}N/100% ^{2}H-labeled talin-F0 in the presence of 0.7 mM unlabeled Rap1b, (4) 0.5 mM $^{15}N/^{13}C$-labeled talin-F0 in the presence of 0.7 mM unlabeled Rap1b prepared in 99.8% D_2O. The following NOESY experiments were performed using the above samples: (i) 3D $^{15}N/^{13}C$-edited NOESY experiment (120 ms mixing time) with sample 1, (ii) 3D $^{15}N/^{13}C$-edited NOESY experiment (120 ms mixing time) with sample 2, (iii) 3D ^{15}N-edited NOESY experiment (300 ms mixing time) with sample 3 (iv) 3D $^{15}N/^{13}C$-filtered NOESY experiment (120 ms mixing time) with sample 4. All these experiments were performed on Bruker 850 MHz or 900 MHz spectrometers at the same condition as mentioned above.

Structure determination

All NMR data were processed and analyzed using nmrPipe[90], PIPP[91], and Sparky[98]. Distance restraints (NOE constraints) were obtained from 3D-NOESY experiments mentioned above, and Xplor-NIH[92] was used to calculate the complex structure. In brief, the individual structures of Rap1b and talin-F0 in complex form were calculated first based on the NOEs collected from sample 1 (2308 NOEs) and sample 2 (1114 NOEs) respectively. 302 dihedral-angle restraints for Rap1b derived from TALOS[93] were applied during Rap1b structure calculation. The initial templates for Rap1b and talin-F0 were derived from PDB database with PDB codes of 4DXA and 3IVF respectively. A total of 78 unambiguous intermolecular NOEs collected from sample 3 and sample 4 were used to calculate complex structure (also see **Table 3.1** for structural statistics). After refinements, a total of 50 final structures were calculated and the 20 lowest energy structures were selected for analysis. The quality of structure was evaluated with PROCHECK[94]. Structures are visualized by PyMOL 1.3 (Schrödinger, LLC.).

Membrane-anchored Rap1b preparation

To prepare large unilamellar vesicles (LUVs), 1-palmitoyl-2-oleoyl-sn-glycero-3-phosphocholine (POPC), L-α-phosphatidylinositol-4,5-bisphosphate (PI(4,5)P_2), and 1,2-dipalmitoyl-sn-glycero-3-phosphoethanolamine-N-[4-(p-maleimidomethyl)cyclohexane-carboxamide] (16:0 PE MCC) were purchased from Avanti Polar Lipids. LUVs which consist of 96% POPC, 1% PIP_2 and 3% PE MCC were prepared by extrusion. In brief,

lipids were first dissolved together in chloroform, and then the chloroform was removed under a stream of nitrogen followed by overnight vacuum pumping. The lipid film was suspended in buffer containing 25 mM NaH_2PO4/Na_2HPO4 (pH 6.8), 100 mM NaCl, and 5 mM $MgCl_2$, and subjected to homogenization with a few freeze–thaw cycles. LUVs were finally formed by extruding the lipid suspension ~20 times through two stacked 0.1 mm polycarbonate filters. Rap1b was tethered to LUVs via Michael addition between the thiol group of Cys 180 and the maleimide group of PE MCC[58,83]. To mimic the physiological condition that only the C-terminal Cys 180 of Rap1b is attached to membrane and meanwhile to avoid non-specific chemical interactions, all the cysteines of Rap1b except Cys 180 were mutated to serines. Rap1b_TM1 (C51S, C118S, C141S) and Rap1b_TM2 (G12V, C51S, C118S, C141S) were generated, purified and loaded with GDP-β-S and GMP-PNP respectively as described above. Rap1b_TM2 was first confirmed to interact with ^{15}N-talin-F0 by HSQC (**Figure 3.21A**). To make Rap1b anchored LUVs, Rap1b_TM1 or Rap1b_TM2 was incubated with freshly prepared LUVs in 1:6 molar ratio overnight at RT in the same buffer. The reaction was terminated by adding β-mercaptoethanol (β-ME) to a final concentration of 5 mM. The achievement of membrane-anchored Rap1b was confirmed by Native-PAGE combined with SDS-PAGE (**Figure 3.21B**). Unanchored Rap1b was dialyzed out in the same buffer using a dialyzer with 100 kDa cut-off membrane (Harvard Apparatus) before use.

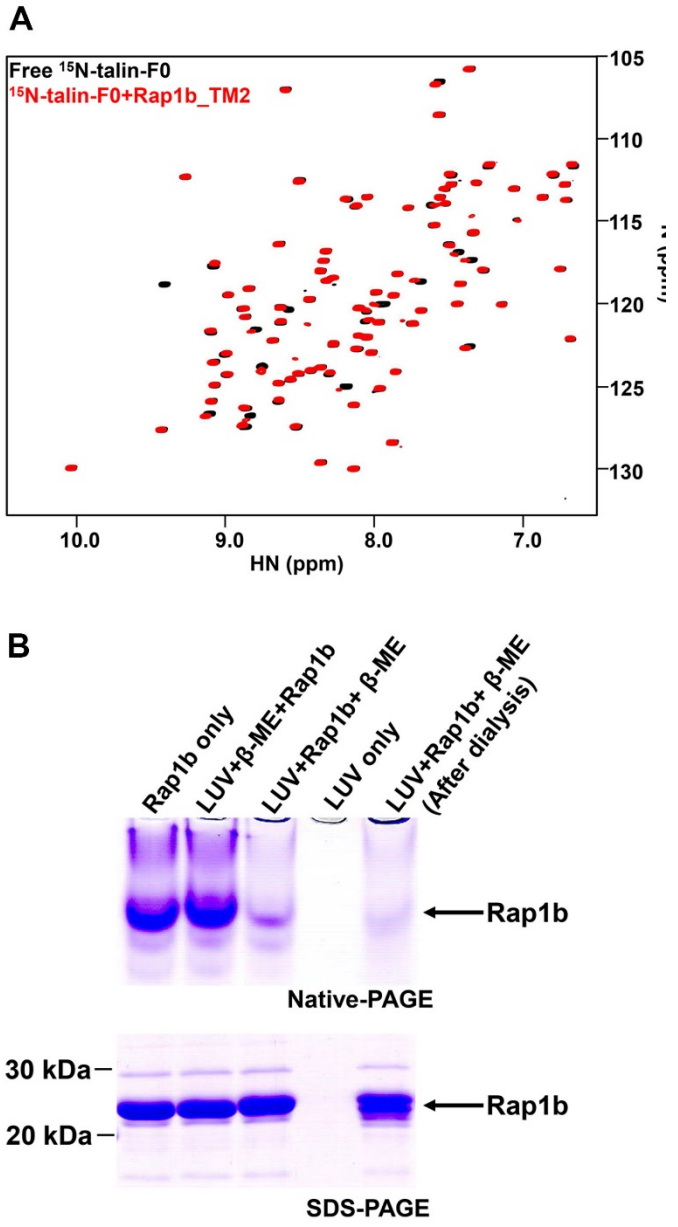

Figure 3.21 The anchorage of Rap1b to membrane vesicles

(A) The HSQC spectra of 45 μM ^{15}N-labeled talin-F0 in the absence (black) and presence of 90 μM GMP-PNP loaded Rap1b_TM2 (red). (B) A combination of Native-PAGE and SDS-PAGE analysis to confirm that Rap1b was anchored to large unilamellar vesicles (LUVs) efficiently. Upper panel, free un-denatured Rap1b migrated into a native-gel, but

LUVs anchored Rap1b couldn't due to the increasing size of the whole molecule, shown as "LUV+Rap1b+β-ME" in which the intensity of Rap1b band was significantly reduced. As a control, LUVs pre-incubated with β-ME failed to anchor Rap1b (shown as "LUV+β-ME+Rap1b") and the intensity of Rap1b band remained unchanged. Lower panel, SDS-PAGE to confirm that the total amount of Rap1b remained the same.

Vesicle co-sedimentation

Multilamellar vesicles (MLVs) rather than LUVs are used in this study since MLVs are larger in size and could be pelleted down easily. MLVs which consist of 87% POPC, 10% PIP2 and 3% PE MCC were prepared similarly to LUVs as described above but without extrusion. MLVs with anchored Rap1b (either GDP-β-S or GMP-PNP) were also prepared similarly as described above. 10 μM talin-H or full-length talin was incubated with 10 μM "MLV-Rap1b (Rap1b-anchored MLVs)", "MLV only" and "MLV+Rap1b (MLVs with unanchored Rap1b)" separately in a "7×21 mm" Polycarbonate tube (Beckman Coulter Inc.) with a total volume of 30 μl at RT for 15 min. Samples were then centrifuged down at 22,000 rpm for 35 min. Membrane pellet was dissolved in 2×SDS loading buffer and subjected to SDS-PAGE analysis. Gels were stained with Coomassie blue, and then scanned and quantified with an Odyssey CLx Imaging System (LI-COR, Inc.). The intensities of protein bands were quantified by the fluorescent signal detected from the 700 nm channel according to the manufacturer's protocol. Experiments were performed in quadruplets. Statistical significance was tested by two-tailed unpaired *t*-test.

Isothermal titration calorimetry

Isothermal titration calorimetry (ITC) experiments were performed using a Microcal iTC 200 system (GE healthcare Life Sciences) at 25 ℃. Before experiments, all samples were dialyzed into the same buffer which contained 25 mM NaH_2PO_4/Na_2HPO_4

(pH 6.8), 100 mM NaCl and 5 mM $MgCl_2$ overnight at 4 ℃. 200 μM talin-H in the syringe (~ 40 μl) was injected 20 times in 2.0 μl aliquots into the sample-cell (~220 μl) containing 15 μM LUV-Rap1b (GMP-PNP). As controls, talin-H was titrated into LUV only, Rap1b only, or buffer only, and talin-H_DM was titrated into LUV-Rap1b (GMP-PNP) using the same condition. ITC Data were analyzed by fitting to a single-site binding model with Origin Software.

Microscale thermophoresis (MST) analysis

The affinity of the interaction between GMP-PNP loaded GFP-Rap1b (G12V) and RIAM-RAPH, talin-F0 or talin-H was measured by using a Monolith NT.115 instrument (NanoTemper Technologies). Rap1b (G12V) was subcloned into a pRSET vector (Thermo Fisher Scientific) which expresses an N-terminal 6xHis tag and a C-terminal GFP fusion tag. RIAM-RAPH, talin-F0 or talin-H was prepared at different concentrations through 1:1 serial dilution and then mixed with 100 nM GFP- Rap1b (G12V) in buffer containing 50 mM Tris-HCl (pH 7.5), 100 mM NaCl, 5 mM $MgCl_2$, 2 mM DTT, and 0.05% Tween 20. The samples were incubated at RT for 10 min and then loaded into Microscale thermophoresis standard or premium capillary tubes. The fluorescent signal of GFP fusion tag was detected by the blue channel of the instrument according to the manufacturer's protocol, and the data were collected using 20% LED power and 40% MST powder at RT. Three independent experiments were performed, and the collected MST data were used to fit the dissociation constant (K_d) by using the MO. Affinity Analysis software (NanoTemper Technologies).

Integrin activation assay

Wild-type talin-H or talin-H_DM (K15A, R35A) was subcloned into a pEGFP-C1 vector. CHO (Chinese hamster ovary) A5 cells stably expressing integrin $\alpha_{IIb}\beta_3$ were transfected with empty vector, wild-type talin-H or talin-H_DM using Lipofectamine 2000 reagent (Life Technologies). After 24 hours, cells were stained with anti-$\alpha_{IIb}\beta_3$ activation-specific mAb PAC1 (1:100 dilution) (Catalog# 340535, BD Biosciences) at RT for 40 min, and later incubated with Alexa Flour 647 Goat Anti-Mouse IgM (Catalog# 115-607-020, Jackson Immunology Laboratories) (1:3,000 dilution) on ice for 30 min. After wash, cells were fixed and subjected to flow cytometry analysis. Values for PAC1 binding were reported as median fluorescent intensities (MFI) and the data were normalized to control with empty vector only and are presented by the means ± S.E.M.. The two-tailed unpaired *t*-test was performed to calculate the *p* value using GraphPad software.

Generation of cell lines and cell culture conditions

Murine talin1 and 2 double knockout fibroblasts ($talin^{1/2dko}$)[80] were retrovirally transduced with pLPCX expression construct containing YPET alone, C-terminally YPET-tagged talin-1 cDNA (talin-WT) or YPET-tagged double mutant talin-1 (talin DM; K15A, R35A) using the Phoenix retroviral expression system. Phoenix cells were transfected using a conventional calcium phosphate protocol and five infection cycles were performed by transferring the phoenix cell culture supernatant supplemented with 5 μg ml^{-1} polybrene to $talin^{1/2dko}$ cells[95,96]. Cells were FACS-sorted using a FACSAria™ IIu

cell sorter (BD Biosciences, Heidelberg, Germany) to isolate cells with comparable expression levels. Cells were characterized by western blotting using mouse α-GFP (home-made), rabbit anti-talin-1(Catalog# sc-15336, Santa Cruz Biotechnology Inc.), rabbit anti-Rap1 (Catalog# sc-65, Santa Cruz Biotechnology Inc.), rabbit anti-RIAM (Catalog# ab92537, Abcam Inc.), mouse anti-GAPDH (Catalog# CB1001-500UG, Millipore), goat anti-rabbit-HRP (Catalog# 111-035-144, Jackson ImmunoResearch Laboratories) and goat anti-mouse-HRP (Catalog# 115-035-003, Jackson ImmunoResearch Laboratories, Inc) antibodies following standard protocols. Rabbit anti-talin-1, rabbit anti-Rap1 and rabbit anti-RIAM antibodies were used at a dilution of 1:1000. Mouse anti-GAPDH, goat anti-rabbit-HRP and goat anti-mouse-HRP antibodies were used at a dilution of 1:20000. Cells were cultured under standard conditions in DMEM GlutaMAX^{TM} (Thermo Fisher Scientific) supplemented with 10% fetal bovine serum, 100 U ml^{-1} penicillin, 100 µg ml^{-1} streptomycin and non-essential amino acids (all Thermo Fisher Scientific).

Adhesion and spreading assays

For adhesion assays, polystyrol flat-bottom 96-well microplates (Greiner Bio-One, Frickenhausen, Germany) were coated with 10 µg ml^{-1} laminin (Sigma) in HBSS (Thermo Fisher Scientific), 5 µg ml^{-1} fibronectin, 0.01 % poly-L-lysine (both Sigma) or 5 µg ml^{-1} vitronectin (STEMCELL technologies, Köln, Germany) in coating buffer (20 mM Tris-HCl pH 9.0, 150 mM NaCl, 2 mM $MgCl_2$) overnight at 4 °C. After blocking with 3% BSA in PBS for 30 min at room temperature, 4x10^4 cells in DMEM containing 0.1 % FBS and 25 mM HEPES, were seeded per well, incubated for 1 h and washed with PBS. Adherent

cells were fixed with 4% paraformaldehyde (PFA) for 15 min and stained with 5 mg ml^{-1} crystal violet in 2% ethanol for 30 min. After washing, remaining crystal violet was dissolved in 2% SDS and quantified by measuring absorbance at 595 nm using a microplate reader (Tecan, Männedorf, Switzerland). All experiments were performed in quadruplets. For spreading analysis, cells were plated on fibronectin (5 µg ml^{-1}) coated dishes and phase contrast pictures were taken using an EVOS™ FL Auto life cell microscope (Thermo Fisher Scientific) 5 min, 15 min, 30 min, 60 min, 120 min and 240 min after seeding the cells. Cell spreading area of 30 cells per group at each time point were measured using ImageJ software (US National Institutes of Health). Statistical significance was tested by two-tailed paired *t*-test.

Flow cytometry

Integrin surface expression was determined by FACS using a LSRFortessa™ X-20 flow cytometer (BD Biosciences). Staining and measurement were performed in PBS supplemented with 2% FBS and 2 mM EDTA. Cells were incubated with biotinylated anti-integrin antibodies and subsequently with Cy5-labeled strepdavidin (Catalog# 016-170-084, Jackson ImmunoResearch Laboratories). Data were analyzed using FlowJo software. The following antibodies were used for flow cytometry: hamster IgM anti-integrin β1 (Catalog# 13-0291-82, eBioscience), rat IgG2a anti-integrin α6 (Catalog# 13-0495-82, eBioscience), rat IgG1 isotype control (Thermo Fisher Scientific), hamster IgG isotype control (Thermo Fisher Scientific), hamster IgG anti-integrin β3 (Catalog# 553345, BD Pharmingen), rat IgG2a anti-integrin α5 (Catalog# 557446, BD Pharmingen™), rat IgG1 anti-integrin αV(Catalog #104104, BioLegend), hamster IgM isotype control

(BioLegend) and rat IgG2a isotype control (BioLegend). All listed antibodies were biotinylated and used at 1:200 dilution.

Immunostaining and focal adhesion analysis

Cells were cultured on fibronectin coated glass coverslips (Thermo Fisher Scientific) over night or on fibronectin-coated micropatterns (disc-shaped with 1100 μm^2 area; Cytoo, Grenoble, France) for 5 h and fixed for 10 min with 4% PFA. Mouse-anti-paxillin with a dilution of 1:300 (Catalog# 610051, BD Transduction Laboratories, Heidelberg, Germany), goat-anti-mouse-Cy3 with a dilution of 1:400 (Catalog# 115-165-146, Jackson ImmunoResearch Laboratories) and Phalloidin-Alexa Fluor 647 with a dilution of 1:100 (Catalog# A22287, Thermo Fisher Scientific) were used for immunostainings. Images were acquired using a Leica TCS SP5 X confocal microscope (Leica Microsystems, Wetzlar, Germany) equipped with 63 × NA 1.40 oil objective lenses and Leica Confocal Software (LAS AF). All pictures were processed with Photoshop (Adobe Systems, San José, California, USA). Focal adhesion area was defined by paxillin staining and quantified using ImageJ software. For quantitative analysis of talin recruitment to focal adhesions, the total ypet signal intensity within the focal adhesion area was normalized to the total ypet fluorescence of the whole cell. Statistical significance was tested by two-tailed paired *t*-test.

Cell lysates preparations

Various types of cells indicated in **Figure 3.16A** were isolated from blood or cultured cells. Cells were washed once with cold PBS, and lysed by adding buffer which contained 50 mM Tris-HCl (pH 6.8) and 1%SDS. The cell lysates were boiled for 5 min, and the concentration of total protein in each cell lysate was quantified with Pierce BCA Protein Assay Kit (Thermo Fisher Scientific). ~8 μg total protein for each lysate was loaded onto SDS-PAGE gels for western-blotting analysis.

Data availability

The complete chemical shift–assignment tables of free Rap1b, bound Rap 1b, and bound talin F0 have been deposited in the Biological Magnetic Resonance Bank (BMRB) with the accession code 30353. The coordinates of Rap1b/talin-F0 complex structure have been deposited in the Protein Data Bank (PDB) with the code 6BA6.

Author contributions

Liang Zhu performed all biochemical/biophysical studies including NMR 2D-HSQC experiments, GST pull down assays, ITC experiments, and Microscale thermophoresis (MST) assay. Liang Zhu and Dr. Jun Yang performed all 3D-NMR studies and determined the solution structure of Rap1b/talin-F0 complex. Thomas Bromberger and Dr. Sarah Klapproth in Dr. Markus Moser's lab (Germany) performed the functional experiments showing that the double mutations of talin resulted in defective cell adhesion and spreading. Dr. Ashely Holly and Dr. Jamila Hirbawi performed the integrin activation assay in CHO A5 cells.

Chapter 4 Summary and Future direction

Summary

Contributed by our studies in this dissertation and others, we have achieved a conclusive mechanism of talin-mediated integrin activation triggered by Rap1. (i) Membrane recruitment of talin (**Figure 4.1A**). Upon extracellular agonist stimulation, membrane-anchored Rap1 gets activated by GEF and transits from an inactive GDP-bound form to an active GTP-bound form (see also **Figure 1.4**). Active Rap1 recruits talin *via* "Rap1-talin" direct pathway (demonstrated in Chapter 3) and/or a canonical "Rap1-RIAM-talin" axis as previously concluded by others. (ii) Activation of talin (**Figure 4.1A**). On one hand, PIPKIγ can be brought to membrane by associating with talin, and promotes the production of PIP2s at the membrane. As a positive feedback, PIP2s "open up" talin *via* an electrostatic "pull-push" mechanism defined previously by our group[14]. It is noteworthy that "Rap1-talin" direct pathway could synergize with "PIPKIγ-PIP2-talin" loop to recruit and activate talin (demonstrated in Chapter 3). On the other hand, "Rap1-RIAM-talin" axis plays an unexpected role in talin activation where the N-terminus of RIAM interacts with talin-F3 domain and sterically repels talin-R domain that otherwise masks the integrin-binding site on talin-F3 to trigger talin activation (demonstrated in Chapter 2). (iii) Activation of integrin (**Figure 4.1B**). Activated talin with an exposed talin-F3 domain catches the cytoplasmic tail of integrin β subunit at the membrane proximal "NPxY" motif and meanwhile, kindlin, a well-known co-activator of talin occupies the second or membrane distal "NPxY" motif. These lead to the separation of

integrin β subunit from α subunit at the cytoplasmic face. Such change is relayed to extracellular domain of integrin and induces the overall conformational change of integrin. Integrin gets activated and binds ECM ligands to initiate cell adhesion.

Our proposed model also provides a basis for understanding how talin gets fully extended to facilitate focal adhesion (FA) assembly following integrin activation (**Figure 4.1B**). Since inactive talin is autoinhibitory and adopts a globular shape, talin needs to get extended to expose binding sites for multiple intracellular adhesion molecules (vinculin, paxillin, etc.). Similar to a spring extension, the anchorage of both ends of talin may facilitate its extension upon force generated by actin network. In this regard, while actin is known to anchor the C-terminus of talin, "Rap1-talin" direct interaction and "PIPKIγ-PIP2-talin" loop (as studied in Chapter 3) guarantee a robust anchorage of talin at its N-terminus.

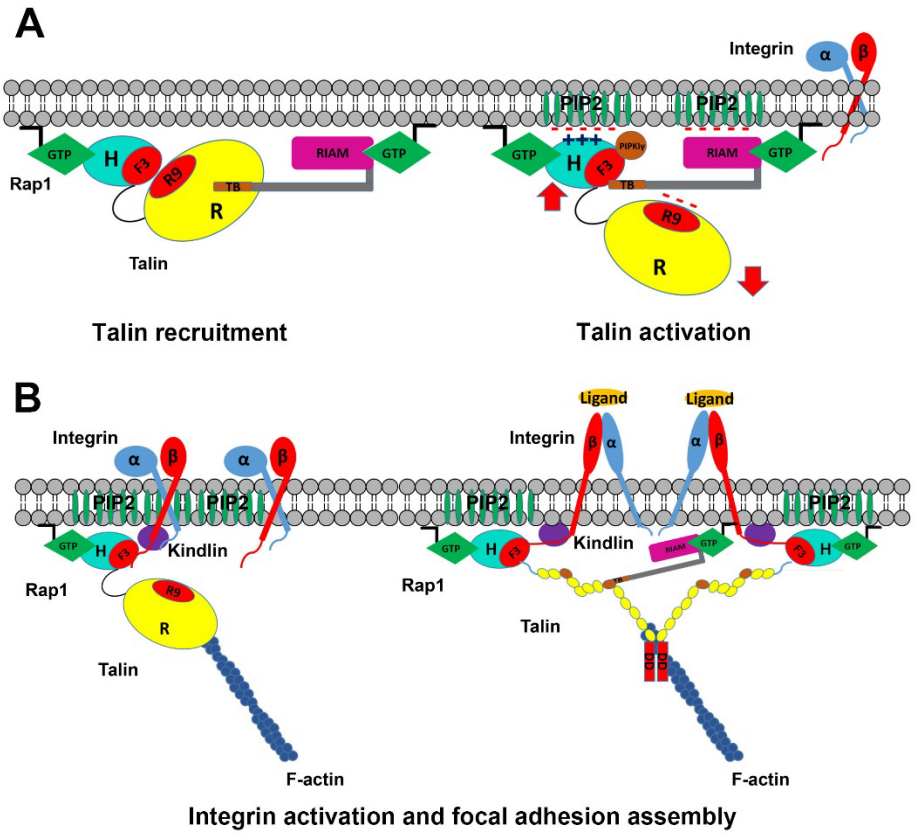

Figure 4.1 The mechanism of talin-mediated integrin activation and focal adhesion assembly triggered by Rap1

(A) Activated Rap1 triggers talin membrane recruitment and activation. "Rap1-RIAM-talin" pathway plays dual roles in both talin recruitment and activation. "Rap1-talin" axis directly targets talin to membrane site. "PIPKIγ-PIP2-talin" loop activates talin and also provides a firm anchorage of talin-H at the membrane site. (B) Integrin activation and focal adhesion assembly. Talin and kindlin cooperate together to activate integrin. Talin is dimeric and autoinhibited in resting state, but it is likely to get full extended to recruit multiple downstream adhesion proteins to trigger focal adhesion assembly upon integrin activation.

Future direction

As concluded by our studies and others, "Rap1-RIAM-talin", "Rap1-talin" and "PIPKIγ-PIP2-talin" pathways may act together to regulate talin-mediated integrin activation (**Figure 4.1A**), however, how these pathways cooperate with one another and how important each of these pathways is in cells still remain as open questions. Therefore, I would like to propose the following questions for future studies and discuss possible approaches to address each of them.

Question1: These pathways regulate the membrane localization and activation of talin, which are two key steps that control talin's action to mediate integrin activation. However, as far as we know, talin mutant that is deficient in RIAM, Rap1 or PIP2 binding only partially affects integrin activation indicating that each of these pathways may still be capable of functioning in the absence of one another. Without impairing the talin-F3/integrin interaction, can we generate a talin "super mutant" that is unable to mediate integrin activation by sufficiently blocking these pathways?

Approach: Three sets of mutations may be combined to generate a talin "super mutant", i.e. K15A/R35A mutations that block Rap1 binding (as studied in Chapter 3), V871Y/V1540Y mutations that are deficient in RIAM binding (as studied in Chapter 2) and K272A/K274A/K322A/K324A mutations that impair PIP2 binding (as studied in Song *et al*. 2012)[14]. It is interesting to investigate if this talin "super mutant" leads to more severely impaired integrin activation, focal adhesion assembly, cell adhesion, and cell

spreading compared to the mutants bearing only one or two sets of these mutations. The specific experiments could be performed as described in Chapter 3. Afterwards, we may have a better understanding about how these pathways cooperate with one another in integrin activaion.

Question 2: As reported, RIAM knock out mice are viable, fertile, and apparently healthy. These mice do not show impaired $\alpha_{IIb}\beta_3$ integrin function or any obvious phenotype in platelets[34]. Only in leukocytes have researchers found that loss of RIAM could lead to deficient leukocyte adhesion or impaired trafficking of lymphocytes[66,67]. Besides, our western-blot analysis also showed that RIAM is highly abundant in leukocytes but barely expressed in non-leukocytes (**Figure 3.16A**). Collectively, these evidences indicate that "Rap1-RIAM-talin" pathway prefers leukocyte-specific β2 integrin signaling and plays a minor role in non-leukocytes. Given that loss of either Rap1 or talin leads to the similar mice phenotypes and talin-mediated integrin activation is Rap1 dependent, we hypothesize that the "Rap1/talin" direct pathway maybe more widely existent in vivo to regulate integrin signaling. How do we test this hypothesis?

Approach: We could generate talin mutant (K15A/R35A) knock-in mice to investigate if the impaired "Rap1/talin" pathway leads to mice phenotypes. First of all, as we showed in **Figure 3.16A** that the expression of Rap1 and talin are extremely high in platelets, so it would be a priority to study the effect of "Rap1/talin" direct pathway in platelet functions (e.g. platelet aggregation response, tail bleeding time, and arterial thrombus formation.). Secondly, we can also examine if these mice show any phenotypes

in β2-integrin mediated leukocyte adhesion or function. This allows us to tell if "Rap1/talin" pathway as well plays a role in leukocyte integrin regulation. Thirdly, it would be interesting to generate RIAM knock-out mice with talin mutant (K15A/R35A) knock-in and investigate their phenotypes. These may help us understand how "Rap1-RIAM-talin" and "Rap1-talin" pathways cooperate with each other in vivo.

Question 3: "Rap1-RIAM-talin" pathway and its significance has been recognized for decades in this field. The fact that little phenotype was observed in RIAM knock-out mice is striking to some extent. How do we understand that RIAM knock-out does not affect overall integrin function in non-leukocytes?

Approach: One of the possibilities is that the absence of "Rap1-RIAM-talin" pathway may tune up other pathways like "Rap1/talin" and/or "PIPKIγ-PIP2-talin" as described above. Therefore, it would be interesting to look at how these two pathways are strengthened in those RIAM-null mice or cell lines. To start with, we could compare the expression levels of Rap1, talin, and PIPKIγ in wild-type cells with those in RIAM-null cells. In addition, we could compare the impact of knocking down these two pathways on integrin activation in wild-type cells with that in RIAM-null cells.

Another possibility could be that RIAM paralogue lamellipodin (Lpd), also from MRL-family, may compensate the loss of RIAM. It has been proved in cells using overexpression method that Lpd has similar function as RIAM does[30,33]. However, another previous study showed that RIAM and Lpd exhibit opposing effects on cell adhesion, suggesting that they are likely to be involved in distinct signaling pathways[29,97]. Thus, the

role of Lpd in integrin signaling remains elusive. Besides, Lpd is barely expressed in platelets as well as in RIAM-null platelets[34]. Therefore, such possibility may be difficult to explore.

Question 4: Rap1 controls multiple downstream effectors (e.g. KRIT1, AF-6, RAPL, RIAM and SHANK)[20,85], to regulate different signaling pathways. Rap1 binds to these effectors through a conserved interface but with a broad range of affinity spanning from nM to sub-mM. Biochemically, these effectors compete with one another for Rap1 binding. How do we understand the relationship among these different Rap1 effectors in cells?

Approach: First, we could simply check the expression levels of these effectors in different types of cells to see if they are expressed in a cell-type dependent manner. As we have observed in (**Figure 3.16A**), at least the expressions of RIAM and talin are cell-type dependent. Second, it is interesting to investigate if the overexpression or depletion of other Rap1 effector (KRIT1, AF-6, or RAPL) affects "Rap1-RIAM-talin" and "Rap1-talin" mediated integrin activation. We could test it in a well-established CHO A5 cell system (as used in both Chapter 2 and 3) where the integrin activation level could be measured. By doing so, we may have a better understanding about how these Rap1 effectors regulate one another in cells.

Question 5: Dysregulated integrin signaling causes many human diseases, including thrombosis, inflammation, and cancer. Integrins are hot therapeutic targets, and

many inhibitors in the forms of monoclonal antibody (mAb), cyclic peptide and small molecule have been developed to directly target the extracellular domain of integrin[3]. However, inhibitors that target talin have yet to be explored. Is it possible to develop inhibitors to modulate talin's action so as to regulate integrin signaling?

Approach: Since talin-mediated integrin signaling is triggered by Rap1 through "Rap1-talin", "Rap1-RIAM-talin" and "PIPKIγ-PIP2-talin" pathways and the interfaces of the key interactions involved in these pathways have been solved, structure-based inhibitors can be developed. (i) We could use computational strategy to search for Rap1 inhibitors to specifically target the "Rap1/talin" or "Rap1/RIAM" binding interface and test their effects in integrin activation. (ii) We could also design and develop peptide-based inhibitors to specifically block "talin/PIPKIγ", "RIAM/talin-R" or "RIAM/talin-F3" interaction that plays a role in talin membrane recruitment or activation. We expect to see this type of inhibitors may have milder effect in integrin activation compared to direct Rap1 inhibitors.

Besides, how talin undergoes conformational change still remains to be explored. A cryo-electron microscopy (Cryo-EM) structure of full-length talin reported in 2013, although with low-resolution, showed that inactive talin is a globular and compact dimer[63]. However, upon integrin activation, talin is likely to get fully extended for initiating focal adhesion assembly (**Figure 4.1B**). To structurally demonstrate it, we may continue pursuing the high-resolution structures of full-length talin in both inactive and extended forms by X-ray crystallography or CryoEM in the future. To experimentally mimic the

extended form of talin, we could generate monomeric talin by introducing mutations that disrupt talin dimerization interface or simply deleting talin dimerization domain (DD).

Reference

1. Barczyk, M., Carracedo, S. & Gullberg, D. Integrins. *Cell Tissue Res* **339**, 269-80 (2010).
2. Hynes, R.O. Integrins: bidirectional, allosteric signaling machines. *Cell* **110**, 673-87 (2002).
3. Goodman, S.L. & Picard, M. Integrins as therapeutic targets. *Trends Pharmacol Sci* **33**, 405-12 (2012).
4. Campbell, I.D. & Humphries, M.J. Integrin structure, activation, and interactions. *Cold Spring Harb Perspect Biol* **3**(2011).
5. Qin, J., Vinogradova, O. & Plow, E.F. Integrin bidirectional signaling: a molecular view. *PLoS Biol* **2**, e169 (2004).
6. Moser, M., Legate, K.R., Zent, R. & Fassler, R. The tail of integrins, talin, and kindlins. *Science* **324**, 895-9 (2009).
7. Calderwood, D.A., Campbell, I.D. & Critchley, D.R. Talins and kindlins: partners in integrin-mediated adhesion. *Nat Rev Mol Cell Biol* **14**, 503-17 (2013).
8. Harburger, D.S. & Calderwood, D.A. Integrin signalling at a glance. *J Cell Sci* **122**, 159-63 (2009).
9. Bennett, J.S. Structure and function of the platelet integrin alphaIIbbeta3. *J Clin Invest* **115**, 3363-9 (2005).
10. Ley, K., Laudanna, C., Cybulsky, M.I. & Nourshargh, S. Getting to the site of inflammation: the leukocyte adhesion cascade updated. *Nat Rev Immunol* **7**, 678-89 (2007).
11. Duong, L.T., Lakkakorpi, P., Nakamura, I. & Rodan, G.A. Integrins and signaling in osteoclast function. *Matrix Biol* **19**, 97-105 (2000).
12. Das, M., Subbayya Ithychanda, S., Qin, J. & Plow, E.F. Mechanisms of talin-dependent integrin signaling and crosstalk. *Biochim Biophys Acta* **1838**, 579-88 (2014).
13. Kim, C., Ye, F. & Ginsberg, M.H. Regulation of integrin activation. *Annu Rev Cell Dev Biol* **27**, 321-45 (2011).
14. Song, X. et al. A novel membrane-dependent on/off switch mechanism of talin FERM domain at sites of cell adhesion. *Cell Res* **22**, 1533-45 (2012).
15. Goult, B.T. et al. The structure of an interdomain complex that regulates talin activity. *J Biol Chem* **284**, 15097-106 (2009).
16. Martel, V. et al. Conformation, localization, and integrin binding of talin depend on its interaction with phosphoinositides. *J Biol Chem* **276**, 21217-27 (2001).
17. Beckerle, M.C., Miller, D.E., Bertagnolli, M.E. & Locke, S.J. Activation-dependent redistribution of the adhesion plaque protein, talin, in intact human platelets. *J Cell Biol* **109**, 3333-46 (1989).
18. Critchley, D.R. Biochemical and structural properties of the integrin-associated cytoskeletal protein talin. *Annu Rev Biophys* **38**, 235-54 (2009).
19. Guidetti, G.F. & Torti, M. The Small GTPase Rap1b: A bidirectional regulator of platelet adhesion receptors. *J Signal Transduct* **2012**, 412089 (2012).

20. Raaijmakers, J.H. & Bos, J.L. Specificity in Ras and Rap signaling. *J Biol Chem* **284**, 10995-9 (2009).
21. Bos, J.L. et al. The role of Rap1 in integrin-mediated cell adhesion. *Biochem Soc Trans* **31**, 83-6 (2003).
22. Chrzanowska-Wodnicka, M., White, G.C., 2nd, Quilliam, L.A. & Whitehead, K.J. Small GTPase Rap1 Is Essential for Mouse Development and Formation of Functional Vasculature. *PLoS One* **10**, e0145689 (2015).
23. Chrzanowska-Wodnicka, M., Smyth, S.S., Schoenwaelder, S.M., Fischer, T.H. & White, G.C., 2nd. Rap1b is required for normal platelet function and hemostasis in mice. *J Clin Invest* **115**, 680-7 (2005).
24. Li, Y. et al. Rap1a null mice have altered myeloid cell functions suggesting distinct roles for the closely related Rap1a and 1b proteins. *J Immunol* **179**, 8322-31 (2007).
25. Roskoski, R., Jr. Protein prenylation: a pivotal posttranslational process. *Biochem Biophys Res Commun* **303**, 1-7 (2003).
26. Takahashi, M. et al. Protein kinase A-dependent phosphorylation of Rap1 regulates its membrane localization and cell migration. *J Biol Chem* **288**, 27712-23 (2013).
27. Bos, J.L., de Rooij, J. & Reedquist, K.A. Rap1 signalling: adhering to new models. *Nat Rev Mol Cell Biol* **2**, 369-77 (2001).
28. Frische, E.W. & Zwartkruis, F.J. Rap1, a mercenary among the Ras-like GTPases. *Dev Biol* **340**, 1-9 (2010).
29. Lafuente, E.M. et al. RIAM, an Ena/VASP and Profilin ligand, interacts with Rap1-GTP and mediates Rap1-induced adhesion. *Dev Cell* **7**, 585-95 (2004).
30. Lee, H.S., Lim, C.J., Puzon-McLaughlin, W., Shattil, S.J. & Ginsberg, M.H. RIAM activates integrins by linking talin to ras GTPase membrane-targeting sequences. *J Biol Chem* **284**, 5119-27 (2009).
31. Wynne, J.P. et al. Rap1-interacting adapter molecule (RIAM) associates with the plasma membrane via a proximity detector. *J Cell Biol* **199**, 317-30 (2012).
32. Watanabe, N. et al. Mechanisms and consequences of agonist-induced talin recruitment to platelet integrin alphaIIbbeta3. *J Cell Biol* **181**, 1211-22 (2008).
33. Lagarrigue, F. et al. A RIAM/lamellipodin-talin-integrin complex forms the tip of sticky fingers that guide cell migration. *Nat Commun* **6**, 8492 (2015).
34. Stritt, S. et al. Rap1-GTP-interacting adaptor molecule (RIAM) is dispensable for platelet integrin activation and function in mice. *Blood* **125**, 219-22 (2015).
35. Zeiler, M., Moser, M. & Mann, M. Copy number analysis of the murine platelet proteome spanning the complete abundance range. *Mol Cell Proteomics* **13**, 3435-45 (2014).
36. Toker, A. The synthesis and cellular roles of phosphatidylinositol 4,5-bisphosphate. *Curr Opin Cell Biol* **10**, 254-61 (1998).
37. Ishihara, H. et al. Type I phosphatidylinositol-4-phosphate 5-kinases. Cloning of the third isoform and deletion/substitution analysis of members of this novel lipid kinase family. *J Biol Chem* **273**, 8741-8 (1998).
38. Di Paolo, G. et al. Recruitment and regulation of phosphatidylinositol phosphate kinase type 1 gamma by the FERM domain of talin. *Nature* **420**, 85-9 (2002).

39. Ling, K., Doughman, R.L., Firestone, A.J., Bunce, M.W. & Anderson, R.A. Type I gamma phosphatidylinositol phosphate kinase targets and regulates focal adhesions. *Nature* **420**, 89-93 (2002).
40. Kong, X., Wang, X., Misra, S. & Qin, J. Structural basis for the phosphorylation-regulated focal adhesion targeting of type Igamma phosphatidylinositol phosphate kinase (PIPKIgamma) by talin. *J Mol Biol* **359**, 47-54 (2006).
41. de Pereda, J.M. et al. Structural basis for phosphatidylinositol phosphate kinase type Igamma binding to talin at focal adhesions. *J Biol Chem* **280**, 8381-6 (2005).
42. Wegener, K.L. et al. Structural basis of integrin activation by talin. *Cell* **128**, 171-82 (2007).
43. Anthis, N.J. et al. The structure of an integrin/talin complex reveals the basis of inside-out signal transduction. *EMBO J* **28**, 3623-32 (2009).
44. Ling, K. et al. Tyrosine phosphorylation of type Igamma phosphatidylinositol phosphate kinase by Src regulates an integrin-talin switch. *J Cell Biol* **163**, 1339-49 (2003).
45. Legate, K.R. et al. Integrin adhesion and force coupling are independently regulated by localized PtdIns(4,5)2 synthesis. *EMBO J* **30**, 4539-53 (2011).
46. Wang, Y. et al. Platelets lacking PIP5KIgamma have normal integrin activation but impaired cytoskeletal-membrane integrity and adhesion. *Blood* **121**, 2743-52 (2013).
47. Shattil, S.J., Kim, C. & Ginsberg, M.H. The final steps of integrin activation: the end game. *Nat Rev Mol Cell Biol* **11**, 288-300 (2010).
48. Vinogradova, O. et al. A structural mechanism of integrin alpha(IIb)beta(3) "inside-out" activation as regulated by its cytoplasmic face. *Cell* **110**, 587-97 (2002).
49. Kim, M., Carman, C.V. & Springer, T.A. Bidirectional transmembrane signaling by cytoplasmic domain separation in integrins. *Science* **301**, 1720-5 (2003).
50. Goksoy, E. et al. Structural basis for the autoinhibition of talin in regulating integrin activation. *Mol Cell* **31**, 124-33 (2008).
51. Saltel, F. et al. New PI(4,5)P2- and membrane proximal integrin-binding motifs in the talin head control beta3-integrin clustering. *J Cell Biol* **187**, 715-31 (2009).
52. Han, J. et al. Reconstructing and deconstructing agonist-induced activation of integrin alphaIIbbeta3. *Curr Biol* **16**, 1796-806 (2006).
53. Worth, D.C. et al. Alpha v beta3 integrin spatially regulates VASP and RIAM to control adhesion dynamics and migration. *J Cell Biol* **189**, 369-83 (2010).
54. Hernandez-Varas, P. et al. Rap1-GTP-interacting adaptor molecule (RIAM) protein controls invasion and growth of melanoma cells. *J Biol Chem* **286**, 18492-504 (2011).
55. Goult, B.T. et al. RIAM and vinculin binding to talin are mutually exclusive and regulate adhesion assembly and turnover. *J Biol Chem* **288**, 8238-49 (2013).
56. Chang, Y.C. et al. Structural and mechanistic insights into the recruitment of talin by RIAM in integrin signaling. *Structure* **22**, 1810-1820 (2014).
57. Anthis, N.J., Wegener, K.L., Critchley, D.R. & Campbell, I.D. Structural diversity in integrin/talin interactions. *Structure* **18**, 1654-66 (2010).

58. Moore, D.T. et al. Affinity of talin-1 for the beta3-integrin cytosolic domain is modulated by its phospholipid bilayer environment. *Proc Natl Acad Sci U S A* **109**, 793-8 (2012).
59. Yang, J. et al. Conformational activation of talin by RIAM triggers integrin-mediated cell adhesion. *Nat Commun* **5**, 5880 (2014).
60. Lee, H.S., Anekal, P., Lim, C.J., Liu, C.C. & Ginsberg, M.H. Two modes of integrin activation form a binary molecular switch in adhesion maturation. *Mol Biol Cell* **24**, 1354-62 (2013).
61. Springer, T.A. Adhesion receptors of the immune system. *Nature* **346**, 425-34 (1990).
62. Arnaout, M.A. Biology and structure of leukocyte beta 2 integrins and their role in inflammation. *F1000Res* **5**(2016).
63. Goult, B.T. et al. Structural studies on full-length talin1 reveal a compact auto-inhibited dimer: implications for talin activation. *J Struct Biol* **184**, 21-32 (2013).
64. Schiemer, J. et al. Galpha13 Switch Region 2 Relieves Talin Autoinhibition to Activate alphaIIbbeta3 Integrin. *J Biol Chem* **291**, 26598-26612 (2016).
65. Xu, X.P. et al. Three-Dimensional Structures of Full-Length, Membrane-Embedded Human alpha(IIb)beta(3) Integrin Complexes. *Biophys J* **110**, 798-809 (2016).
66. Klapproth, S. et al. Loss of the Rap1 effector RIAM results in leukocyte adhesion deficiency due to impaired beta2 integrin function in mice. *Blood* **126**, 2704-12 (2015).
67. Su, W. et al. Rap1 and its effector RIAM are required for lymphocyte trafficking. *Blood* **126**, 2695-703 (2015).
68. Nieswandt, B. et al. Loss of talin1 in platelets abrogates integrin activation, platelet aggregation, and thrombus formation in vitro and in vivo. *J Exp Med* **204**, 3113-8 (2007).
69. Petrich, B.G. et al. Talin is required for integrin-mediated platelet function in hemostasis and thrombosis. *J Exp Med* **204**, 3103-11 (2007).
70. Goult, B.T. et al. Structure of a double ubiquitin-like domain in the talin head: a role in integrin activation. *EMBO J* **29**, 1069-80 (2010).
71. Plak, K., Pots, H., Van Haastert, P.J. & Kortholt, A. Direct Interaction between TalinB and Rap1 is necessary for adhesion of Dictyostelium cells. *BMC Cell Biol* **17**, 1 (2016).
72. White, G.C., 2nd, Crawford, N. & Fischer, T.H. Cytoskeletal interactions of Rap1b in platelets. *Adv Exp Med Biol* **344**, 187-94 (1993).
73. Hancock, J.F. Ras proteins: different signals from different locations. *Nat Rev Mol Cell Biol* **4**, 373-84 (2003).
74. Gloerich, M. & Bos, J.L. Regulating Rap small G-proteins in time and space. *Trends Cell Biol* **21**, 615-23 (2011).
75. Chrzanowska-Wodnicka, M. Rap1 in endothelial biology. *Curr Opin Hematol* (2017).
76. Vaynberg, J. & Qin, J. Weak protein-protein interactions as probed by NMR spectroscopy. *Trends Biotechnol* **24**, 22-7 (2006).

77. Perera, H.D. et al. Membrane binding of the N-terminal ubiquitin-like domain of kindlin-2 is crucial for its regulation of integrin activation. *Structure* **19**, 1664-71 (2011).
78. Li, X. et al. Structural basis for small G protein effector interaction of Ras-related protein 1 (Rap1) and adaptor protein Krev interaction trapped 1 (KRIT1). *J Biol Chem* **287**, 22317-27 (2012).
79. Bouaouina, M., Lad, Y. & Calderwood, D.A. The N-terminal domains of talin cooperate with the phosphotyrosine binding-like domain to activate beta1 and beta3 integrins. *J Biol Chem* **283**, 6118-25 (2008).
80. Theodosiou, M. et al. Kindlin-2 cooperates with talin to activate integrins and induces cell spreading by directly binding paxillin. *Elife* **5**, e10130 (2016).
81. Pollard, T.D., Blanchoin, L. & Mullins, R.D. Molecular mechanisms controlling actin filament dynamics in nonmuscle cells. *Annu Rev Biophys Biomol Struct* **29**, 545-76 (2000).
82. Elliott, P.R. et al. The Structure of the talin head reveals a novel extended conformation of the FERM domain. *Structure* **18**, 1289-99 (2010).
83. Gureasko, J. et al. Membrane-dependent signal integration by the Ras activator Son of sevenless. *Nat Struct Mol Biol* **15**, 452-61 (2008).
84. Pizon, V., Lerosey, I., Chardin, P. & Tavitian, A. Nucleotide sequence of a human cDNA encoding a ras-related protein (rap1B). *Nucleic Acids Res* **16**, 7719 (1988).
85. Lilja, J. et al. SHANK proteins limit integrin activation by directly interacting with Rap1 and R-Ras. *Nat Cell Biol* (2017).
86. Gavin, A.C. et al. Functional organization of the yeast proteome by systematic analysis of protein complexes. *Nature* **415**, 141-7 (2002).
87. Hein, M.Y. et al. A human interactome in three quantitative dimensions organized by stoichiometries and abundances. *Cell* **163**, 712-23 (2015).
88. Williamson, M.P. Using chemical shift perturbation to characterise ligand binding. *Prog Nucl Magn Reson Spectrosc* **73**, 1-16 (2013).
89. Xu, Y., Wang, X., Yang, J., Vaynberg, J. & Qin, J. PASA--a program for automated protein NMR backbone signal assignment by pattern-filtering approach. *J Biomol NMR* **34**, 41-56 (2006).
90. Delaglio, F. et al. NMRPipe: a multidimensional spectral processing system based on UNIX pipes. *J Biomol NMR* **6**, 277-93 (1995).
91. Garrett, D.S., Powers, R., Gronenborn, A.M. & Clore, G.M. A common sense approach to peak picking in two-, three-, and four-dimensional spectra using automatic computer analysis of contour diagrams. 1991. *J Magn Reson* **213**, 357-63 (2011).
92. Schwieters, C.D., Kuszewski, J.J., Tjandra, N. & Clore, G.M. The Xplor-NIH NMR molecular structure determination package. *J Magn Reson* **160**, 65-73 (2003).
93. Shen, Y., Delaglio, F., Cornilescu, G. & Bax, A. TALOS+: a hybrid method for predicting protein backbone torsion angles from NMR chemical shifts. *J Biomol NMR* **44**, 213-23 (2009).
94. Laskowski, R.A., Rullmannn, J.A., MacArthur, M.W., Kaptein, R. & Thornton, J.M. AQUA and PROCHECK-NMR: programs for checking the quality of protein structures solved by NMR. *J Biomol NMR* **8**, 477-86 (1996).

95. Austen, K. et al. Extracellular rigidity sensing by talin isoform-specific mechanical linkages. *Nat Cell Biol* **17**, 1597-606 (2015).
96. Austen, K., Kluger, C., Freikamp, A., Chrostek-Grashoff, A. & Grashoff, C. Generation and analysis of biosensors to measure mechanical forces within cells. *Methods Mol Biol* **1066**, 169-84 (2013).
97. Krause, M. et al. Lamellipodin, an Ena/VASP ligand, is implicated in the regulation of lamellipodial dynamics. *Dev Cell* **7**, 571-83 (2004).
98. Goddard T. D. and Kneller D. G.. SPARKY 3, University of California, San Francisco. (http://www.cgl.ucsf.edu/home/sparky/)